Studies of structural, dielectric and electrical properties of A/B site modified $(Na_{0.5}Bi_{0.5})TiO_3$ ceramic oxides

Barun Kumar Barick

DEPARTMENT OF PHYSICS

NATIONAL INSTITUTE OF TECHNOLOGY ROURKELA

2011

Studies of structural, dielectric and electrical properties of A/B site modified $(Na_{0.5}Bi_{0.5})TiO_3$ ceramic oxides

Thesis submitted to the
National Institute of Technology, Rourkela
For award of the degree

of

Master of Technology (Res)

By

Barun Kumar Barick

Under the guidance of

Dr. Dillip Kumar Pradhan

DEPARTMENT OF PHYSICS
NATIONAL INSTITUTE OF TECHNOLOGY
ROURKELA
JULY 2011

Dedicated to
My Loving Family,
Friends and Teachers

CERTIFICATE

This is to certify that the thesis entitled "**Studies of structural, dielectric, and electrical properties of A/B site modified ($Na_{0.5}Bi_{0.5}$)TiO_3 ceramic oxides**", submitted by **Barun Kumar Barick** to National Institute of Technology, Rourkela, is a record of bona fide research work under my supervision and I consider it worthy of consideration for the award of the degree of Master of Technology (Res) of the Institute.

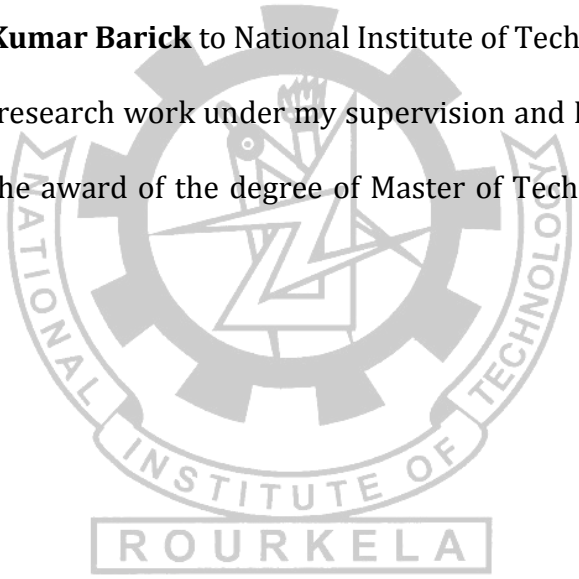

(Dr. Dillip Kumar Pradhan)
Supervisor

Date:

DECLARATION

I certify that

a. The work contained in the thesis is original and has been done by myself under the general supervision of my supervisor.

b. The work has not been submitted to any other Institute for any degree or diploma.

c. I have conformed to the norms and guidelines given in the Ethical Code of Conduct of the Institute.

d. Whenever I have used materials (data, theoretical analysis, and text) from other sources, I have given due credit to them by citing them in the text of the thesis and giving their details in the references.

Signature of the Student

ACKNOWLEDGEMENT

At the beginning, I would like to place on record my deep sense of gratitude to Prof. Dillip Kumar Pradhan, Dept. of Physics, NIT, Rourkela-769008, INDIA, for his generous guidance, help and useful suggestions.

I express my sincere gratitude to Prof. R. N. P. Choudhary, Dept. of Physics, Institute of Technical Education and Research, SOA University, Bhubaneswar-751030, India, for his stimulating guidance, continuous encouragement and well equipped laboratory facility throughout the course of present work.

I am extremely grateful to chairman and M.S.C members Prof. B. Ganguli, Prof S. Jena, Prof. D. K. Bisoyi, Prof. S. C. Mishra, Prof. S. K. Pratihar for their insightful comments and constructive suggestions to improve the quality of this research work.

I am thankful to N Sahoo, T Badapanda, Subrat, Mousoumi, Ponuatoya, Surbala, Satyabrata, Jashashree, Shanghamitra, Shreedevi and Achutya for their valuable suggestion and discussion at every step of my research work. I owe gratefulness to my “Hall-6” borders Satish, Auro, Krushna, Paresh etc. for joyful environment and helping me out in different ways.

I would like to show my sincere thanks to Prakash Palei and V Senthil for selfless help and useful suggestions. I am also great full to “Ferroelectric lab” members of IIT Kharagpur, especially Nabnit, Prakash, Shubhadrsini, Dhiren for their help and various suggestions. I express special thanks to labmates Satyanarayan, Asoka, and Smrutirekha, for necessary help to accomplishing this work.

Finally, I am forever indebted to my parents, sisters, brothers and DIDI for their blessings, love, inspiration, encouragement, and strong supports in every moments of my life.

Barun Kumar Barick

ABSTRACT

In recent years, there is an urgent need for the development of lead-free alternative ferroelectrics to replace the most dominant lead-based ferroelectrics (e.g., Lead zirconate titanate (PZT)) due to the toxicity of lead. Sodium bismuth titanate $(Na_{0.5}Bi_{0.5})TiO_3$ (NBT) based ferroelectrics are supposed to be the future materials for solid state electronics devices because of their relatively high Curie temperatures and high remnant polarization among the non-lead ferroelectrics. The present work deals with the synthesis and analysis of the electrical properties of NBT based lead free ferroelectric materials with suitable substitution at A and B sites.

In this context, the systematic studies of lanthanum (La) / yttrium (Y) and zirconium (Zr) substitution at A and B sites of NBT have been undertaken through structural, dielectric and impedance spectroscopy studies. NBT and modified NBT samples were synthesized by conventional solid state reaction route. The desired phase and crystal structure formation of the synthesized materials were confirmed by X-ray diffraction (XRD) analysis. The preliminary XRD analysis of the material revealed rhombohedral crystal system with hexagonal axis. The scanning electron micrographs (SEM) were taken at different magnifications to visualize the microstructure (grain size, grain distribution, voids etc.) of the materials. The appearance of the characteristic peak of BO_6 octahedra in FTIR spectrum confirms the formation of perovskite phase.

The temperature dependent dielectric constant of NBT and modified NBT showed a diffuse phase transition at the Curie temperature (T_c). The diffusivity of phase transition increases with increase in the concentration of substitutions. In the case of La and Y modified NBT, three phase transitions were observed. The phase transitions are ferroelectric to antiferroelectric phase ~150^oC (T_d), rhombohedral to tetragonal structure ~220^oC (T_{R-T}) and antiferroelectric to paraelectric phase (T_c) ~330^oC. The value of dielectric constant at T_c was found to be decreased with the La, Y and Zr modification**,** which may be due to the reduction of distortion in the unit cell. The Curie temperature (T_c) increases with La, Y and Zr substitution. The ac conductivity spectrum of NBT and modified NBT exhibited power law features. The calculated dc conductivity follows Arrhenius behavior. The Jump Relaxation Model (JRM) has been used to describe the observed conductivity spectrum. The conduction mechanism in the material may be due to oxygen vacancy and A-site ionic vacancies.

Complex impedance spectroscopic (CIS) methods have been used for the study of structure-property relationship of polycrystalline materials in a wide range of frequencies and temperatures. An asymmetric and temperature dependent relaxation peak has been observed in the variation of imaginary part of impedance with frequency, following Arrhenius behavior. Two overlapped depressed semicircular arcs in complex impedance plot (Nyquist plot) correspond to grain and the grain boundary contribution of the material. On the basis of brick layer model an equivalent electrical circuit has been proposed, which is a combination of two parallel RC elements connected in series for the electrical response of the material. The reduction of grain and grain boundary resistances (R_g and R_{gb}) of the materials with increase in

temperature showed negative temperature coefficient of resistance (NTCR) type behavior similar to that of semiconductors.

The modulus formalism has been adopted to study the conductivity relaxation mechanism in the material. The advantage of complex electric modulus formalism is that it suppresses the electrode effect. The imaginary part of electrical modulus vs. frequency spectrum shows a broad (FWHM>1.14), asymmetric and temperature dependent peak suggesting the non-Debye type relaxation in the material. The asymmetric nature of the peak may be due to the stretched exponential character of relaxation time. The imaginary part of modulus vs. frequency spectrum shows two well resolved peaks for the contribution of grain and grain boundary phenomena in the material at higher temperatures. The activation energies obtained in modulus spectrum are comparable to the activation energies obtained from impedance spectrum.

CONTENTS

List of Table:

List of Figure:

List of Symbols and Abbreviations:

ε	Dielectric constant
γ	Diffusivity
δ	Phase angle
ω	Angular frequency
σ_{ac}	A.C. conductivity
σ_{dc}	D.C. conductivity
Z'	Real part of impedance
Z''	Imaginary part of impedance
M'	Real part of electric modulus
M''	Imaginary part of electric modulus
λ	Wave length
β	Full width at half maximum
T_c	Curie temperature
T_d	Depolarization temperature
T_{R-T}	Rhombohedral to Tetragonal transition temperature
d	Inter planer spacing in crystal
a, b, c	Crystal unit cell parameter
h, k, l	Miller indices
NBT	Sodium bismuth titanate
RT	Room temperature
DC	Direct current
AC	Indirect current
Hrs	Hours
SEM	Scanning electron microscope
XRD	X-ray diffraction
FTIR	Fourier transform infrared spectroscopy
CIS	Complex impedance spectroscopy

Chapter 1

INTRODUCTION

1.1 Preamble

Ceramics are defined as the solid compounds that consist of metallic and nonmetallic elemental solids which are formed by the application of heat and/or pressure [1]. In general, the most common properties of ceramics are: hard, wear-resistant, brittle, refractory, thermal insulators, electrical insulators, nonmagnetic, oxidation resistance, thermal shock prone and chemically stable [2]. Nowadays ceramic materials are used everywhere. The properties of ceramic materials depend on the types of atoms present, the nature of bonding between the atoms and the way the atoms are packed together. The atoms in ceramic materials are held together by a chemical bond. Two most common chemical bonds for ceramic materials are covalent and ionic bonding. In comparison to metals, ceramics have very low electrical conductivity due to ionic-covalent bonding which does not form free electrons [3].

Most of the ceramic materials are dielectrics which possess very low electrical conductivity but supports electrostatic field. Electrical conductivity of ceramics varies with the frequency of the applied field and also with temperature [4]. This is due to the fact that charge transport mechanisms are frequency dependent and thermal energy provides the activation energy for the charge migration. In general, ceramic materials have high dielectric strength and high dielectric constant. Dielectric ceramic materials are used for manufacturing capacitors, insulators and resistors for electronic devices [5].

The dielectrics are electrical insulating materials, which can be polarized by the application of electric field. All the dielectrics are insulators but all the insulators are not dielectrics. Dielectrics are classified into nonpolar and polar types. When an electric field is applied to dielectric materials, displacement of center of positive and center of negative charge occurs, which creates a dipole moment. By this way it stores energy. The elementary dipoles in the dielectric materials interact with each other under certain thermodynamic conditions. The internal electric field produced by the interaction of dipoles aligns the dipoles in the same direction. This gives rise, the spontaneous polarization in the dielectric material. The polar dielectric materials with spontaneous polarization even in the absence of externally applied electric field are called as ferroelectric materials [6]. In the present study, we will discuss about the polar dielectrics in general and ferroelectric ceramic oxide in particular.

1.2 Ferroelectrics and related materials

The periodic arrangements of atoms influence the physical properties of a material. In crystallography, periodicity is understood by 7 crystal systems. These 7 crystal systems are classified into 14 Bravais lattices. Further, these 7 crystal systems are classified into 32 crystal classes known as point groups. Among them 11 point groups are centrosymmetric and so they do not possess any polarity. The other 21 point groups out of the 32 point groups are non-centrosymmetric. All non-centrosymmetric point groups, except the '432' point group, exhibit piezoelectric effect i.e., can be polarized under the influence of mechanical stress. Whereas 432 point group does not have polar axis due to any other type of symmetry. Only 10 out of 20 piezoelectric groups exhibit pyroelectric behavior i.e., the polarization occurs along a particular polar axis due to application of thermal energy. When the temperature of such crystals is altered, the change in polarization can be observed through the change in pyroelectric current. The ferroelectric materials are a sub-group of pyroelectric materials in which polarization can be reversed or reoriented by applying a reverse electric field [7].

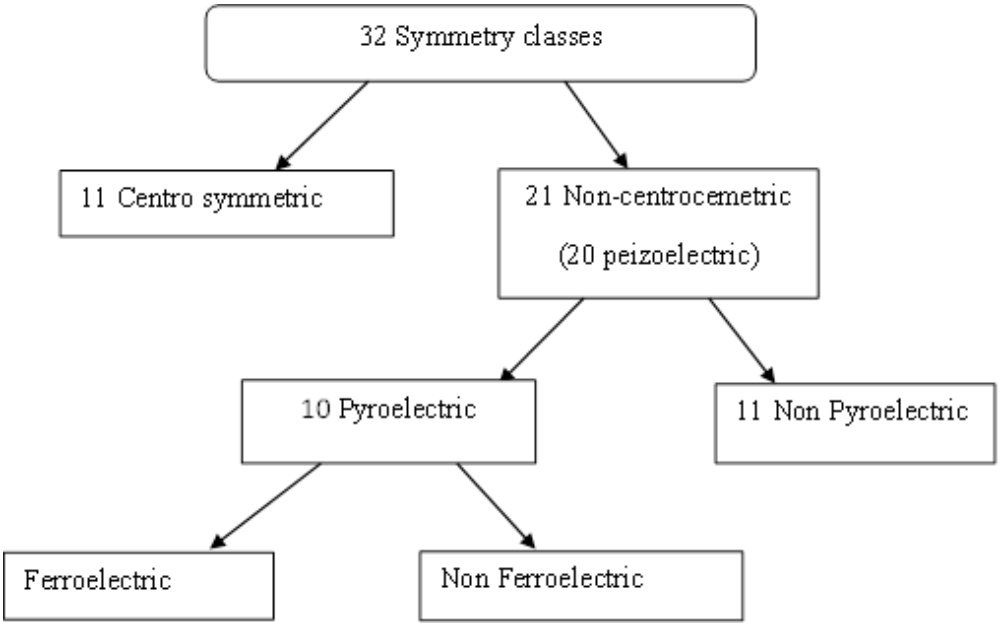

Fig. 1.1 Schematic representation of the classification of point groups

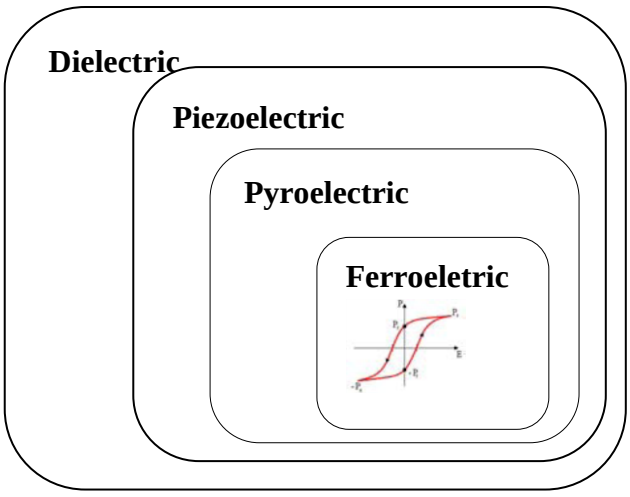

Fig. 1.2 Diagrammatic representations of the relationship between ferroelectrics, pyroelectrics and piezoelectrics.

In ferroelectric materials, the direction of spontaneous polarization (P_s) can be reoriented between two or more equilibrium symmetry equivalent states by the application of an appropriate electric field. A ferroelectric crystal generally has certain regions which exhibit a uniform alignment of electric dipoles and the spontaneous polarization in such regions may be different from one another. Such regions with uniform polarization are called ferroelectric domains. The interface between two domains is called the domain wall.

The most important property of ferroelectric materials is the formation of hysteresis loop due to its polarization reversal property. Figure 1.3 shows the ferroelectric hysteresis loop of ferroelectric materials.

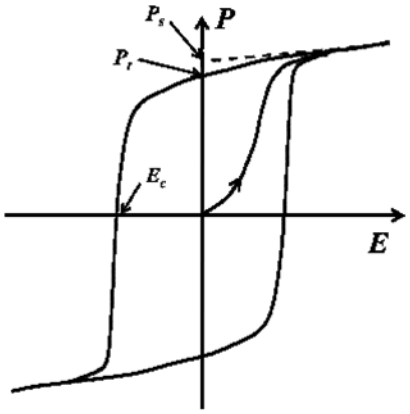

Fig. 1.3 A typical P-E hysteresis loop of ferroelectric material.

Up to certain electric field the ferroelectric material shows the linear relationship between electric field (E) and polarization (P). At relatively high electric field polarization shows a nonlinear relationship with the field. Polarization gets saturated at a certain higher field called saturation polarization. When the applied field is

removed the material possesses some polarization as some domains do not come back to the original direction. This polarization is called remnant polarization. In order to remove the remnant polarization in the material, an extra amount of opposite electric field is required which is known as coercive field. With an increasing electric field more domains will align in the opposite direction. Hence a cycle can be obtained by inverting the electric field once again.

The ferroelectricity phenomenon was first observed in Rochelle salt in 1920s [8]. Unfortunately, Rochelle salt loses its ferroelectric properties if the composition is slightly changed, which made it rather unattractive for industrial applications. In 1945s, ferroelectric behavior was reported in $BaTiO_3$ having perovskite structure [9]. Then after a lot of structural families with ferroelectric properties have been discovered. Ferroelectric materials are classified as corner sharing oxygen octahedral (Perovskite, Tungsten bronze, Pyrochlore, Bismuth layer), hydrogen bonded radicals (e.g., KDP, KH_2PO_4,), organic polymers (e.g., PVDF, $(CH_2\text{-}CF_2)_n$). Although all the structural families mentioned above shows ferroelectricity, but perovskite structural family shows greater potential for industrial device application [10].

The perovskite family is one of the fundamental crystal lattice structures. The general chemical formula for perovskite compounds is ABO_3, where 'A' and 'B' are two cations of different size, and 'O' is an anion, which makes bonds with both A and B. The valence of the A cation ranges from +1 to +3 and the B cation from +3 to +6. The 'A' atoms are larger than the 'B' atoms. The perovskite structure consists of

corner shared oxygen octahedral with B site cation in the middle. The A cations are situated at interstitial sites created by oxygen octahedral.

The stability of the perovskite structure is described by Goldschmidth tolerance factor t defined as

$$t = \frac{r_A + r_O}{r_B + r_O} \qquad (1.1)$$

where r_A, r_B and r_O are the ionic radii of the A, B, and oxygen ions respectively. It was found that the stable perovskite structure may be expected when t = 0.88 to 1.09. For an ideal perovskite structure, t = 1. In B-site driven perovskites (the ionic radius B-site atom too small for its site (t > 1)), the B atom has a tendency to move off center e.g., $BaTiO_3$. A-site driven structures (the ionic radius of B-site atom too big for its site (t < 1)) are often not ferroelectric and make favorable bond by tilting the oxygen octahedral e.g., $SrTiO_3$ or $CaTiO_3$.

The unit cell of perovskite structure can be distorted in many different directions like [100], [110], [111], [hk0] or [hkl] accompanied by the tilting of oxygen octahedra. The tolerance factor can be used to predict the crystal system at room temperature. [11]

Among different types of ferroelectric materials, barium titanate (BT) has become one of the most widely studied ferroelectric materials due to its better ferroelectric properties, chemical and mechanical stability. By 1950s, the ferroelectric

solid solution system $Pb(Ti,Zr)O_3$ (PZT) perovskite structure was invented. Since then, the PZT compositions are extensively exploited for piezoelectric and ferroelectric application both in research and industry.

1.3 Phase transition

The changes of spontaneous polarization of ferroelectric material by the change of crystal structure with temperature are called as ferroelectric phase transitions. A phase transition occurs due to changes in the forces of interaction between the atoms in the crystals. When the crystal undergoes the ferroelectric phase transition, the direction of this spontaneous polarization may arise in any one of the possible directions in the crystal structure. An asymmetrical shift in the equilibrium ion position gives rise to polarization catastrophe and hence a permanent dipole moment in the material.

Ferroelectric phase transitions are either displacive or order-disorder type. The displacive transition in perovskite ferroelectric ($BaTiO_3$) occurs by the ionic displacement of B-site ion within the oxygen octahedral cage. In an order-disorder ferroelectric, the randomly directed dipole moment of unit cell points in the same direction within a domain upon lowering the temperature [12]. The spontaneous polarization (P_s) of the ferroelectric system increases with decrease in temperature and appears discontinuously or some time continuously at a certain temperature, called Curie temperature or transition temperature (T_C). In the ferroelectric phase, at least one set of ions in the crystal sits in a double well potential, where either of two

positions, is equally energetically favorable. Above T_C, the particles in the double well have enough kinetic energy to move back and forth over the barrier that separates the wells, so that the time average position of the atom is midway between the wells. If the shape of the well stays the same above T_C, and the ion kinetic energy $k_\beta T$ becomes large, the transition is an order-disorder phase transition. If the minima of the well actually move together to form a single well above T_C, then the transition is displacive.

There are two types of phase transitions, first and second order phase transition. These are named depending on how the order parameter changes during the transition. In ferroelectric system, polarization is the order parameter. The order of the phase transition is defined by the discontinuity in the partial derivatives of the Gibbs free energy (G) of the ferroelectric at the phase transition temperature. For n^{th}-order phase transition, the n^{th}-order derivative of G is a discontinuous function at the transition temperature. A first order transition has a discontinuity in the order parameter, while a second order transition has a discontinuity in the first derivative of the order parameter at the transition temperature. The spontaneous polarization and strain change continuously at the second order ferroelectric phase transition and are discontinuous at for the first-order ferroelectric phase transitions [13].

The symmetry of the crystal changes at a phase transition point. The change in temperature or pressure, changes the atomic arrangements in the crystals without any change in chemical compositions. At this Curie temperature, the material

undergoes a transition from paraelectric (PE) symmetric phase to a ferroelectric (FE) lower symmetric phase i.e., at temperature $T>T_C$ the crystal does not exhibit ferroelectricity, while for $T<T_C$ it is ferroelectric. If there is more than one ferroelectric phase, the temperature at which the crystal transforms from one ferroelectric phase to another is called the transition temperatures.

Near the Curie point or phase transition temperature, thermodynamic properties including dielectric, elastic, optical, and thermal constants show an anomalous behavior. This is due to the distortion in the crystal as the phase changes. The temperature dependence of the dielectric constant above the Curie point ($T>T_C$) in most of the ferroelectric crystals is governed by the Curie-Weiss law:

$$\epsilon = \epsilon_0 + \frac{C}{T-T_0} \qquad (1.2)$$

where, ε is the permittivity of the material, ε_0 is the permittivity of the vacuum, C is the Curie constant and T_0 is the Curie-Weiss temperature. In the case of ceramic polar dielectrics the value of ε, P_s and other properties are very sensitive to dopants, defects in the crystal, porosity, grain size, sintering time and sintering temperature etc. In general the Curie-Weiss temperature T_0, is different from the Curie temperature T_C. For first order transitions, $T_0<T_C$ while for second order phase transitions, $T_0=T_C$. Other ferroelectrics show diffuse phase transition behavior. An additional subset of the ferroelectric phase transition called diffuse phase transition.

1.4 Diffuse phase transition

In macroscopic homogeneous materials, the observed transition temperature is not sharply defined. The transition is smeared out over a certain temperature interval, resulting in a gradual change of physical properties in this temperature region. This phase transition is called as diffuse phase transition temperature (DPT). Though this phenomenon is observed in several types of materials, however the most remarkable examples of DPT are found in ferroelectric materials. Ferroelectric diffuse phase transitions (FDPT) are first mentioned in the literature in the early 1950's. Some characteristics of the DPT are (a) broadened maxima in the permittivity-temperature curve, (b) gradual decrease of spontaneous and remnant polarizations with rising temperature, (c) transition temperatures obtained by different techniques which do not coincide, (d) relaxation character of the dielectric properties in transition region and (e) no Curie-Weiss behavior in certain temperature intervals above the transition temperature [14].

The diffuseness of the phase transition is assumed to be due to the occurrence of fluctuations in a relatively large temperature interval around the transition. Usually two kinds of fluctuations are considered: (a) compositional fluctuation and (b) polarization (structural) fluctuation. From the thermodynamic point of view, it is clear that the compositional fluctuation is present in ferroelectric solids-solutions and polarization fluctuation is due to the small energy difference between high and low temperature phases around the transition. This small entropy difference between ferroelectric and paraelectric phases will cause a large probability of fluctuation.

According to Fritsberg, substances of less stability are expected to have a more diffuse transition [15]. For relaxor as well as other FDPT, the width of the transition region is mainly important for practical applications. Smolenskii *et al.* [16] studied the DPT by fitting with a Gaussian distribution function at transition. The mean square deviation parameter of fitting indicates about the degree of diffusivity of the DPT. Complex perovskite type ferroelectrics with distorted cation arrangements show DPT which is characterized by a broad maximum for the temperature dependence of dielectric constant (ε) and dielectric dispersion in the transition region. For DPT, ε follows modified temperature dependence Curie Weiss law.

$$\epsilon = \epsilon_0 + \frac{C}{(T - T_m)^{\gamma}} \qquad (1.3)$$

where, T_m is the temperature at which ε reaches maximum (ε_m), C is the modified Curie constant and γ is the critical exponent. The γ factor explains the diffusivity of the materials, which lies in the range $1<\gamma<2$. In case of γ equals to unity, normal Curie–Weiss law is followed and it shows the normal ferroelectric phase transition. The value of γ is equal to two for complete diffusive phase transitions [17]. The smeared out ε vs. T response has generally been attributed to the presence of micro-regions with local compositions varying from the average composition over a length scale of 100 to 1000 Å. Different micro-regions in a macroscopic sample are assumed to transfer at different temperatures, so-called Curie range, leading DPT which is due to compositional fluctuations. In DPT the peak at dielectric maxima is much curved and polarization persists for a short range of temperatures above T_m.

1.5 NBT and Related materials

The polycrystalline perovskite ferroelectric ceramic materials have enormous applications in electronic and solid state devices such as actuators, piezoelectric motor, transducers, filter, resonator, micro-electromechanical system (MEMS). For most of the industrial application, $PbTiO_3$ (PT), $PbZrTiO_3$(PZT), $PbLaZrTiO_3$(PLZT), $PbMg_{1/3}Nb_{2/3}O_3$-$PbTiO_3$ (PMN-PT) like lead based multicomponent systems are used for their excellent ferroelectric and piezoelectric properties.

Despite the excellent ferroelectric and piezoelectric properties of lead based ferroelectric materials, these materials contain a large amount of lead (> 60 wt. %) which is toxic. While processing these materials, lead (Pb) normally exposed or released into the environment. The restoring and recycling of the lead-based materials have extensive environmental issues. Since lead remains for a long time in the environment and accumulates in living tissues, it damages the brain and nervous system [18]. On the other hand, improper disposing of lead, such as disposing to open environments, it could introduce the ecosystem and cause “acid rain”. Hence, for the environmental concern, there is a requirement of an alternative for lead based peizoceramic. Particularly the alternative materials should have properties comparable with lead-based counterparts. Furthermore, the lead free transducer is required for therapeutic and ultrasound devices used to study about living systems. The European Union (EU) has been enforced a legislation such as Waste from Electrical and Electronic (WEEE) on January 1, 2004, Restriction of Hazardous

substances (RoHS) on July 1, 2006 and End of Life Vehicles (ELV) on July, 2003 to stop the use of toxic materials like lead in industrial applications [11].

Many research groups around the globe are actively involved in ferroelectric research to find out an alternative to lead based system. There are various lead free perovskite ferroelctric materials e.g., $BaTiO_3$ (BT), $Na_{0.5}Bi_{0.5}TiO_3$ (NBT), $K_{0.5}Bi_{0.5}TiO_3$ (KBT), $KNbO_3$ (KN), $K_{0.5}Na_{0.5}NbO_3$ (KNN), $BaZrTiO_3$ (BZT), $BaSrTiO_3$ (BST) and their solid solutions have been studied for lead free applications [19]. Among the lead free ferroelectric materials, $Na_{0.5}Bi_{0.5}TiO_3$ (NBT) is considered to be an excellent candidate for applications.

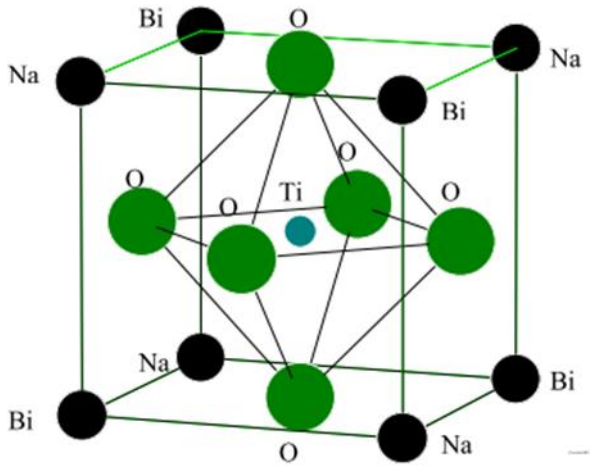

Fig. 1.5 Perovskite structure of NBT [21].

Sodium bismuth titanate (NBT) was discovered in 1960 by Smolenskii*et al.* [20]. NBT is an ABO_3 distorted perovskite with a rhombohedral (R3c) crystal structure at room temperature. In NBT, the bismuth and sodium cations occupy the

corners of a cubic unit cell, oxygen cations occupying the face centers forming an octahedral and a titanium cation in the center of the oxygen octahedra.

NBT is one among the few A-site disorder perovskite material, having a mixture of Bi^{3+} and Na^{1+} ions. The phase transitions and crystal structures of NBT at various temperatures was studied by Jones and Thomas, 2002 [22]. With decreasing temperature, NBT transforms from cubic Pm3m to tetragonal P4bm and then to rhombohedral R3c with coexistence regions between them.

There are some important features of the NBT material given below

i. NBT has the special ability to form a stable chemical compound through substitution on the A-site cation in the perovskite structure [23].

ii. NBT shows the peculiar nature of temperature dependent phase transitions. On cooling NBT transforms from a paraelectric phase to an anti-ferroelectric phase and then to a ferroelectic phase [24].

iii. Many relaxor ferroelectrics have pairs of isovalent A cations or chemically different B cations, but NBT has unlike valency Na^{+1} and Bi^{+3}cations at the A sites.

iv. The polarization of Pb^{+2} plays a special role in the ferroelectric properties of lead based materials. Bi^{+3} ions are isoelectronic configuration with Pb^{+2}, both showing a lone pair effect.

Studies on the structural and electrical properties have been performed on NBT and its dopants. Some of them trying to improve the dielectric properties, while other trying to improve the piezoelectric properties. NBT is a good material for both applications because it can be modified to enhance a specific desirable behavior.

The structural phase transitions in sodium bismuth titanate with the variation of pressure (up to 19 GPa) has been investigated using Raman spectroscopy by Kreisel *et al*. [23]. Zhu *et al.* [25] studied the effect of sintering temperature on $74Bi_{1/2}Na_{1/2}TiO_3–20.8Bi_{1/2}K_{1/2}TiO_3–5.2BaTiO_3$ ceramics. They observed that with the increase in Curie–Weiss temperature T_C, the sintering temperature increases, and the depolarization temperature T_d decreases. East *et al.* [26] reported that the bulk permittivity of NBT did not show any peak in the region 450 to 540 ^{0}C confirming the tetragonal polymorph is non-polar. A relaxor behavior was reported in the NBT-KBT system and it is due to the cation disorder in 12 fold coordination site. The tetragonal phase of the system is anti-ferroelectric due to loosely packed A-site cation [27]. The complex substitutions of Ba^{+2}, Sr^{+2} and Mn^{+4} cations reduces coercive field and increases the polarization of NBT were reported using first principle derived approach [28]. Isupov *et al.* [29] summarized the phase transition of NBT; it has three phase transitions of four structural phases. The transition of ferroelectric to antiferroelectric at temperature 200 ^{0}C named as ferroelectric (FE) transition. The transition of antiferroelectric to ferroelastic at temperature 320 ^{0}C named as antiferroelectric (AFE) transition. The transition of ferroelastic to paraelastic at

temperature 540 ^{0}C named as ferroelastic (FElast) transition. The complex impedance, electric modulus, dielectric loss and dc conductivity analyses of NBT was carried out by Saradhi *et al.* [30]. Dorcet *et al.* [31] studied the nanoscale structure and local structure due to the A- site order-disorder in NBT using TEM. The composition (1-3x) NBT-2xKBT-xBT shows the morphotropic phase boundary at x=0.025-0.035 between rhombohedral and tetragonal phase reported by Li *et al.* [32]. Ranjan *et al.* [33] studied structural and dielectric properties of $(Na_{0.50}Bi_{0.50})_{1-x}Ba_xTiO_3$ with $0 \leq x \leq 0.10$. The above system shows rhombohedral structural up to x=0.055 and above that it becomes nearly cubic. Suchanicz [34] explained the deformed hysteresis loops above 200 ^{0}C of NBT in terms of electro-mechanical interaction between polar-regions and nonpolar matrix. The relaxor behavior of $Na_{0.5}Bi_{0.5}TiO_3$–$K_{0.5}Bi_{0.5}TiO_3$ was explained as the cation disorder due to Na^{+1}, K^{+1}, Bi^{3+}at A-site. In tetragonal symmetry, the loosely packed A-site cations make the material anti-ferroelectric [35]. The relaxor ferroelectric nature of NBT was studied using Brillouin scattering by Schmidt *et al.* [36]. Structure and phase transition behavior of La doped sodium bismuth titanate ceramics were studied by Lee *et al.* [37]. Lanthanum incorporation creates both A-site and B-site vacancies. In A-site vacancies the phase transition near 200 °C becomes pronounced and it contributes to the incommensurate antiferroelectric phase. But, B-site vacancies produced by La doping do not contribute to the incommensurate phase. Barium doped BNT was studied for peizoelectric application by Chu *et al.* [38]. The addition of ZrO_2 to NBT increases the T_m as well as T_d to higher temperature and decreases the dielectric loss [39]. Jian-Xiu *et al.* [40] studied the dielectric and peizoelectric properties of NBT

with KCe substtution. It shows high Curie temperature (>650 ^{0}C) and high piezoelectric properties (d_{33}=27 pC/N). Kim *et al.* [41] studied that the coercive field decreases in La modified $Na_{1/2}Bi_{1/2}TiO_3$ (NBT) for the composition $Na_{1/2}Bi_{1/2-x}La_xTiO_3$ (x=0, 0.01, 0.03, 0.05, 0.07, 0.10). Phase Transitions in $Na_{1/2}Bi_{1/2}TiO_3$-$SrTiO_3$-$PbTiO_3$ solid solution were studied by Dunce *et al.* [42]. This composition shows relaxation depending on various concentrations of $PbTiO_3$. Lin *et al.* [43] studied the dielectric properties of silver particles incorporated $Na_{0.5}Bi_{0.5}TiO_3$. The dielectric constant increases with the increase in the amount of metallic silver particles which is ascribed to the effective electric fields developed between the dispersed particles in the matrix and the percolation effect. Hiruma *et al.* [44] determined the depolarization temperature T_d, rhombohedral-tetragonal phase transition temperature T_{R-T}, and the temperature of maximum dielectric constant T_m from the temperature dependent dielectric and piezoelectric properties of $Bi_{1/2}Na_{1/2}TiO_3$–$Bi_{1/2}A_{1/2}TiO_3$, A=Li and K. Microstructures and mechanical properties of zirconium doped NBT ceramics were studied by Watcharapasorn *et al.* [45]. The solution of (NBT–x$PbMg_{1/3}Nb_{2/3}O_3$) has been investigated by Lee *et al.* [46]. An addition of PMN into NBT transformed the structure of sintered samples from rhombohedral to pseudocubic phase for x larger than 0.1. A significant improvement of the piezoelectric and dielectric properties of the La_2O_3 (0–0.8 wt. %) doped $(Bi_{0.5}Na_{0.5})_{0.94}Ba_{0.06}TiO_3$ ceramics reported by Fu *et al.* [47]. Relaxor-like dielectric behavior was induced by barium doping to $Na_{0.5}Bi_{0.5}TiO_3$ was reported by Suchanicz [48]. Structure and dielectric properties of Sr^{2+} doped $(Na_{1/2}Bi_{1/2})TiO_3$ was studied by Park *et al.* [49]. The decrease of T_{max} and typical relaxor ferroelectric phase transition

behavior was found above 18 % of Sr^{2+} concentration. Sakata *et al.* [50] reported the AFE properties of the NBT phase above 200 ^{0}C in the NBT-$SrTiO_3$ solid solutions. Buhrer [51] reported that the Curie temperature went through a minimum at x=0.1–0.2 for the solid solutions of $(1-x)Na_{0.5}Bi_{0.5}TiO_3 + xK_{0.5}Bi_{0.5}TiO_3$, while the lattice parameters grew with x. Takenaka *et al.* [52] has reported the MPB at x=0.06–0.07 in $(1-x)NBT+xBaTiO_3$ system. The phase transition temperature and dielectric permittivity of A-site ion (A=Pb, Sr) substituted $(Na_{1/2}Bi_{1/2})TiO_3$ solid solutions with the aid of structural analysis has been investigated by Lee *et al.* [53]. They observed first order phase transition with the increase in the substitutions of Pb. However, substitution of Sr in the solid solutions exhibited relaxor ferroelectrics behavior. The phase transition temperature, electrical properties and the relationship between the substituted divalent ions (Ca^{2+}, Sr^{2+} and Ba^{2+}) in $(Bi_{1/2}Na_{1/2})TiO_3$-based ceramics were investigated by Watanabe *et al.* [54]. Hiruma *et al.* [55] demonstrated the relationship between various phases and the electrical properties of solid solutions of $(Bi_{1/2}Na_{1/2})$ TiO_3 with $NaNbO_3$ and $KNbO_3$ substitutions. The addition of bismuth aluminate ($BiAlO_3$) increases the broadness of dielectric peak and reduces the coercive field as reported by Yu *et al.* [56]. Boucher *et al.* [57] studied the structure and ferroelectric properties of $Na_{0.5}Bi_{0.5}TiO_3$-$BiScO_3$ system. Chen *et al.* [58] studied the electrical properties of $1-x(Bi_{0.5}Na_{0.5})TiO_3–xBa(Zr_{0.04}Ti_{0.96})O_3$ solid solutions and they reported that the solid solutions showed a MPB with the addition of 6 mole percent BZT in BNT. Yi *et al.* [59] have investigated the microstructure of lanthanum doped BNT and it was found that the substitution of La^{3+} ions at the A-site (Bi^{3+} or Na^+ ions), inducing A-site vacancies, resulted in inhibition of grain growth as well as

improvement of densification. Dielectric and piezoelectric properties of yttrium modified $(Bi_{0.5}Na_{0.5})_{0.94}Ba_{0.06}TiO_3$ was studied by Zhou *et al.* [60]. Senda *et al.* [61] compared the properties of lead based and lead free NBT composition of NBT-PT, NBT-KBT systems. The relationship between depolarization temperature and maximum permittivity temperature, influence of non-stoichiometry and doping on the structures and piezoelectric properties of $Na_{1/2}Bi_{1/2}TiO_3$–$BaTiO_3$ ceramics ware studied by Chu *et al.* [62]. Dai *et al.* [63] reported that the addition of $(0.96Bi_{0.5}Na_{0.5}TiO_3–0.04BaTiO_3)$ reduces the phase transition temperature of cubic to tetragonal and tetragonal to orthorhombic phases of $(0.98K_{0.5}Na_{0.5}NbO_3–0.02LiTaO_3)$. The addition of La_2O_3 to NBT results in high piezoelectric constant and low dissipation factor (tanδ) and reduction of Curie temperature was obtained by Fu *et al.* [64]. The reduction of domain size of Mn-doped $Na_{1/2}Bi_{1/2}TiO_3$ crystal with enhanced dielectric, piezoelectric and ferroelectric properties were observed in comparison with that of pure $Na_{1/2}Bi_{1/2}TiO_3$ crystal [65]. Setasuwon *et al.* [66] reported the synthesis of $Na_{1/2}Bi_{1/2}TiO_3$ anisotropic particles with grain orientation by conversion of $Na_{0.5}Bi_{4.5}Ti_4O_{15}$ crystals. The materials, $Bi_{0.5}(Na_{1-x-y}K_xLi_y)_{0.5}TiO_3$ (BNKLT−x/y) possess higher piezoelectric constant (d_{33}=230.8 pC/N), higher electromechanical coupling factor (k_p=0.41), larger remnant polarization (P_r=40 μC/cm^2) and a better P–E hysteresis loop below 200 °C [67]. Structural and dielectric properties studies by Liao *et el.* [68] shows the existence of a MPB in the composition range of $0.175 \leq x \leq 0.20$ of $Bi_{0.5}(Na_{1-x-y}K_xAg_y)_{0.5}TiO_3$ piezoelectric ceramics at room temperature.

Xu et al. [69] successfully synthesizes the $(Na_{0.5}Bi_{0.5})TiO_3$ and $(Na_{0.5}Bi_{0.5})_{0.92}Ba_{0.08}TiO_3$ powders by a citrate method. The compound $(1–x)Bi_{0.5}Na_{0.5}TiO_3–xBaNb_2O_6$ shows diffuse phase transition character and the diffuse character increases with increasing concentration of $BaNb_2O_6$ [70]. NBT doped BT synthesized by the citrate method and shows a high piezoelectric constant of 180 pC/N [71]. The substitution of $(Mg_{1/3}Nb_{2/3})^{+4}$ at B-site of $(Bi_{1/2}Na_{1/2})TiO_3$-based piezoelectric ceramic by a conventional ceramic technique and its effect on the microstructure, dielectric and piezoelectric properties were investigated [72]. The dielectric relaxation and electrical conduction in the Zr doped NBT systems were studied by Lily *et al.* [73]. The diffused phase transitions in the NBT-KBT system is due to structural disorder as well as compositional fluctuations in the crystal structure and relaxation phenomena is Maxwell–Wagner type as reported by Li *et al.* [74]. Li *et al.* [75] observed that the crystalline structure varies from rhombohedral to cubic with the increase in concentration of $KNbO_3$. The phase transition temperatures decreased and compounds showed relaxor ferroelectric behavior due to the introduction of $KNbO_3$. The composition $(1–3x)NBT–2xKBT–xBT$ shows a morphotropic phase boundary (MPB) between rhombohedral and tetragonal phase locates in the range of x=0.025–0.035 and show a relatively low coercive field of E_c $=4.55 kVmm^{-1}$. The transformation of relaxor type ferroelectrics to normal ferroelectrics increases with increase of KBT and BT concentration [76]. Prasad *et al.* [77] reported that the addition of WO_3 to NBT shifts phase transition temperature and depolarization temperature to a higher temperature. Raghavender *et al.* [78, 79] studies the effect of Ce^{+3} and Sm^{+3}substitution on electrical properties $Na_{0.5}Bi_{0.5}TiO_3$.

The peak in dielectric constant of NBT at 320 ^{0}C is associated with relaxation processes which can be recognized as the results of interaction (both of electric and mechanical nature) between polar-regions and nonpolar matrix, but cannot be a phase transition i.e., no changes in structure, specific heat, domain structure etc. are observed in this temperature [80]. Electrical properties of $(Bi_{0.5}Na_{0.5}TiO_3)$-$(Ba(Hf_{0.05},Ti0_{.95})O_3$, (BHT5) was studied by Tian *et al.* [81]. A small amount of BHT5 substitution increases the phase transition temperature (T_m) but the reverse trend is observed for higher concentration. And also (1–x)BNT–xBHT5 shows the morphotropic phase boundary at x=0.08. The compound $(1-x)Na_{0.5}Bi_{0.5}TiO_3-xK_{0.5}Bi_{0.5}TiO_3$for x=0.50, showed high piezoelectric properties, high T_d and low dielectric loss are reported by Zhao *et al.* [82]. Preparation and properties of sol–gel-derived $Bi_{0.5}Na_{0.5}TiO_3$ lead-free ferroelectric thin film was reported by Yu *et al.* [83]. At low temperature, the substitution of Ba, Mn, Nb, on NBT single crystal or ceramic has a small effect on thermal properties [84]. The addition of Mn decreases the T_c and increases the resistivity of the NBT [85]. Zhou *et al.* [86] studied the relaxor behavior of $Bi_{0.5}Na_{0.5}TiO_3–Bi_{0.5}K_{0.5}TiO_3–BiFeO_3$ ferroelectrics. The structure of NBT and Ba modified NBT were studies using diffuse X-ray scattering by Thomas *et al.* [87]. Grain growth kinetics of Dy modified BNT studied by Watcharapasorn *et al.* [88]. The dielectric properties of $(Bi_{1/2}Na_{1/2})Ti_{1-x}(Ni_{1/3}Nb_{2/3})_xO_3$ with x=0, 0.01, 0.02, 0.03 and 0.04 was studied by Zhou *et al.* [89]. They observed that grain size decreases with increasing x. The piezoelectric increases, up to x = 0.03 and then decreases with increasing x with a maximum value of 101 pC/N.

The morphotropic phase boundary (MPB) exists in $(Bi_{1/2}Na_{1/2})Ti_{1-x}(Zn_{1/3}Nb_{2/3})_xO_3$ ceramics between rhombohedral and tetragonal in the range of $0.5\% \leq x \leq 2.0\%$ [90]. The substitution of Eu on NBT shows a phase transition of rhombohedral to cubic reported by Lin *et al.* [91]. Kim *et al.* [92] studies the electrical properties $(1-x)(Bi_{0.5}Na_{0.5})TiO_3–xBaTiO_3$ $(x=0–0.10)$ powders synthesized by the emulsion method. Densification and reduction of sintering temperature of NBT ceramics were observed by substitution of Fe_2O_3 [93]. Dielectric and ferroelectric measurements of $(Bi_{0.95}Na_{0.75}K_{0.20-x}Li_x)_{0.5}Ba_{0.05}TiO_3$ showed that the Curie temperature shifts from 570K to 620K, but the maximum value of the dielectric constant decreases from 6700 to 4700 with the increase of lithium substitution as reported by Wang *et al.* [94].

The structure of $(Na_{0.5}Bi_{0.5})_{1-x}Ba_xTiO_3$ system showed MPB between rhombohedral–tetragonal phase lies in the composition range of $0.04<x<0.08$ at room temperature [95]. Mehboob *et al.* [96] studied the electrical properties of $(Na_{0.5}Bi_{0.5})(Nd_xTi_{1-2x}Nb_x)O_3$ ceramic by impedance spectroscopy. The effect of KBT on dielectric properties of NBT was studied by Li *et al.* [97] using impedance spectroscopy. The observed relaxation phenomenon in the system is Maxwell–Wagner type. Qu *et al.* [98] reported that the Ba^{+2} substitutions in A-site improve the dielectric properties of NBT ceramics. The composition of BNT–BZT shows a MPB and improves piezoelectric properties in the range of 3 to 12 mol% BZT [99]. The ternary system, $(Na_{1/2}Bi_{1/2})TiO_3$-$NaNbO_3$-$BaTiO_3$ ceramics, which shows pseudo-cubic crystal structure was studied by Wu *et al.* [100]. The change in crystal structure of

$(Bi_{0.5}Na_{0.5})_{0.94}Ba_{0.06}TiO_3$–$Ba(Zr_{0.04}Ti_{0.96})O_3$ from rhombohedral to tetragonal symmetry along with increasing BZT content was studied by Chen *et al.* [101].

The improved piezoelectric property with reduced coercive field was observed in 0–1.0 wt% CeO_2 doped $Bi_{0.5}Na_{0.44}K_{0.06}TiO_3$ piezoelectric ceramics [102]. The Curie temperature (T_c) and piezoelectric constants decreases in Mn modified $(Na_{0.5}Bi_{0.5})_{0.92}Ba_{0.08}TiO_3$ceramic [103]. Wang *et al.* [104] observed that cobalt doped $(Na_{0.5}Bi_{0.5})TiO_3$ exhibit a weak ferromagnetic order at room temperature and possess ferroelectric property. The Bi doped NBT was studied by Wang *et al.* [105] and reported that it reduces poling leakage current, enhances the piezoelectric properties and increases the dielectric constant and the dielectric loss of the NBT ceramics.

The dielectric constant of Nd_2O_3 doped $0.82Bi_{0.5}Na_{0.5}TiO_3$–$0.18Bi_{0.5}K_{0.5}TiO_3$ lowers with an increase in the Nd_2O_3 content [106]. There exists a morphotropic phase boundary (MPB) between rhombohedral and tetragonal lattices in the range of $0.18 < x < 0.21$ and $0 < y < 0.05$ in (0.97–x)BNT–xBKT–0.03BF and (0.82 – y)BNT–0.18BKT–yBF systems reported by Zhou *et al.* [107]. Shieh *et al.* [108] studied the switching characteristics of the MPB compositions of the $(Bi_{0.5}Na_{0.5})TiO_3$–$BaTiO_3$–$(Bi_{0.5}K_{0.5})TiO_3$ system by examining their polarization and strain hysteresis. The addition of CeO_2 with 0-1wt% $(Bi_{1/2}Na_{1/2})$¼0.94Ba0.06TiO_3 (BNBT) ceramics showed an increase in coupling factor and decrease in dissipation factor of systems without change in the co-existence of NBT-$BaTiO_3$ structure [109]. The T_d and T_{R-T} decrease, while T_m increases linearly with increase in $BiCrO_3$ contents in NBT reported by

Selvamani *et al.* [110]. Ramana *et al*. [111] investigated microwave sintered NBT showed high density, high dielectric properties and improved microstructure in comparison to conventionally sintered NBT. Piezoelectric coefficients and thermal stability of Fe and Mn substituted $Na_{0.5}Bi_{0.5}TiO_3$ ceramics were studied at high temperature by Davies *et al*. [112]. Rout *et al.* investigated various phase transformations in a solid solution series of $(100-x)Na_{0.5}Bi_{0.5}TiO_3–xSrTiO_3(0\leq x\leq 40)$ by x-ray diffraction, dielectric, and Raman scattering techniques [113].

Problems

Based on the literature survey, some of the main drawbacks found in the NBT based material are:

1. High coercive field.
2. High conductivity. The issue of high conductivity was attributed to volatilization of Bi ions during sintering [63].
3. High dielectric loss.
4. Low peizoelectric properties.

1.6 Main Objectives

In order to overcome the above problems, following are the main objectives of the proposed work.

- Preparation of new complex ferroelectric compounds using a high-temperature solid-state reaction technique.

- Studies of the structural, vibrational and micro-structural properties of the materials for better understanding of their structural parameters and surface morphology.
- Study of the dielectric responses as a function of frequency and temperature to find out the phase transitions in the material.
- Study of ac and dc conductivity of materials at various temperatures.
- Studies of complex impedance, complex electric modulus, complex permittivity and relaxation process of the materials by a complex impedance spectroscopy (CIS) method to establish structural (micro-structural) property relationship.

1.7 Materials under present investigation

The parent material is NBT and substitution of lanthanum, yttrium at A site and zirconium at B site of NBT.

$(Na_{0.5}Bi_{0.5})TiO_3$

$(Na_{0.5}Bi_{0.5})_{(1-x)}La_xTi_{(1-x/4)}O_3$ x=0.02, 0.04, 0.06, 0.08

$(Na_{0.5}Bi_{0.5})Ti_{(1-x)}Zr_xO_3$ x=0.05, 0.1, 0.2, 0.3

$(Na_{0.5}Bi_{0.5})_{(1-x)}Y_xTi_{(1-x/4)}O_3$ x=0.02, 0.04, 0.06, 0.08

1.8 Organization of Thesis

Chapter 1:

Introduction about ceramic materials, dielectric materials, and peizoelectric, pyroelectric, ferroelectric phenomena are given in chapter 1. First and second order phase transition of ferroelectric materials, detailed literature survey on NBT material, objective and addressed problems of research, list of materials under study and details about the thesis are also presented in this chapter.

Chapter 2:

This chapter deals with the chemical and solid state synthesis route of ceramic material. The procedure adopted for the solid state reaction route is also presented here. It also includes a brief description about the synthesis of desired material and description about different material characterization techniques e.g., XRD, SEM, FTIR, impedance spectroscopy.

Chapter 3:

The structural study is presented in this chapter. Preliminary study of the crystal structure of materials is carried out by X-ray diffraction analysis. The surface morphology and vibrational studies of the materials were carried out by scanning electron microscopy and FTIR spectroscopy, respectively.

Chapter 4:

In this chapter, detailed study of dielectric properties of materials is presented. The variation of dielectric constant and dielectric loss with frequency and temperature has been studied. Various phase transitions observed in these materials are discussed here.

Chapter 5:

Conductivity, one of the important phenomena of ferroelectric materials has been discussed in this chapter. The electrical properties of the materials are studied by complex Impedance spectroscopy. An equivalent circuit has been modeled for the observed electrical response of the material. The detailed understanding of long range conductivity and the localized relaxation process have been discussed using modulus spectroscopic studies on the materials is presented in this chapter.

Chapter 6:

It contains major conclusions drawn from the present investigation and some possible future work about the study of the NBT system.

References

[1] M. W. Barsoum, Fundamental of ceramics. Taylor and Francis, (2003)

[2] V. G. Sukumaran and N. Bharadwaj, Ceramics in dental applications. Trends in Biomaterials and Artificial Organs, 20 (2006) 7.

[3] M. W. Barsoum, Fundamentals of ceramic. Mc Graw-Hill Companies, Inc. International Edition, (1997).

[4] A. K. Jonscher, Dielectric relaxation in solids. Journal of Physics D: Applied Physics 32 (1999) 57.

[5] M. E. Lines and A. M. Glass, Principles and applications of ferroelectrics and related materials, Clarendon Press, Oxford (1977).

[6] Y. Xu, Ferroelectric materials and their applications, North-Holland Elsevier Sci. Publ., Amsterdam (1991).

[7] V. K. Wadhawan, Introduction to ferroic materials, CRC Press (2000).

[8] J. Valasek, Piezoelectric and allied phenomena in Rochelle Salt. Physcial Review, 17 (1921) 475.

[9] K. Uchino, Ferroelectric Devices. Marcel Dekker, Inc (2000).

[10] J. Kulawik, D. Szwagierczak and B. Groger, Investigations of properties of ceramic materials with perovskite structure in chosen electronic applications. Bulletin of the Polish Academy of Sciences. Technical Sciences, 55 (2007) 293.

[11] J Rodel, W. Jo, K. T. P. Seifert, E. M. Anton, T. Granzow and D. Damjanovic Perspective on the development of Lead-free piezoceramics. Journal of the American Ceramic Society, 92 (2009) 1153.

[12] C. Kittel, Introduction to Solid State Physics, 5th Ed., New York: Wiley, (1976).

[13] D. Damjanovic, Ferroelectric, dielectric and piezoelectric properties of ferroelectric thin films and ceramics. Reports on Progress in Physics, 61 (1998) 1267.

[14] G. H. Jonker, On dielectric Curie-Weiss law and diffuse phase transition in ferroelectrics. Material Research Bulletin, 18 (1983) 301.

[15] J. Fritesberg, Proc. 4th Int. Meeting on Ferroelectricity, Leningrad (1977).

[16] G. A. Smolesnky and V. A. Isupov, Soviet Journal of Technology and Physics 24, (1954) 1375.

[17] A. Shukla and R. N. P. Choudhary, Ferroelectric phase-transition and conductivity analysis of La^{3+}/Mn^{4+} modified $PbTiO_3$nanoceramics.Physica B: Condensed Matter, 405 (2010) 2508.

[18] M. Demaeder, D. Damjanovic and N. Setter, Lead-free piezoelectric materials. J. Electroceramic, 13 (2004) 385.

[19] T. Takenaka, Piezoelectric properties of some lead-free ferroelectric ceramics. Ferroelectrics, 230 (1999) 87.

[20] G. A. Smolenskii, V. A. Isupov, A. I. Agranovskaya and N. N. krainic, New ferroelectrics of complex composition. Soviet Physics.-Solid State, 2 (1961) 2651.

[21] C. J. Walsh, Bond valence structure analysis of doped bismuth titanate. Thesis, Alfred university, Alfred, New York (2004).

[22] G. O. Jones and P. A. Thomas, Investigation of the structure and phase transitions in the novel A-site substituted distorted perovskite compound $Na_{0.5}Bi_{0.5}TiO_3$. Acta Crystallography, Section B: Structural Science, 58 (2002) 168.

[23] J. Kreisel, A. M. Glazer, P. Bouvier and G. Lucazeau, High pressure Raman study of a relaxor ferroelectric: The $(Na_{0.5}Bi_{0.5})TiO_3$ perovskite. Physcial Review B, 63 (2001) 174106.

[24] C. S. Tu, I. G. Siny and V. H. Schmidt, Sequence of dielectric anomalies and high-temperature relaxation behavior in $Na_{1/2}Bi_{1/2}TiO_3$. Physcial Review B, 49 (1994) 11550.

[25] M. Zhu, H. Hu, N. Lei, Y. Hou and H. Yan, Dependence of depolarization temperature on cation vacancies and lattice distortion for lead-free74$(Bi_{1/2}Na_{1/2})TiO_3$–20.8$(Bi_{1/2}K_{1/2})TiO_3$–5.2$BaTiO_3$ferroelectric ceramics. Applied Physics Letter, 94 (2009) 182901.

[26] J. East and D. C. Sinclair, Characterization of $(Bi_{1/2}Na_{1/2})TiO_3$ using electric modulus spectroscopy. Journal of Materials Science Letters, 16 (1997) 422.

[27] Y. Li, W. Chen, J. Zhou, Q. Xu, H. Sun and M. Liao, Dielectric and ferroelectric properties of lead free NBT-KBT ferroelectric ceramic. Ceramic International, 31 (2005) 139.

[28] J. Zhou, W. W. Peng, D. Zhang, X. Y. Yang and W. Chen, Polarization properties of $Na_{1/2}Bi_{1/2}TiO_3$ system: First-principles calculation and experiment. Computational Materials Science, 44 (2008) 67.

[29] V. A. Isuprov and A. F. Ioffe, Ferroelectric $Na_{0.5}Bi_{0.5}TiO_3$ and $K_{0.5}Bi_{0.5}TiO_3$ perovskites and their solid solutions. Ferroelectrics, 315 (2005) 123.

[30] B.V. BahugunaSaradhi, K. Srinivas, G. Prasad, S. V. Surynarayan and T. Bhimasankaram, Impedance spectroscopy studies in ferroelectric $(Na_{1/2}Bi_{1/2})TiO_3$. Material Science and Engineering B, 98 (2003) 10.

[31] V. Dorcet, G. Trolliard and P. Boullay, The structural origin of the antiferroelectric properties and relaxor behavior of $Na_{0.5}Bi_{0.5}TiO_3$. Journal of Magnetism and Magnetic Materials, 321 (2009)1758.

[32] Y. Li, W. Chen, Q. Xu, J. Zhou and X. Gu, Piezoelectric and ferroelectric properties of $Na_{0.5}Bi_{0.5}TiO_3$–$K_{0.5}Bi_{0.5}TiO_3$–$BaTiO_3$ piezoelectric ceramics. Materials Letters, 59 (2005) 1361.

[33] R. Ranjan and A. Dviwedi, Structure and dielectric properties of $(Na_{0.50}Bi_{0.50})_{1-x}Ba_xTiO_3$: $0 \le x \le 0.10$. Solid State Communications, 135 (2005) 394.

[34] J. Suchanicz, Behavior of $Na_{0.5}Bi_{0.5}Ti0_3$ ceramics in the ac electric field. Ferroectrics, 209 (1998) 561.

[35] Y. Li, W. Chena, J. Zhou, Q. Xu, H. Sun and M. Lia. Dielectric and ferroelectric properties of lead-free $Na_{0.5}Bi_{0.5}TiO_3$–$K_{0.5}Bi_{0.5}TiO_3$ ferroelectric ceramics. Ceramics International, 31 (2005) 139.

[36] V. H. Schmidt, C. S. Tu and I. G. Siny, Dielectric and brillouin scattering anomalies in an $Na_{l/2}Bi_{l/2}TiO_3$ (NBT) relaxor ferroelectric crystal. DOI:10.1109/ISAF.1994.522294.

[37] J. K. Lee, J. Y. Yi and K. S. Hong, Dependence of incommensurate phase formation on vacancy type in La-doped $(Na_{1/2}Ba_{1/2})TiO_3$. Journal of Applied Physics, 96 (2004) 1174.

[38] B. J. Chu, J. H. Cho, Y. H. Lee, B. I. Kim and D. R. Chen, The potential application of BNT-based ceramics in large displacement actuation. Journal of Ceramic Processing Research, 3 (2002) 231.

[39] K. Kumari and K. Prasad, Structural and dielectric properties of ZrO_2 added $(Na_{1/2}Bi_{1/2})TiO_3$ ceramic. Brazilian Journal of Physics, 39 (2009) 297

[40] X. J. Xiu, Z. Liang and Z. C. Ju, Dielectric and piezoelectric properties of Sodium Bismuth Titanate ceramics with KCe substitution. Chinese Physics Letter, 25 (2008) 4414.

[41] J. S. Kim, B. C. Choi, J. H. Jeong, K. S. Lee and S. B. Cho, Ferroelectric properties of La doped $Na_{1/2}Bi_{1/2}TiO_3$ (NBT) lead-free ferroelectric ceramics. Ferroelectrics, 384 (2009) 120.

[42] M. Dunce, E. Birks, M. Antonova, M. Kundzinsh and A. Sternberg, Phase transitions in $Na_{1/2}Bi_{1/2}TiO_3$-$SrTiO_3$-$PbTiO_3$ solid solutions. Integrated Ferroelectrics, 108 (2009) 125.

[43] Y. Lin, C. W. Nan, J. Wang, G. Liu, J. Wu and N. Cai, Dielectric behavior of $Na_{0.5}Bi_{0.5}TiO_3$-based composites incorporating silver particles. Journal of the American Ceramic Society, 87 (2004) 742.

[44] Y. Hiruma, K. Yoshii, H. Nagata and T. Takenaka, Phase transition temperature and electrical properties of $Bi_{1/2}Na_{1/2}TiO_3$–$Bi_{1/2}$ $A_{1/2}TiO_3$, A=Li and K lead-free ferroelectric ceramics. Journal of Applied Physics, 103 (2008) 084121.

[45] A. Watcharapasorn, S. Jiansirisomboon and T. Tunkasiri, Microstructures and mechanical properties of zirconium-doped bismuth sodium titanate ceramics. Chiang Mai Journal of Science, 33 (2006) 169.

[46] J. Kun Lee, Yi, Jae Yun, Hong and Kug Sun, Structural and electrical properties of $(1-x)(Na_{1/2}Bi_{1/2})TiO_3$-$xPb(Mg_{1/3}Nb_{2/3})O_3$ solid solution. Journal of Solid State Chemistry, 177 (2004) 2850.

[47] P. Fu, Z. Xu, R. Chu, W. Li, G. Zang and J. Hao, Piezoelectric, ferroelectric and dielectric properties of La_2O_3-doped $(Bi_{0.5}Na_{0.5})_{0.94}Ba_{0.06}TiO_3$ lead-free ceramics. Materials & Design, 31 (2010) 796.

[48] J. Suchanicz, J. Kusz, H. Bohm and G. Stopa, Structural and electric properties of $(Na_{0.5}Bi_{0.5})_{0.88}Ba_{0.12}TiO_3$. Journal of Material Science, 42 (2007) 7827.

[49] S. E. Park and K. S. Hong, Variations of structure and dielectric properties on substituting A-site cations for Sr^{2+} in $(Na_{1/2}Bi_{1/2})TiO_3$. Journal of Material Research, 12 (1997) 2152.

[50] K. Sakata and Y. Masuda, Ferroelectric and antiferroelectric properties of $(Na_{0.5}Bi_{0.5})TiO_3$-$SrTiO_3$ solid solution ceramics. Ferroelectrics, 7 (1974) 347.

[51] C. F. Buhrer, Some properties of bismuth perovskites. Journal of Chemical Physics, 36 (1962) 798.

[52] T. Takenaka, K. Maruyama and K. Sakata, $(Bi_{1/2}Na_{1/2})TiO_3$-$BaTiO_3$ system for lead-free piezoelectric ceramics. Japanese Journal of Applied Physics, 30 (1991) 2236.

[53] J. K. Lee, K. S. Hong, C. K. Kim and S. E. Park, Phase transitions and dielectric properties in A-site ion substituted $(Na_{1/2}Bi_{1/2})TiO_3$ ceramics (A=Pb and Sr). Journal of Applied Physics, 91 (2002) 4538.

[54] Y. Watanabe, Y. Hiruma, H. Nagata and T. Takenaka, Phase transition temperatures and electrical properties of divalent ions (Ca^{2+}, Sr^{2+} and Ba^{2+}) substituted $(Bi_{1/2}Na_{1/2})TiO_3$ ceramics. Ceramics International, 34 (2008) 761.

[55] Y. Hiruma, H. Nagata and T. Takenaka, Phase diagrams and electrical properties of $(Bi_{1/2}Na_{1/2})TiO_3$-based solid solutions. Journal of Applied Physics, 104 (2008) 124106.

[56] H. Yu and Z. Ye, Dielectric, ferroelectric and piezoelectric properties of the Lead free $(1-x)Na_{0.5}Bi_{0.5}TiO_3$–x $BiAlO_3$ solid solution. Applied Physics Letter, 93 (2008) 112902.

[57] E. Boucher, P. Marchet and J. P. Mercurio, Structural and ferroelectric study of $Na_{0.5}Bi_{0.5}TiO_3$-$BiScO_3$ system. Journal De Physique. IV: JP, 128 (2005) 3.

[58] Z. W. Chen, A. Z. Sui, Z. Y. Lu and P. A. Liu, Electrical properties of $(Bi_{0.5}Na_{0.5})TiO_3$–$Ba(Zr_{0.04}Ti_{0.96})O_3$ ceramics. Journal of Ceramic Society Japan, 114 (2006) 857.

[59] J. Y. Yi, J. K. Lee and K. S. Hong, Dependence of the microstructure and the electrical properties of Lanthanum-substituted $(Na_{1/2}Bi_{1/2})TiO_3$ on cation Vacancies. Journal of American Ceramic Society, 85 (2002) 3004.

[60] C. Zhou, X. Liu, W. Li and C. Yuan, Dielectric and piezoelectric properties of Y_2O_3 doped $(Bi_{0.5}Na_{0.5})_{0.94}$ $Ba_{0.06}TiO_3$ lead-free piezoelectric ceramics. Materials Research Bulletin, 44 (2009) 724.

[61] S. Said and J. P. Mercurio, Relaxor behaviour of low lead and lead free ferroelectric ceramics of the $Na_{0.5}Bi_{0.5}TiO_3$–$PbTiO_3$ and $Na_{0.5}Bi_{0.5}TiO_3$–$K_{0.5}Bi_{0.5}TiO_3$systems. Journal of the European Ceramic Society, 21 (2001) 1333.

[62] B. J. Chu, D. R. Chen, G. R. Li and Q. R. Yin. Electrical properties of $Na_{1/2}Bi_{1/2}TiO_3$–$BaTiO_3$ ceramics. Journal of the European Ceramic Society, 22 (2002) 2115.

[63] Y. Dai and X. Zhang. Phase transition behavior and electrical properties of lead-free $(1-x)(0.98K_{0.5}Na_{0.5}NbO_3-0.02LiTaO_3)-x(0.96Bi_{0.5}Na_{0.5}TiO_3-0.04BaTiO_3)$ piezoelectric ceramics. Journal of the European Ceramic Society, 28 (2008) 3193.

[64] P. Fu, Z. Xu, R. Chu, W. Li, G. Zang and J. Hao, Piezoelectric, ferroelectric and dielectric properties of La_2O_3-doped $(Bi_{0.5}Na_{0.5})_{0.94}Ba_{0.06}TiO_3$ lead-free ceramics. Materials and Design, 31 (2010) 796.

[65] H. Liu, W. Ge, X. Jiang, X. Zhao and H. Luo, Growth and characterization of Mn-doped $Na_{1/2}Bi_{1/2}TiO_3$ lead-free ferroelectric single crystal. Materials Letters, 62 (2008) 2721.

[66] P. Setasuwon and S. Kijamnajsuk, Synthesis of $Na_{0.5}Bi_{0.5}TiO_3$ anisotropic particles with grain orientation by conversion of $Na_{0.5}Bi_{4.5}Ti_4O_{15}$ crystals. Science and Technology of Advanced Materials, 7 (2006) 780.

[67] D. Q. Xiao, D. M. Lin, J. G. Zhu and P. Yu, Studies on new systems of BNT-based lead-free piezoelectric ceramics. Journal of Electroceramic, 21 (2008) 34.

[68] Y. W. Liao, D. Q. Xiao, Y. P. Zhao and Y. L. Deng, Dielectric characteristics and phase structure of lead-free $Bi_{0.5}(Na_{1-x-y}K_xAg_y)_{0.5}TiO_3$ piezoelectric ceramics. Materials Chemistry and Physics, 107 (2008) 413.

[69] Q. Xu, S. Chen, W. Chen, Duanping Huang, Jing Zhou, Huajun Sun and Yueming Li, Synthesis of $(Na_{0.5}Bi_{0.5})TiO_3$ and $(Na_{0.5}Bi_{0.5})_{0.92}Ba_{0.08}TiO_3$ powders by a citrate method. Journal of Material Science, 41 (2006) 6146.

[70] C. R. Zhou and X. Y. Liu, Dielectric properties and relaxation of $Bi_{0.5}Na_{0.5}TiO_3-BaNb_2O_6$ lead-free ceramics. Bulletin of Material Science, 30 (2007) 575.

[71] Q. Xua, X. Chena, W. Chena, S. Chena, B. Kimb and J. Lee, Synthesis, ferroelectric and piezoelectric properties of some $(Na_{0.5}Bi_{0.5})TiO_3$ system compositions. Materials Letters, 59 (2005) 2437.

[72] Z. C. Rong, L. X. Yu, L. W. Zhou and Y. C. Lai. Effect of substitution of titanium by magnesium and niobium on structure and piezoelectric properties in $(Bi_{1/2}Na_{1/2})TiO_3$ceramics. Bulletin of Material Science, 32 (2009) 99.

[73] Lily, K Kumari, K Prasada and R. N. P. Choudhary. Impedance analysis of $(Na_{0.5}Bi_{0.5})(Zr_{0.25}Ti_{0.75})O_3$ ceramic. Indian Journal of Engineering & Materials Sciences, 15 (2008) 147.

[74] Y. M. Li, R. H. Liao, X. P. Jiang and Y. P. Zhang, Impedance spectroscopy and dielectric properties of $Na_{0.5}Bi_{0.5}TiO_3–K_{0.5}Bi_{0.5}TiO_3$ ceramics. Journal of Alloys and Compounds, 484 (2009) 961.

[75] Y. Li, W. Chen, Q. Xu and J. Zhou, Relaxor behavior and ferroelectric properties of $Na_{0.5}Bi_{0.5}TiO_3$-$K_{0.5}Bi_{0.5}TiO_3$-$KNbO_3$ lead-free ceramics. Journal of Materials Science, 40 (2005) 3625.

[76] Y. Li, W. Chenb, Q. Xub, J. Zhoub, X. Gua and S. Fanga. Electromechanical and dielectric properties of $Na_{0.5}Bi_{0.5}TiO_3–K_{0.5}Bi_{0.5}TiO_3–BaTiO_3$ lead-free ceramics. Materials Chemistry and Physics, 94 (2005) 328.

[77] K. Prasad, K. Kumari, Lily, K. P. Chandra, K. L. Yadav, and S. Sen, Glass-like response of $(Na_{1/2}Bi_{1/2})TiO_3–WO_3$ ceramic. Solid State Communications, 144 (2007) 42.

[78] M. Raghavender, G. S. Kumar and G. Prasad, A-site substitution-controlled dielectric dispersion in lead-free sodium bismuth titanate. Pramana-Journal of Physics, 72 (2009) 999.

[79] M. Raghavender, G. S. Kumar and G. Prasad, Modification of dielectric relaxations in sodium bismuth titanate with samarium doping. Journal of Physics and Chemistry of Solids, 67 (2006) 1803.

[80] J. Suchanicz, Peculiarities of phase transitions in $Na_{0.5}Bi_{0.5}TiO_3$. Ferroelectric, 190 (1997) 77.

[81] H. Y. Tian, D. Y. Wang, D. M. Lin, J. T. Zeng, K. W. Kwok and H. L. W. Chan. Diffusion phase transition and dielectric characteristics of $Bi_{0.5}Na_{0.5}TiO_3$–$Ba(Hf,Ti)O_3$ lead-free ceramics. Solid State Communications, 142 (2007) 10.

[82] S. Zhao, G. Li, A. Ding, T. Wang and Q. Yin. Ferroelectric and piezoelectric properties of $(Na, K)_{0.5}Bi_{0.5}TiO_3$ lead free ceramics. Journal of Physics D: Applied Physics, 39 (2006) 2277.

[83] T. Yu, K. W. Kwok and H. L. W. Chan. Preparation and properties of sol-gel-derived $Bi_{0.5}Na_{0.5}TiO_3$ lead-free ferroelectric thin film. Thin Solid Films, 515 (2007) 3563.

[84] J. Suchanicz. A. Jezowski, R. Poprawski and S. Dacko, Thermal and dielectric behavior of pure and doped $Na_{0.5}Bi_{0.5}TiO_3$ at low temperature. Physica Status Solid (b), 221 (2000) 789.

[85] H. Nagata and T. Takenaka, Additive effect on electrical properties of $(Na_{1/2}Bi_{1/2})TiO_3$ ferroelectric ceramics. Journal of the European Ceramic Society, 21 (2001) 1299.

[86] C. R. Zhou, X. Y. Liu, W. Z. Li and C. L. Yuan, Dielectric relaxor behavior of A-site complex ferroelectrics of $Bi_{0.5}Na_{0.5}TiO_3$–$Bi_{0.5}K_{0.5}TiO_3$–$BiFeO_3$. Solid State Communications, 149 (2009) 481.

[87] P. A. Thomas , S. Trujillo, M. Boudard, S. Gorfman and J. Kreisel, Diffuse X-ray scattering in the lead-free piezoelectric crystals $(Bi_{1/2}Na_{1/2})TiO_3$ and Ba-doped $(Bi_{1/2}Na_{1/2})TiO_3$. Solid State Sciences, 12 (2010) 311.

[88] A. Watcharapasorn and S. Jiansirisomboon, Grain growth kinetics in Dy-doped $Na_{0.5}Bi_{0.5}TiO_3$ ceramics. Ceramics International, 34 (2008) 769.

[89] C. R. Zhou and X. Y. Liu, Effect of B-site substitution by $(Ni_{1/3}Nb_{2/3})^{4+}$ for Ti^{4+}on microstructure and piezoelectric properties in $(Bi_{1/2}Na_{1/2})TiO_3$ piezoelectric ceramics. Journal of Alloys and Compounds, 466 (2008) 563.

[90] C. Zhou and X. Liu, Effect of B-site substitution of complex ions on dielectric and piezoelectric properties in $(Bi_{1/2}Na_{1/2})TiO_3$ piezoelectric ceramics. Materials Chemistry and Physics, 108 (2008) 413.

[91] Y. Lin, S. Zhao, N. Cai, J. Wu, X. Zhou and C. W. Nan, Effects of doping Eu_2O_3 on the phase transformation and piezoelectric properties of $Na_{0.5}Bi_{0.5}TiO_3$ -based ceramics. Materials Science and Engineering B, 99 (2003) 449.

[92] B. H. Kim, S. J. Han, J. H. Kim, J. H. Lee B. K. Ahn and Q. Xu, Electrical properties of (1-x)$(Bi_{0.5}Na_{0.5})TiO_3$–$xBaTiO_3$ synthesized by emulsion method. Ceramics International, 33 (2007) 447.

[93] A. Watcharapasorn, S. Jiansirisomboon and T. Tunkasiri, Sintering of Fe-doped $Bi_{0.5}Na_{0.5}TiO_3$ at <1000 °C. Materials Letters, 61 (2007) 2986.

[94] X. Y. Wang, C. L. Wang, M. L. Zhao, J. F. Wang, K. Yang and J. C. Li, Ferroelectric properties of lithium-doped $(Bi_{0.95}Na_{0.75}K_{0.20})_{0.5}Ba_{0.05}TiO_3$ ceramics. Materials Letters, 61 (2007) 3847.

[95] Q. Xu, S. Chen, W. Chen, S. Wu, J. Lee, J. Zhou, H. Sun and Y. Li, Structure, piezoelectric properties and ferroelectric properties of $(Na_{0.5}Bi_{0.5})_{1-x}Ba_xTiO_3$ system. Journal of Alloys and Compounds, 381 (2004) 221.

[96] S. Mahboob, G. G. Prasad and S. Kumar, Impedance spectroscopy and conductivity studies on B site modified $(Na_{0.5}Bi_{0.5})(Nd_xTi_{1-2x}Nb_x)O_3$ ceramics. Journal of Material Science, 42 (2007) 10275.

[97] Y. M Li, R. H. Liao, X. P. Jiang and Y. P. Zhang, Impedance spectroscopy and dielectric properties of $Na_{0.5}Bi_{0.5}TiO_3$–$K_{0.5}Bi_{0.5}TiO_3$ ceramics. Journal of Alloys and Compounds, 484 (2009) 961.

[98] Y. Qu, D. Shan and J. Song, Effect of A-site substitution on crystal component and dielectric properties in $Bi_{0.5}Na_{0.5}TiO_3$ ceramics. Materials Science and Engineering B, 121 (2005) 148.

[99] C. Peng, J. F. Li and W. Gong, Preparation and properties of $(Bi_{1/2}Na_{1/2})TiO_3$–$Ba(Ti,Zr)O_3$ lead-free piezoelectric ceramics. Materials Letters, 59 (2005) 1576.

[100] Y. Wu, H. Zhang, Y. Zhang, J. Ma and D. Xie, Lead-free piezoelectric ceramics with composition of $(0.97-x)Na_{1/2}Bi_{1/2}TiO_3$-$0.03NaNbO_3$-$xBaTiO_3$. Journal of Materials Science, 38 (2003) 987.

[101] Z. Chen and J. Hu, Piezoelectric and dielectric properties of $(Bi_{0.5}Na_{0.5})_{0.94}Ba_{0.06}TiO_3$–$Ba(Zr_{0.04}Ti_{0.96})O_3$ lead-free piezoelectric ceramics. Ceramics International, 35 (2009) 111.

[102] Y. Li, W. Chen, Q. Xu, J. Zhou, Y. Wang and H. Sun, Piezoelectric and dielectric properties of CeO_2–doped $Bi_{0.5}Na_{0.44}K_{0.06}TiO_3$ lead-free ceramics. Ceramics International, 33 (2007) 95.

[103] X. Y. Zhou, H. S. Gu, T. Y. Wang, W. Y. Li and T. S. Zhou. Piezoelectric properties of Mn doped $(Na_{0.5}Bi_{0.5})_{0.92}Ba_{0.08}TiO_3$ ceramics. Materials Letters, 59 (2005) 1649.

[104] Y. Wang, G. Xu, X. Ji, Z. Ren, W. Weng, P. Du, G. Shen and G. Han. Room-temperature ferromagnetism of Co-doped $Na_{0.5}Bi_{0.5}TiO_3$: Diluted magnetic ferroelectrics. Journal of Alloys and Compounds, 475 (2009) 25.

[105] X. X. Wang, K. W. Kwok, X. G. Tang, H. L. W. Chan and C. L. Choy, Electromechanical properties and dielectric behavior of $(Bi_{1/2}Na_{1/2})_{(121.5x)}Bi_xTiO_3$ lead-free piezoelectric ceramics. Solid State Communications, 129 (2004) 319.

[106] Z. Yang, Y. Hou, B. Liu and L. Wei, Structure and electrical properties of Nd_2O_3–doped$0.82Bi_{0.5}Na_{0.5}TiO_3$–$0.18Bi_{0.5}K_{0.5}TiO_3$ ceramics. Ceramics International, 35 (2009) 1423.

[107] C. Zhou, X. Liu, W. Li and C. Yuan. Structure and piezoelectric properties of $Bi_{0.5}Na_{0.5}TiO_3$–$Bi_{0.5}K_{0.5}TiO_3$–$BiFeO_3$ lead-free piezoelectric ceramics. Materials Chemistry and Physics, 114 (2009) 832.

[108] J. Shieh, K. C. Wu and C. S. Chen, Switching characteristics of MPB compositions of $Bi_{0.5}Na_{0.5}TiO_3$–$BaTiO_3$–$(Bi_{0.5}K_{0.5})TiO_3$ lead-free ferroelectric ceramics. Acta Materialia, 55 (2007) 3081.

[109] X. Wang, H. L. W. Chan and C. l. Choy, Piezoelectric and dielectric properties of CeO_2–added $(Bi_{0.5}Na_{0.5})_{0.94}Ba_{0.06}TiO_3$ lead-free ceramics. Solid State Communications, 125 (2003) 395.

[110] R. Selvamani, G. Singh, V. Sathe, V. S. Tiwari and P. K. Gupta. Dielectric, structural and Raman studies on $(Na_{0.5}Bi_{0.5}TiO_3)_{(1-x)}(BiCrO_3)_x$ ceramic. Journal of Physics: Condensed Matter, 23 (2011) 055901.

[111] M. V. Ramana, S. R. Kiran, N. R. Reddy, K. V. S. Kumar, V. R. K. Murthy, B. S. Murty, Synthesis of lead free sodium bismuth titanate (NBT) ceramic by conventional and microwave sintering methods. Journal of Advanced Dielectrics (JAD) New, 1 (2011) 71.

[112] M. Davies, E. Aksel and J. L. Jones, Enhanced high-temperature piezoelectric coefficients and thermal stability of Fe- and Mn-substituted $Na_{0.5}Bi_{0.5}TiO_3$ ceramics. Journal of American Ceramic Society, 94 (2011) 1314.

[113] D. Rout, K. S. Moon, S. J. L. Kang and I. W. Kim, Dielectric and Raman scattering studies of phase transitions in the $(100-x)Na_{0.5}Bi_{0.5}TiO_3–xSrTiO_3$ system. Journal of Applied Physics, 108 (2010) 084102.

Chapter 2

EXPERIMENTAL TECHNIQUE

2.1 Introduction

The requirement of polycrystalline ceramic materials now-a-days has been increased for various industrial applications. Modern ceramics have huge applications in electronics, aerospace, automotive, medical, etc. The synthesis of materials plays the vital role in tailoring the physical properties of material. Ceramic powder synthesis as a field of materials processing is undergoing rapid expansion. One of the challenges faced by materials scientists today is the synthesis of materials with desired composition, structure, and properties for specific applications. There are developments of new techniques to get high quality materials with affordable cost and minimum required time. The synthesis of materials requires knowledge of crystal chemistry, thermodynamics, phase equilibrium, and reaction kinetics [1]. There is an interrelationship between the structures, properties with the processing of ceramic [2]. The ceramic processing is a sequence of operations that systematically changes

the chemical composition and physical aspects of the structure which ultimately affect the physical properties of the material. The aim of the science behind ceramic processing is to identify the important properties and to understand the effect of processing parameters on the structural and physical properties of the materials. A general problem in the synthesis of ceramic powders is the agglomeration because of Van der Waals forces, voids, and formation of secondary phases in final product. Ferroelectric ceramic materials can be synthesized in two forms i.e., single crystal and powder form. Single crystals are relatively difficult to prepare and need utmost care for device applications [3]. However ceramic powders are easier to synthesize and it has interesting microstructure phenomena like grain, grain boundary, porosity etc. Further, the polycrystalline powder is thermally, chemically and mechanically more stable than single crystal. In many cases ferroelectric properties shown by powder ceramic are comparable to single crystal ceramic.

This chapter describes the various steps of the synthesis technique and different methods of characterizations of the studied materials.

2.2 Various types of synthesis technique

Ceramic powder synthesis is the most important technology in chemical engineering and the ceramics related areas of materials science. The basic idea is that synthesis technique should give uniformity in the microstructure of a single phase ceramic for better properties. Numerous techniques are available in the literature for the synthesis of ceramic samples. Selection of the synthesis route is crucial to control the composition, structure, and morphology of a chosen material. There are

mainly two approaches for synthesis of ceramic powder. One is the chemical method and the other one is the mechanical method. Mechanical methods are (a) mixed oxide process or solid state reaction process and (b) high energy ball milling (ball mill, planetary ball mill, rotator ball mill, etc.). The chemical methods of synthesis of ceramic powders are sol-gel methods, co-precipitation method, hydrothermal method, combustion method, molten salts, liquid-phase and gas-phase reactions, polymer pyrolysis, pechini method, citrate gel methods, aerosols and emulsions etc. [4]. The chemical method gives a better product as compared to the mechanical method by the absence of secondary phase, chemically and structurally homogeneous, morphologically identical sample. But the disadvantages of chemical method are it is time consuming, reaction procedures are complex and requirement of costly ingredients. The initial product obtained from chemical method is also calcined at temperatures 500 ^{0}C to 1000 ^{0}C depending on the material which is same as in solid state reaction route. The chemical precursors taken in chemical method are hydrophobic, unstable at room temperature, hence reacts with other materials. The disadvantage of solid state reaction assists synthesized powders has imperfect surface structure, non-uniform strain and coarse particle size due to prolonged heating at high temperature [5]. Still the solid state reaction route method is well appreciated for a large-scale production of bulk ceramic powders. It requires low cost precursors which are readily available and needs easier preparation technique.

2.3 Solid state reaction route

The solid state reaction route is the most convenient and widely used method for the preparation of polycrystalline solids from a mixture of solid oxide and carbonates as precursors. Heat is required for solid precursors to proceed for reaction, as generally solids do not participate in reaction at room temperature. The thermodynamic free energy determines the feasibility of the reaction of precursors. The rate of reaction depends upon reaction conditions, structural properties of the reactants, surface area of the solids and their reactivity [6]. In solid state synthesis the reactants are heated for a variety of reasons. The precursors have to be thermally decomposed to produce the required fragments for direct combination. In addition, the higher temperature allows some movement or flow of atoms through the solid at a sufficient rate so that the desired product can eventually be obtained. This process is enhanced if one of the components melts, thus overcomes the 'solid state diffusion barrier'[7]. This barrier arises because the reactions can only occur between neighboring atoms. In a solid, the atoms have to migrate through the rigid solid lattice. This process is slow unless the temperature is raised significantly to allow rapid migration. A number of procedures are used to reduce the time needed for synthesis. The starting materials are often intimately grinded together, thus ensuring good mixing and hence increasing contact between the reacting grains.

2.3.1 Reagents

Reagents are the raw materials for the reaction from which the required solid crystalline compound will form as product. The nature of raw material has a major

effect on the properties of the final ceramic material. The quality of raw materials depends upon the purity percentage and particle size. The reagents are selected on the basis of reaction conditions and the nature of the product. The reactants are dried thoroughly before weighing, to remove the moisture. The surface area of reagents influences the reaction rate for which fine grained materials should be used. If the raw materials contain some impurities, it will affect the physical properties of the final product material [8].

2.3.2 Weighing and mixing

The reactants have been taken in a stoichiometric ratio for a desired compound to form. Let 'M' be the molecular weight of the desired ceramic and 'm' be the amount of prepared material. 'M_a' is the molecular weight of the a^{th} metallic oxide/carbonate used in the synthesis of the ceramic and 'z' is the fraction of "a" metallic ion in the ceramic. Then weight required for a^{th} metallic oxide/carbonate is given by

$$m_a = \frac{M_a m z}{M} \qquad (2.1)$$

These precursors are manually mixed in an agate mortar and pestle. Some organic volatile liquid (preferably acetone or alcohol) is added to the mixture and grinded till it dry. The liquid is used for a homogenous mixture of precursors to avoid formation of secondary phase. If the reactant quantities are much larger than ~20g, mechanical mixing is usually done using a ball mill and the process may take several hours.

2.3.3 Calcination

The heating of the mixture depends on the form and reactivity of the reactants. Calcination is used to achieve the desired crystal phase and particle size. For the heating of material a chemically inert and high melting point container is used, generally noble metals (platinum, gold). The calcination process is an endothermic decomposition reaction which gives oxide as a solid product and liberates gases [9].

2.3.4 Sintering

Sintering is the removal of pores between the calcined particles by the shrinkage of the powder as well as the growth of particle and formation of the strong bond between adjacent particles. The powder is mixed with a binder and then compacted into a pellet form using a hydraulic press. The binder will burn out at the time of sintering. The sintering transforms the pallet to a strong, dense ceramic body with closely packed grains and randomly distributed crystallographic orientation. The reduction of excess energy associated with the surface is the driving force of the sintering process [10]. The solid/vapor interface becomes solid/solid interface which gives rise to the grain boundary area and the grain growth mechanism gives densification to the sample. The sintering temperature is always higher than calcination temperature.

2.3.5 Electroding

The sample surfaces were polished for smoothness and then silver paint or any conducting paint is used as an electrode. The material is now in between two

electrodes like dielectric material in between parallel plate capacitor. The electroding material should adhere the sample surface perfectly. The electrode should have zero electrical resistance. The conducting paint should be in thin layer form. The electrodes also can be made by a deposition method using sputtering. Also conventional photolithography and chemical etching techniques were employed to make the desired electrode.

2.4 Experimental Details

The materials were synthesized by a conventional solid-state reaction route. The high purity carbonate (Na_2CO_3) and oxides (Bi_2O_3, TiO_2, La_2O_3, ZrO_2, Y_2O_3) (LOBA Chemie Private Limited, Mumbai, India) of required precursors were weighed according to the particular stoichiometric ratios. The above weighed powder was mixed by agate mortar and pestle for 2 hours. Then again mixed in acetone (CH_3COCH_3) (Merck Specialities Private Limited, Mumbai, India.) medium till it dry for homogeneous mixture. The dried mixture was put in alumina crucible and calcined at temperature 950 ^{0}C for 4 hours in air circulate furnace. The above heated powder formed into a lump and it was grinded till it became fine powder. Again it was calcined at temperature 1000 ^{0}C for 4 hours for complete reaction. The calcined powder was grinded for fine powder and phase formation was checked by XRD at room temperature. The above calcined powder was mixed with 7% PVA (polyvinyl alcohol) as a binder in mortar and pestle. The binder mixed powder was compacted to form pallet by a hydraulic press at 6 x 10^7 kg/m^2 pressure using die set. The sintering of the pellet sample was carried out at an optimized temperature of 1080 ^{0}C

for 4 hours for densification. The sintered pallets were polished by emery paper and painted with silver paste as an electrode for electrical measurement. The painted samples were kept in the oven for 10 hours to evaporate the moisture in the sample. The flow chart of synthesis procedure is given below.

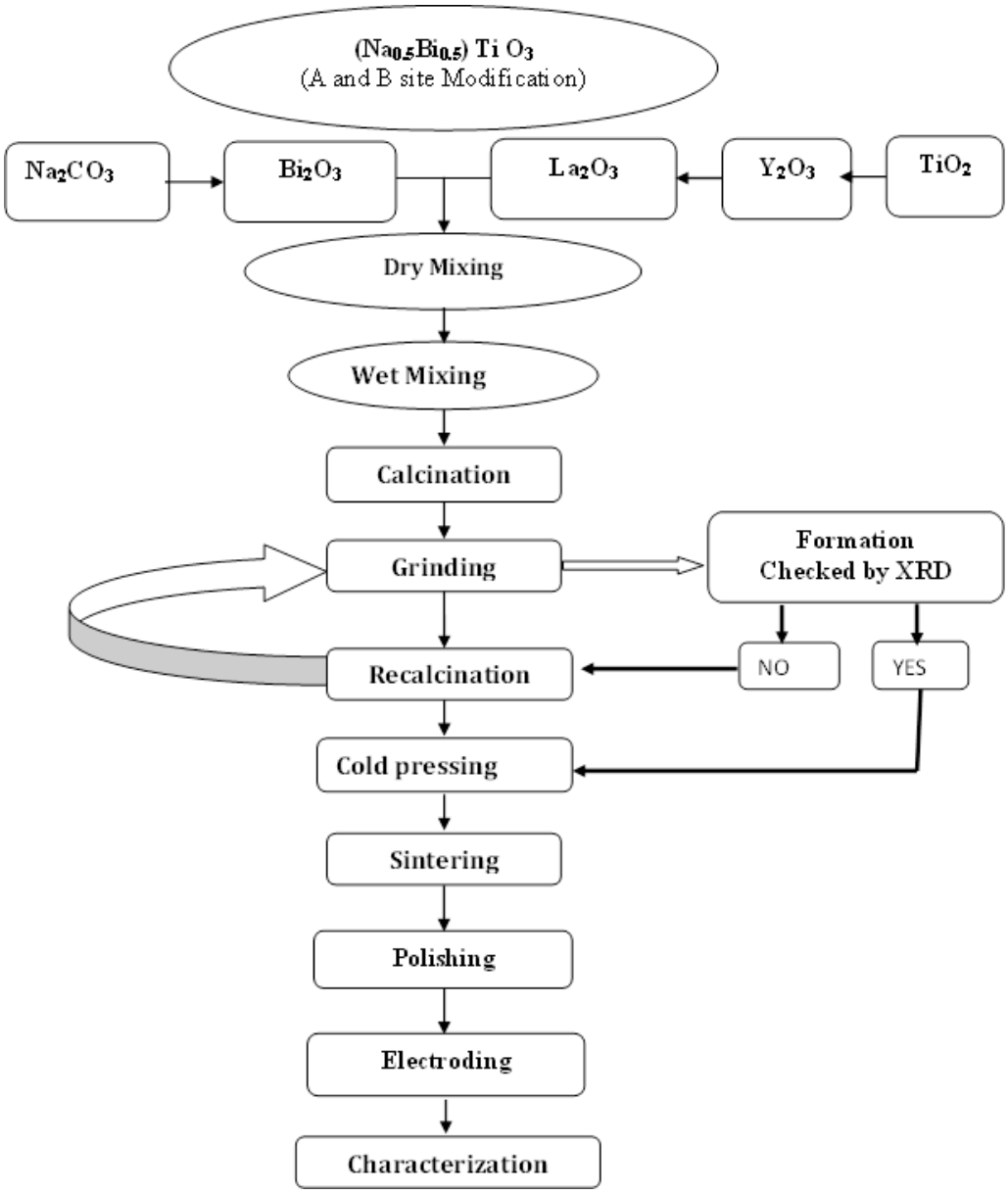

Fig. 2.1 Flow chart for the preparation of ceramic samples by a solid-state reaction technique.

Table 2.1 Abbreviated names, tolerance factor, diameter and thickness of synthesized sample.

Compound	Abbreviated name	Tolerance factor (t)	Diameter in cm	Thickness in cm
$(Na_{0.5}Bi_{0.5})TiO_3$	NBT	0.8568	0.945	0.147
$(Na_{0.5}Bi_{0.5})_{(1-0.02)}La_{0.02}Ti_{(1-0.02/4)}O_3$	NBLT02	0.8573	0.894	0.141
$(Na_{0.5}Bi_{0.5})_{(1-0.04)}La_{0.04}Ti_{(1-0.04/4)}O_3$	NBLT04	0.8578	0.883	0.175
$(Na_{0.5}Bi_{0.5})_{(1-0.06)}La_{0.06}Ti_{(1-0.06/4)}O_3$	NBLT06	0.8583	0.892	0.154
$(Na_{0.5}Bi_{0.5})_{(1-0.08)}La_{0.08}Ti_{(1-0.08/4)}O_3$	NBLT08	0.8587	0.9	0.088
$(Na_{0.5}Bi_{0.5})Ti_{(1-0.05)}Zr_{0.05}O_3$	NBTZ05	0.8545	0.971	0.193
$(Na_{0.5}Bi_{0.5})Ti_{(1-0.1)}Zr_{0.1}O_3$	NBTZ1	0.8520	0.957	0.105
$(Na_{0.5}Bi_{0.5})Ti_{(1-0.2)}Zr_{0.2}O_3$	NBTZ2	0.8474	0.951	0.127
$(Na_{0.5}Bi_{0.5})Ti_{(1-0.3)}Zr_{0.3}O_3$	NBTZ3	0.8427	0.922	0.150
$(Na_{0.5}Bi_{0.5})_{(1-0.02)}Y_{0.02}Ti_{(1-0.02/4)}O_3$	NBYT02	0.8431	0.89	0.113
$(Na_{0.5}Bi_{0.5})_{(1-0.04)}Y_{0.04}Ti_{(1-0.04/4)}O_3$	NBYT04	0.8295	0.89	0.103
$(Na_{0.5}Bi_{0.5})_{(1-0.06)}Y_{0.06}Ti_{(1-0.06/4)}O_3$	NBYT06	0.8160	0.887	0.112
$(Na_{0.5}Bi_{0.5})_{(1-0.08)}Y_{0.08}Ti_{(1-0.08/4)}O_3$	NBYT08	0.8028	0.91	0.141

2.5 Characterization Techniques

The above synthesized materials are characterized by various experimental techniques at different measurement conditions to study its physical properties. The basic fundamental principle and use of XRD, FTIR, SEM, along with preliminary ideas about impedance spectroscopy, dielectric study and conductivity study are described below.

2.5.1 X-ray diffraction

X-ray diffraction (XRD) characterization technique is a powerful tool for detailed structural study of the material. It gives information about atomic arrangements of materials, determination of the crystal structure, the identification of the chemical species present in materials which are the origin of physical properties of materials. As the wavelength (λ) of X-ray comparable to the interplaner placing (d) of crystals, diffraction occurs at particular angle (θ). The diffraction satisfies the Bragg equation,

$$2d\sin\theta = n\lambda \qquad (2.2)$$

Where n is the order of diffraction. The intensity of the diffracted beams depends on the arrangements and atomic number of the atoms in the unit cell. Unit cells describe the symmetry of all structures.

Atoms are not point like objects in a mathematical sense rather its radius is of the order of X-ray wavelengths and the electrons are distributed over the entire atomic volume. Hence there will be phase differences occur between scattered waves which decrease the intensity of the scattered wave with increase in scattering angle.

This decrease is described by the atomic form factor f_j. The structure factor can be expressed as the Fourier sum of f_j over all atoms j in a unit cell, with the phase (Ø) of the reflection.

$$F_{hkl} = \sum_{j=i}^{N} f_j \exp\left[2\pi i\left(hx_j + ky_j + lz_j\right)\right] = |F|\exp(i\emptyset) \quad (2.3)$$

The intensity of a diffraction peak is proportional to the squared value of the structure factor

$$I \approx |F_{hkl}|^2 = \left(\sum_{j=i}^{N} f_j \exp\left[2\pi i\left(hx_j + ky_j + lz_j\right)\right]\right)^2 \quad (2.4)$$

The calculation of lattice constants from the line positions or d spacing can be found from a general formula

$$\frac{1}{d_{hkl}^2} = V^2[h^2b^2c^2\sin^2\alpha + k^2c^2a^2\sin^2\beta + l^2a^2b^2\sin^2\gamma] \quad (2.5)$$

where, V = volume of the unit cell

$$= abc(1 - \cos^2\alpha - \cos^2\beta - \cos^2\gamma + \cos\alpha\cos\beta\cos\gamma)^{1/2} \quad (2.6)$$

where, a, b, c, α, β and γ are lattice parameters and h, k, l are the miller indices. The above formula is used to calculate lattice parameters for all the compositions [11].

2.5.2 FTIR

Infrared vibrational spectroscopy is a most common technique for structural elucidation and compound identification. Molecules naturally vibrate (stretch, contract, bend etc.) at particular frequencies which is characteristic of the constituent bonds. The vibrational frequencies of most molecules correspond to the frequencies of infrared light. When an infrared light interacts with the matter, the chemical functional group tends to adsorb infrared radiation corresponding to the natural

frequency of vibration of bond or group regardless of the structure of the rest of the molecule. Infrared light and a molecule only interact when the dipole moment of the molecule changes due to vibration of molecules. Strength of absorption of infrared light depends on the size of deformation of the dipole moment due to vibration. The IR spectra are like finger print of a molecule i.e., no two unique molecular structures produce the same infrared spectrum [12]. Typically, this technique is used to study compounds using light radiation of 4000-400 cm^{-1} (mid-infrared).

The usefulness of infrared spectroscopy for several types of analysis is [13]

- It can identify unknown materials.
- It can determine the quality or consistency of a sample.
- It can determine the amount of components in a mixture.

2.5.3 SEM

The scanning electron microscope (SEM) uses a focused beam of high energy electrons. The kinetic energy of the accelerated electrons in the focused beam is dissipated by the electron-sample interactions when the incident electrons are decelerated in the solid sample and produced a variety of signals [14]. These signals are secondary electrons (that produce SEM images), backscattered electrons (BSE), diffracted backscattered electrons (EBSD that are used to determine crystal structures and orientations of minerals), photons (characteristic X-rays that are used for elemental analysis and continuum X-rays), visible light (cathodoluminescence CL), and heat. Secondary electrons and backscattered electrons are commonly used for imaging samples. Secondary electrons are most valuable for showing morphology and

topography on samples and backscattered electrons are most valuable for illustrating contrasts in composition in multiphase samples. The SEM is also capable of performing semi-quantitative chemical composition analysis by energy dispersive X-ray spectroscopy (EDXS) and wavelength dispersive X-ray spectroscopy (WDXS) analysis [15]. Data are collected over a selected area of the surface of the sample, and a 2-dimensional image is generated which displays spatial variations in these properties. Areas ranging from approximately 1 cm to 5 microns in width can be imaged in a scanning mode using conventional SEM techniques (magnifications ranging from 20x to approximately 30,000x with spatial resolution of 50 to 100 nm).

2.5.4 Dielectric study

The polarization in the dielectric material occurs when it is subjected to the external field and it is classified according to their origin. Types of polarizations are [16]

1. Electronic polarization
2. Atomic or ionic polarization
3. Dipolar polarization
4. Interface or space charge polarization

At optical frequency ($\sim 10^{15}$) only electronic polarization present in material. Ionic polarization arises at $\sim 10^{13}$ Hz range with electronic polarization in the material. At 10^{6} to 10^{10} Hz range contribution due to oriental polarization gets added to the ionic and electronic polarization, while space charge polarization contributes only below the 10^{2} Hz frequency range [17]. The effect of temperature on both electronic and ionic polarizations is small. The electronic and ionic polarizations are temperature

independent but orientation polarization and space charge polarization are affected by temperature. At higher temperatures, polarization increases due to ionic and crystal imperfection mobility. The total polarization is a sum of these four polarizations.

When a dielectric is subjected to the ac voltage, the electrical energy is absorbed by the material and is dissipated in the form of heat. The dissipation is called dielectric loss. When the applied frequency is in the same range as the relaxation time, resonance occurs. So the current lead the voltage by (90-δ), where δ is called the loss angle and tanδ is the electrical loss due to resonance and called as tangent loss. Loss tangent can be expressed as:

$$\tan\delta = \frac{\epsilon_r''}{\epsilon_r'} \tag{2.7}$$

where, $\epsilon_r'$and ϵ_r'' are real and imaginary part of relative permittivity.

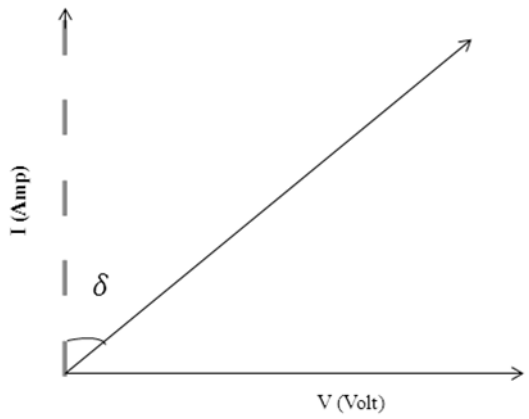

Fig. 2.2 Phase diagram between current and voltage.

The current can be resolved into two components

i. The component in phase with the applied voltage is $I_x = V\omega\epsilon''C_0$. It gives the dielectric loss.

ii. The component leading the applied voltage by 90^0 is $I_y = V\omega\epsilon'C_0$.

The dielectric constant depends strongly on the frequency of the alternating electric field and on the chemical structure, imperfection of the material, temperature and pressure.

2.5.5 Impedance spectroscopic studies

The complex impedance spectroscopic (CIS) technique is used to analyze the electrical response of a polycrystalline sample in a wide range of frequencies. Ac electrical data may be represented in any of the four basic formalisms which are interrelated to each other [18].

Complex impedance: $Z^* = Z' - jZ''$

Complex admittance: $Y^* = (Z^*)^{-1}$

Complex permittivity: $\varepsilon^* = (j\omega C_0 Z^*)^{-1} = \varepsilon' - j$

Complex electric modulus: $M^* = j\omega C_0 Z^* = M' + jM''$ (2.8)

where, (Z', M', ε') and (Z'', M'', ε'') are the real and imaginary components of impedance, modulus, and permittivity, respectively. j=-1, $\omega=2\pi f$ is the angular frequency and $C_0=\varepsilon_0 A\ell^{-1}$ in which C_0 is the vacuum capacitance of the cell without the sample, ε_0 the permittivity of free space, 8.854×10^{-14} F/cm, ℓ and A are the thickness and area of the sample.

There are several ways of presenting the data and the most common are as follows [19]:

(1) Plots of the real and imaginary components either in logarithmic or in linear coordinates against frequency.

(2) Polar plots of the imaginary component against the real component on a linear presentation. The type of relaxation can be understood by the shape of the plot such as Debye, Cole–Cole, Cole–Davidson etc., and also as a means of finding the equivalent circuit for the material.

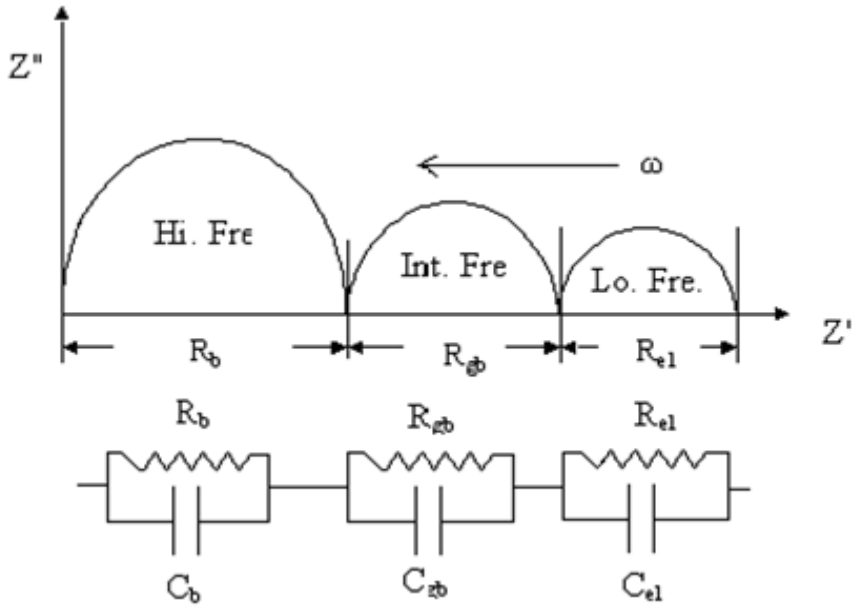

Fig.2.3 Nyquist plot and its equivalent circuit representation.

The relationship between microstructure and electrical properties can be obtained from complex impedance plot. The semi-circle at lower frequency in Fig. 2.3 is due to the contribution of electrode-material interface, another semicircular arc at

intermediate frequency is due to the contribution of grain boundary, and at high frequency the semicircular arc is due to the bulk response of the material.

The time is required for decaying the polarization of a dielectric material after the removal of the applied direct voltage and also it takes finite time for the polarization to build up to maximum value by the application of field. This phenomenon is called dielectric relaxation. There are various relaxations among them Debye and Cole-Cole relaxations are prominent in the solid ferroelectric materials.

2.5.6 Conductivity study

Many dielectrics possess conductivity due to motion of charges and such conductivity is usually expressed by volume conductivity. The motion of charges in the dielectric gives rise to the conduction current and additionally polarizes the dielectric [20]. The conductivity may therefore be contributes to the dielectric loss. The equation below gives the contribution of conductivity to the dielectric loss:

$$\sigma_{dc} = \sigma' + j\sigma'' = \omega\epsilon_0[\epsilon'' + j(\epsilon' - \epsilon_\infty)] \quad (2.9)$$

The Ac conductivity of the material having relative permittivity ϵ_r and dielectric loss tanδ at frequency ω is calculated using the equation given by

$$\sigma_{ac} = \epsilon_0\epsilon_r\omega \tan\delta \quad (2.10)$$

where, ϵ_0 is the permittivity in the vacuum.

Jonscher has suggested the conductivity as a function of frequency in a large number of materials follows a relation as

$$\sigma = \sigma_0 + A\omega^n \quad (2.11)$$

The value of "n" varies between 0 to 1. The variation in "n" is associated with displacement of carriers which move within the sample by discrete hops between randomly distributed localized sites. The term $A\omega^n$ can often be explained on the basis of two distinct mechanisms for carrier conduction:

(i) Quantum mechanical tunneling (QMT) through the barrier separating the localized sites

(ii) Correlated barrier hopping (CBH) over the same barrier.

D.C. conductivity is a thermally activated quantity and it obeys the Arrhenius behavior.

$$\sigma_{dc} = \sigma_0 \exp(-E_a/kT) \tag{2.12}$$

where, σ_0 is a preexponential factor, E_a is the activation energy, k is the Boltzmann constant, and T is the absolute temperature.

At low frequency conductivity is dominated by dc conductivity. The electrical conductivity transforms from frequency independent dc conductivity to frequency dependent ac conductivity upon increasing the frequency. The frequency at which this transition occurs is called as hopping frequency ω_p which follows the relation

$$\sigma(\omega) = k\omega_p \left[1 + \left(\frac{\omega}{\omega_p}\right)\right]^n \tag{2.13}$$

References

[1] K. C. Patil Chemistry of nanocrystalline oxide materials - Combustion Synthesis, Properties and Applications. World Scientific Publishing Co. Pte. Ltd. (2008)

[2] C. B. Carter and M. G. Norton, Ceramic materials: science and engineering. Springer, (2007).

[3] W. A. Bonner and G. J. Zydzik, Growth of single crystal lead molybdate for acousto-optic applications. Journal of Crystal Growth, 7 (1970) 65.

[4] G. Cao, Nanostructures & nanomaterials Synthesis, Properties & Applications. Imperial College Press, (2004).

[5] Y. P. Fu, Y. H. Su and C. H. Lin, Comparison of microwave-induced combustion and solid-state reaction for synthesis of $LiMn_{2-x}Cr_xO_4$ powders and their electrochemical properties. Solid State Ionics, 166 (2004) 137.

[6] Editor, P. Hagenmuller, Preparative methods in Solid State Chemistry. Academic press, (1972).

[7] I. P. Parkin, Solid state metathesis reaction for metal borides, silicides, pnictides and chalcogenides: ionic or elemental pathways. Chemical Society Reviews, 25, (1996) 199.

[8] A. R. West, Solid State Chemistry and its Applications. Wiley and Sons, (2005).

[9] J. D. Gilchrist, Extraction Metallurgy (3rd Ed.). Oxford: Pergamon Press, (1989).

[10] M. W. Barsoum, Fundamentals of Ceramic. McGraw-Hill Companies,Inc. International Edition, (1997).

[11] B. D. Cullity, S. R. Stock, Elements of X-Ray Diffraction. (3rd Edition) Prentice Hall, (2001).

[12] K. Nakamoto, Infrared and Raman spectra of inorganic and coordination compounds. Fourth edition, John Wiley and Sons, (1986).

[13] F. A. Settle, Editor, Handbook of Instrumental Techniques for Analytical Chemistry. Prentice-Hall, (1997).

[14] D. Brandon, W. D. Kaplan, Microstructural characterization of materials. 2nd Edition, John Wiley & Sons, (2008).

[15] J. Goldstein, Scanning electron microscopy and x-ray microanalysis. Kluwer Adacemic/Plenum Pulbishers, (2003).

[16] R. V. Hippe, Dielectric materials and applications. Cambridge Technology Press of MIT, (1995).

[16] K. C. Kao, Dielectric phenomena in solids with emphasis on physical concepts of electronic processes. Elsevier Academic Press, (2004).

[18] E. Barsoukov, J. R. Macdonald, Impedance spectroscopy: theory, experiment, and applications. John Wiley and Sons, (2005)

[19] A. K. Jonseher, Dielectric relaxation in solids, Chelsea Dielectric Press, (1983).

[20] G. G. Raju, Dielctrics in electic Fields. Mervel Dekker, (2003).

Chapter 3

STRUCTURAL, MICROSTRUCTURAL AND VIBRATIONAL STUDY

3.1 Introduction

The structural, microstructural and vibrational characterizations of the synthesized materials were carried out by XRD, SEM, and FTIR analysis respectively. X-ray diffraction analysis has been used to study the phase formation of the materials and preliminary idea about the crystal structure of the sample. Size and distribution of grain, porosity of the materials have been analyzed by SEM. The formation of perovskite phase has been studied from the FTIR spectra by observing the characteristic peak of BO_6 octahedra of perovskite structure.

3.2 XRD analysis

X-ray diffraction experiments were performed on a PANalytical'sX'Pert PRO diffractometer in a wide range of Bragg angle ($20 \leq 2\theta \leq 80^0$) with Cu $K_{\alpha 1}$ radiation (λ=1.5405 Å) at a continuous scan type having step size of 0.0167 degree at room temperature. All the peaks of the XRD patterns of all the compounds were indexed in cubic to orthorhombic crystal systems and different cell configuration using 2θ values and/or inter-planer spacing (d) of each peak by a computer software "POWD". The best agreement between experimental and calculated value of d (i.e. $\Sigma(d_{exp}-d_{cal})=\Delta d$=minimum) was found in the rhombohedral system with hexagonal axis. The least squares refined lattice parameters of each composition were tabulated in the respective tables.

3.2.1 $(Na_{0.5}Bi_{0.5})TiO_3$

The XRD pattern of the calcined powder of $Na_{0.5}B_{0.5}TiO_3$ at room temperature is shown in Fig. 3.1. The presence of sharp diffraction peaks in the pattern, which are different from the ingredients, suggests the formation of a new single phase compound. The peak position (on 2θ scale), full width at half maximum (FWHM) and intensity are calculated using a commercially available software PEAK FIT [1] for each peak from the XRD data. Indexing of all peaks of XRD pattern is carried out using 2θ and intensity value of each peak by a standard computer software POWD [2]. The best agreement between the observed and the calculated interplaner spacings (d) and Bragg angles was found for the rhombohedral crystal structure (space group:R3c with hexagonal axis). The least-squares refined lattice parameters are found to be

a=5.4880(43) Å, *b*=13.5384(43)Å (i.e., the standard deviations are in parenthesis) and the unit cell volume is found to be 353.116(Å)^3. The indexing of h, k, l planes are shown in Fig. 3.1.

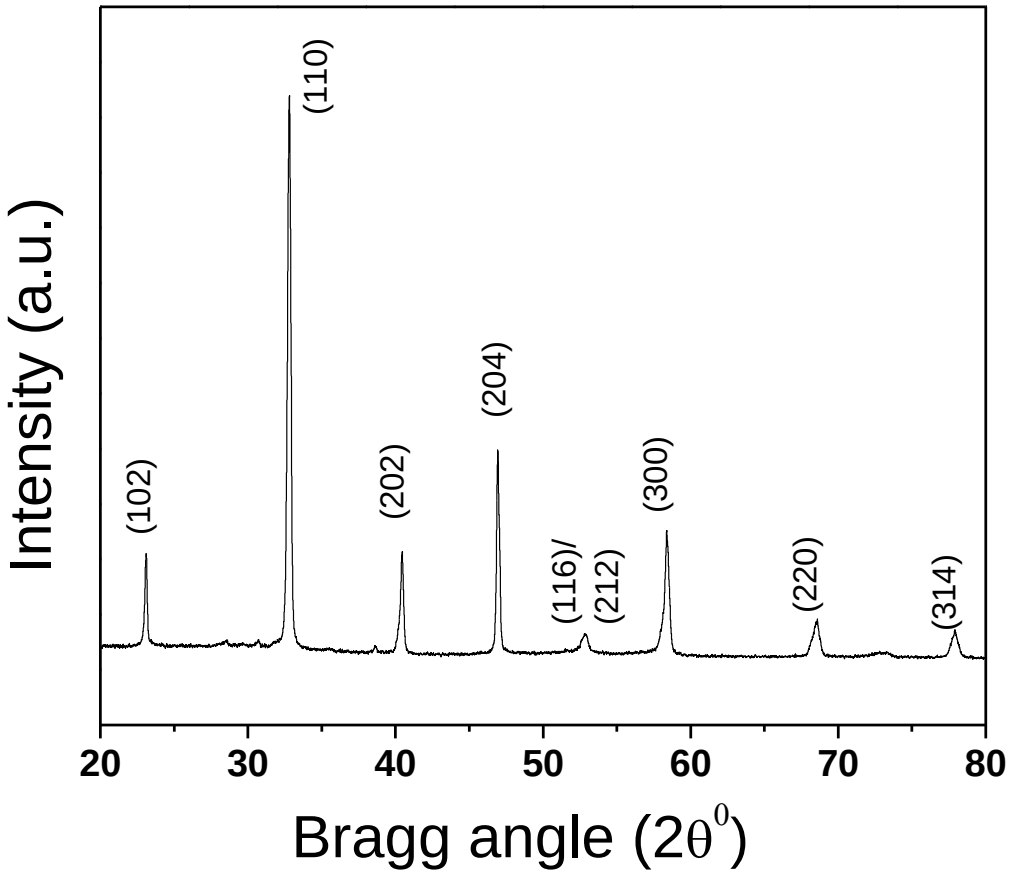

Fig. 3.1 XRD pattern of $Na_{0.5}Bi_{0.5}TiO_3$ at room temperature.

Table 3.1 Comparison of observed (d_{obs}) and calculated (d_{cal}) *d* spacing (in Å), relative intensity, miller indices of $Na_{0.5}Bi_{0.5}TiO_3$.

Peak No.	d-spacing (Å)		I/I_0	Miller Indices		
	d-observed	*d*-calculated		h	k	l
1	3.8486	3.8801	16	1	0	2
2	2.7289	2.7344	100	1	1	0
3	2.2291	2.2351	18.5	2	0	2
4	1.9340	1.9401	34.5	2	0	4
5	1.7370	1.7400	2	1	1	6
6	1.7293	1.7306	2.5	2	1	2
7	1.5791	1.5787	21.5	3	0	0
8	1.3688	1.3672	6	2	2	0
9	1.2255	1.2245	5	3	1	4

3.2.2 La modified NBT

Figure 3.2 compares XRD patterns of calcined powder of $(Na_{0.5}Bi_{0.5})_{(1-x)}La_xTi_{(1-x/4)}O_3$, (a) x=0.0, (b) x=0.02, (c) x=0.04, (d) x=0.06, (e) x=0.08 at room temperature. The XRD patterns suggest the formation of a new compound with a small amount of secondary or impurity phase, which increases with increase in La content. The star marked peak of XRD pattern is the impurity phase of the sample. The reflection of the impurity phase corresponds to $Na_{0.5}Bi_{4.5}Ti_4O_{15}$ (ICDD No 74-1318). The crystal structure of compounds is found to be rhombohedral with an expected R3c space group (hexagonal axes).

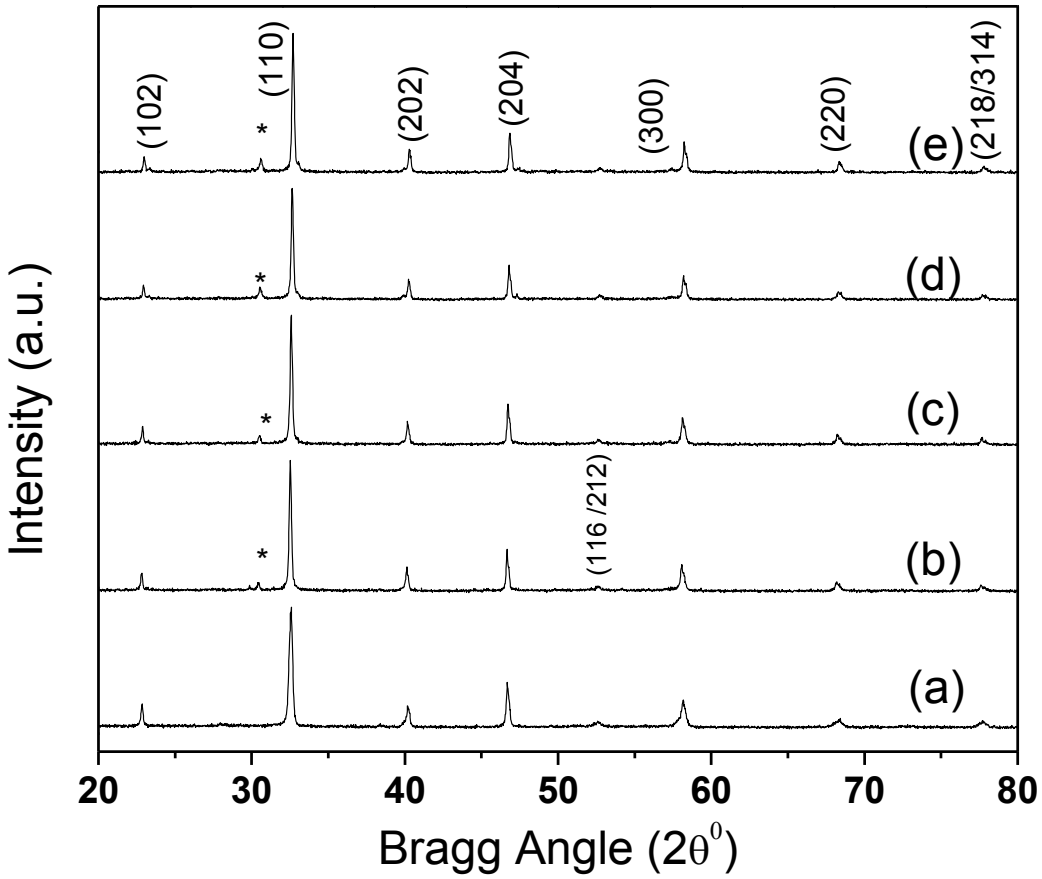

Fig. 3.2 XRD patterns of $(Na_{0.5}Bi_{0.5})_{(1-x)}La_xTi_{(1-x/4)}O_3$, (a) x=0.0, (b) x=0.02, (c) x=0.04, (d) x=0.06, (e) x=0.08 at room temperature.

Table 3.2 Comparison of observed (d_{obs}) and calculated (d_{cal}) *d* spacing (in Å), relative intensity, miller indices of $(Na_{0.5}Bi_{0.5})_{(0.98)}La_{0.02}Ti_{(1-0.02/4)}O_3$.

Peak No.	*d*-spacing		I/I_0	Miller Indices		
	d-observed	*d*-calculated		h	k	l
1	3.8852	3.8873	14.5	1	0	2
2	2.7477	2.7453	100	1	1	0
3	2.2429	2.2425	19	2	0	2
4	1.9426	1.9437	35.0	2	0	4
5	1.5855	1.5850	22.5	3	0	0
6	1.3730	1.3727	9	2	2	0
7	1.2295	1.2302	3	2	1	8
8	1.2282	1.2284	6	3	1	4

Table 3.3 Comparison of observed (d_{obs}) and calculated (d_{cal}) *d* spacing (in Å), relative intensity, miller indices of $(Na_{0.5}Bi_{0.5})_{(0.96)}La_{0.04}Ti_{(1-0.04/4)}O_3$

Peak No.	*d*-spacing		I/I_0	Miller Indices		
	d-observed	*d*-calculated		h	k	l
1	3.8986	3.891	12	1	0	2
2	2.7526	2.7556	100	1	1	0
3	2.2462	2.2441	19	2	0	2
4	1.945	1.9455	37	2	0	4
5	1.7409	1.7423	3	1	1	6
6	1.7366	1.7379	2	2	1	2
7	1.5873	1.5877	22.5	3	0	0
8	1.3742	1.3735	8	2	2	0
9	1.2293	1.2293	5	3	1	4

Table 3.4 Comparison of observed (d_{obs}) and calculated (d_{cal}) *d* spacing (in Å), relative intensity, miller indices of $(Na_{0.5}Bi_{0.5})_{(0.94)}La_{0.06}Ti_{(1-0.06/4)}O_3$.

Peak. No.	*d*-spacing		I/I_0	Miller Indices		
	d-observed	*d*-calculated		h	k	l
1	3.8685	3.8833	9	1	0	2
2	2.7378	2.7410	100	1	1	0
3	2.2371	2.394	20	2	0	2
4	1.9379	1.9416	32	2	0	4
5	1.5828	1.5825	23.5	3	0	0
6	1.3714	1.3705	9	2	2	0
7	1.2277	1.2293	3.5	2	1	8
8	1.2262	1.2267	3	3	1	4

Table 3.5 Comparison of observed (d_{obs}) and calculated (d_{cal}) d spacing (in Å), relative intensity, miller indices of $(Na_{0.5}Bi_{0.5})_{(0.92)}La_{0.08}Ti_{(1-0.08/4)}O_3$.

Peak No.	*d*-spacing		I/I_0	Miller Indices		
	d-observed	*d*-calculated		h	k	l
1	3.8768	3.8854	15	1	0	2
2	2.7419	2.7433	100	1	1	0
3	2.2392	2.2410	17	2	0	2
4	1.9399	1.9427	33	2	0	4
5	1.5840	1.5838	24	3	0	0
6	1.3721	1.3716	8	2	2	0
7	1.2279	1.2276	4.5	3	1	4

The lattice parameters and unit cell volume of the NBT decreases with increase in La concentration. The reduction in unit cell volume may be due to the reduction in distortion of *c*–axis.

Table 3.6 Comparison of lattice parameters (*a* and *c* in Å) and unit cell volume (V in $(Å)^3$), of $(Na_{0.5}Bi_{0.5})_{(1-x)}La_xTi_{(1-x/4)}O_3$. The estimated standard deviations in cell parameters are given in parenthesis.

x	***a***	***c***	**Volume(*V*)**
0.0	5.4880(43)	13.5384(43)	353.116
0.02	5.4942(30)	13.5208(30)	353.46
0.04	5.4906(20)	13.5003(20)	352.46
0.06	5.4865(30)	13.5002(30)	351.93
0.08	5.4821(50)	13.5001(50)	351.36

3.2.3Zr modified NBT

Figure 3.3 compares the room temperature XRD patterns of calcined powder of $(Na_{0.5}Bi_{0.5})Ti_{(1-x)}Zr_xO_3$, (a) x=0.0, (b) x=0.05, (c) x=0.1, (d) x=0.2, (e) x=0.3. The diffraction patterns suggest the formation of the compound with a small amount of impurity phase (star marked) at higher concentrations (20 and 30% Zr). The star marked peak corresponds to the reflections of ZrO_2 (ICDD No 80-0966). The crystal structure of compounds is found to be rhombohedral (space group:R3c) with hexagonal axis. As the Zr concentration increases the XRD peak shifted to lower 2θ

values (higher *d* spacing). This may be due to the higher ionic radius of Zr as compared to Ti.

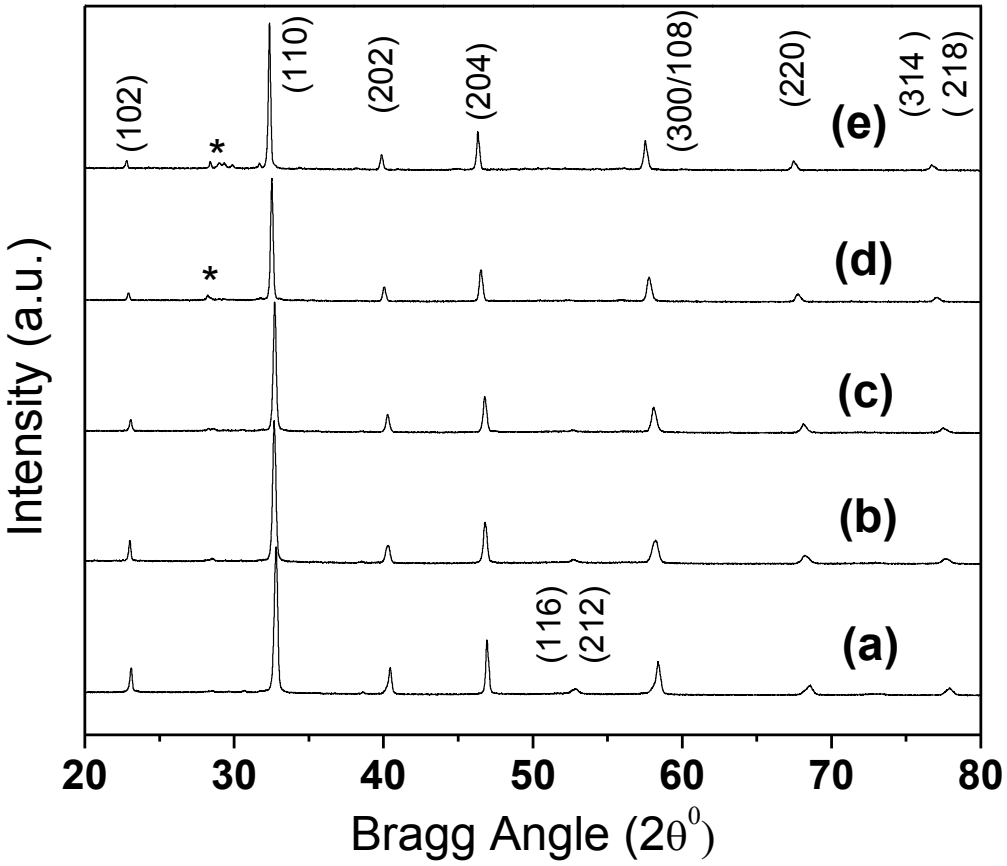

Fig. 3.3 XRD patterns of $(Na_{0.5}Bi_{0.5})Ti_{(1-x)}Zr_xO_3$, (a) x=0.0,(b) x=0.05, (c) x=0.1, (d) x=0.2, (e) x=0.3 at room temperature.

Table 3.7 Comparison of observed (d_{obs}) and calculated (d_{cal}) d spacing (in Å), relative intensity, miller indices of $(Na_{0.5}Bi_{0.5})Ti_{(1-0.05)}Zr_{0.05}O_3$.

Peak No.	*d*-spacing		I/I_0	Miller Indices		
	d-observed	*d*-calculated		h	k	l
1	3.8618	3.8859	14.5	1	0	2
2	2.7378	2.7434	100	1	1	0
3	2.2365	2.2411	13	2	0	2
4	1.9391	1.9429	29.5	2	0	4
5	1.5840	1.5839	16	3	0	0
6	1.3730	1.3717	6	2	2	0
7	1.2285	1.2277	3.5	2	1	8

Table 3.8 Comparison of observed (d_{obs}) and calculated (d_{cal}) *d* spacing (in Å), relative intensity, miller indices of $(Na_{0.5}Bi_{0.5})Ti_{(1-0.1)}Zr_{0.1}O_3$

Peak No.	*d*-spacing		I/I_0	Miller Indices		
	d-observed	*d*-calculated		h	k	l
1	3.8518	3.8822	9	1	0	2
2	2.7351	2.7390	100	1	1	0
3	2.2371	2.2381	13	2	0	2
4	1.9399	1.9412	27	2	0	4
5	1.5860	1.5838	18.5	3	0	0
6	1.3748	1.3757	6.5	2	2	0
7	1.2303	1.2294	3.5	2	1	8

Table 3.9 Comparison of observed (d_{obs}) and calculated (d_{cal}) *d* spacing (in Å), relative intensity, miller indices of $(Na_{0.5}Bi_{0.5})Ti_{(1-0.2)}Zr_{0.2}O_3$.

Peak No.	*d*-spacing		I/I_0	Miller Indices		
	d-observed	*d*-calculated		h	k	l
1	3.8768	3.8492	6	1	0	2
2	2.7509	2.7496	100	1	1	0
3	2.2494	2.2685	11.75	2	0	2
4	1.9501	1.9246	26	2	0	4
5	1.5941	1.5985	19.75	1	0	8
6	1.3817	1.3748	6.5	2	2	0
7	1.2367	1.2449	4	3	1	4

Table 3.10 Comparison of observed (d_{obs}) and calculated (d_{cal}) *d* spacing (in Å), relative intensity, miller indices of $(Na_{0.5}Bi_{0.5})Ti_{(1-0.3)}Zr_{0.3}O_3$.

Peak No.	*d*-spacing		I/I_0	Miller Indices		
	d-observed	*d*-calculated		h	k	l
1	3.8986	3.8412	5	1	0	2
2	2.7642	2.7497	100	1	1	0
3	2.2591	2.2735	10.5	2	0	2
4	1.9580	1.9206	25.25	2	0	4
5	1.6001	1.6008	19	1	0	8
6	1.3866	1.3902	6	2	2	0
7	1.2407	1.2404	3.5	3	1	4

Table 3.11 Comparison of latticeparameters (*a* and *c* in Å) andunitcellvolume(*V* in (Å)^3)of $(Na_{0.5}Bi_{0.5})Ti_{(1-x)}Zr_xO_3$.

x	*a*	*c*	Volume(V)
0.0	5.4880(43)	13.5384(43)	353.116
0.05	5.5037(16)	13.4870(16)	353.799
0.10	5.5210(50)	13.5219(50)	356.951
0.20	5.5465(56)	13.5901(56)	362.067
0.30	5.5607(34)	13.6211(34)	364.761

3.2.4 Y modified NBT

The compared XRD patterns of calcined powder of $(Na_{0.5}Bi_{0.5})_{(1-x)}Y_xTi_{(1-x/4)}O_3$, (a) x=0.0, (b) x=0.02, (c) x=0.04, (d)x=0.06, (e) x=0.08 at room temperature is shown in Fig. 3.4. The diffraction patterns suggest the formation of the compounds with small amount of impurity phase (star marked peak). The star marked peak corresponds to the reflections of $Na_{0.5}Bi_{4.5}Ti_4O_{15}$ (ICDD No 74-1319). The crystal structure is found to be rhombohedral (space group R3c) with hexagonal axis. The lattice parameter and unit cell volume decreased with the increase in the concentration of the Y atom. This may due to the smaller ionic radius of yttrium than bismuth and sodium.

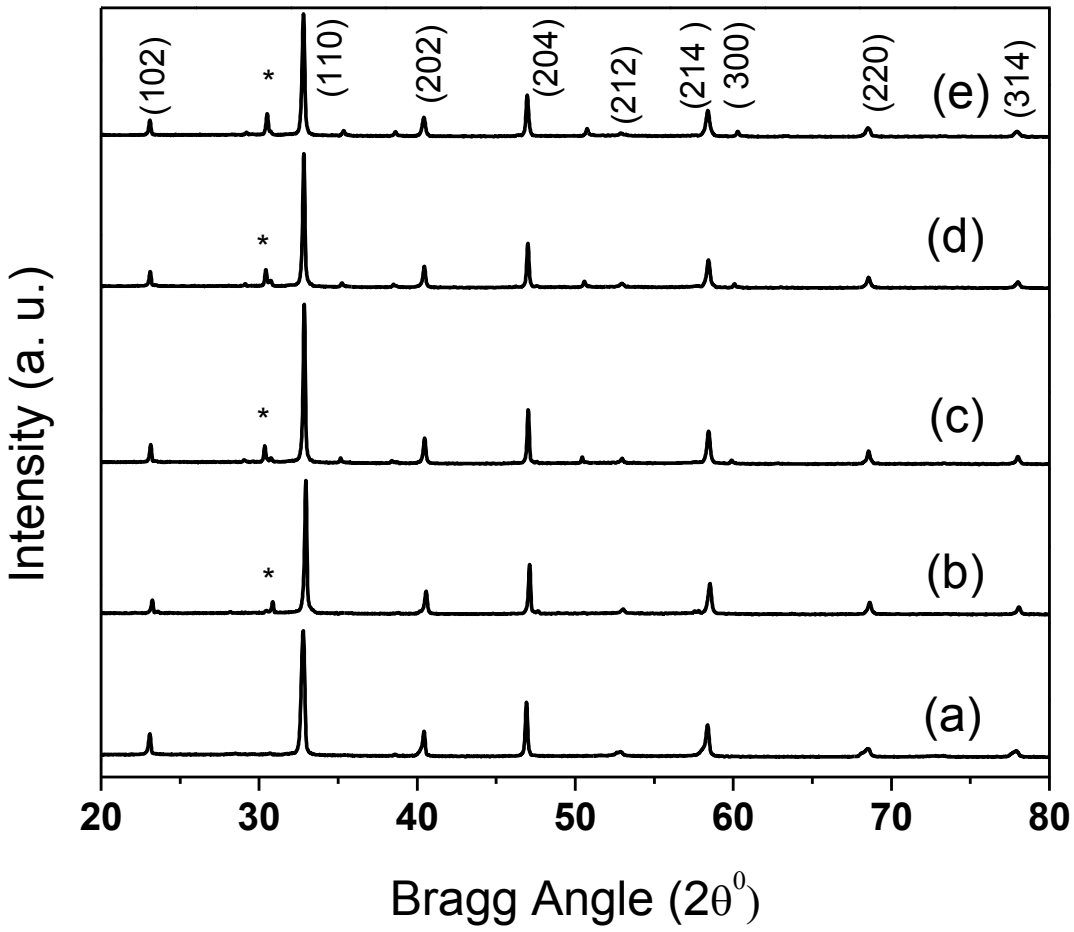

Fig. 3.4 XRD pattern of XRD patterns of $(Na_{0.5}Bi_{0.5})_{(1-x)}Y_xTi_{(1-x/4)}O_3$, (a) x=0.0, (b) x=0.02, (c) x=0.04, (d) x=0.06, (e) x=0.08 at room temperature.

Table 3.12 Comparison of observed (d_{obs}) and calculated (d_{cal}) *d* spacing (in Å), relative intensity, miller indices of $(Na_{0.5}Bi_{0.5})_{(0.98)}Y_{0.02}Ti_{(1-0.02/4)}O_3$.

Peak No.	*d*-spacing		I/I_0	Miller Indices		
	d-observed	*d*-calculated		h	k	l
1	3.8225	3.8518	9.5	1	0	2
2	2.7144	2.7088	100	1	1	0
3	2.2212	2.2320	16	2	0	2
4	1.9282	1.9259	31	2	0	4
5	1.7248	1.7302	3	2	1	2
6	1.5752	1.5754	19	2	1	4
7	1.3655	1.3621	7	2	2	0
8	1.2225	1.2221	4.5	3	1	4

Table 3.13 Comparison of observed (d_{obs}) and calculated (d_{cal}) *d* spacing (in Å), relative intensity, miller indices of $(Na_{0.5}Bi_{0.5})_{(0.96)}Y_{0.04}Ti_{(1-0.04/4)}O_3$.

Peak No.	*d*-spacing		I/I_0	Miller Indices		
	d-observed	*d*-calculated		h	k	l
1	3.8388	3.8737	12	1	0	2
2	2.7224	2.7305	100	1	1	0
3	2.2259	2.2318	15	2	0	2
4	1.9294	1.9369	30	2	0	4
5	1.7269	1.7280	2.5	2	1	2
6	1.5769	1.5765	18	3	0	0
7	1.3675	1.3653	6.5	2	2	0
8	1.2239	1.2227	4	3	1	4

Table 3.14 Comparison of observed (d_{obs}) and calculated (d_{cal}) *d* spacing (in Å), relative intensity, miller indices of $(Na_{0.5}Bi_{0.5})_{(0.94)}Y_{0.06}Ti_{(1-0.06/4)}O_3$.

Peak No.	*d*-spacing		I/I_0	Miller Indices		
	d-observed	*d*-calculated		h	k	l
1	3.8437	3.8836	11	1	0	2
2	2.7241	2.7309	100	1	1	0
3	2.2270	2.2339	10	2	0	2
4	1.9301	1.9276	28	2	0	4
5	1.7281	1.7291	2	2	1	2
6	1.5771	1.5767	18	3	0	0
7	1.3675	1.3655	6.5	2	2	0
8	1.3641	1.3642	3	3	0	5
9	1.2238	1.2240	4	3	1	4

Table 3.15 Comparison of observed (d_{obs}) and calculated (d_{cal}) *d* spacing (in Å), relative intensity, miller indices of $(Na_{0.5}Bi_{0.5})_{(0.92)}Y_{0.08}Ti_{(1-0.08/4)}O_3$.

Sl. No.	*d*-spacing		I/I_0	Miller Indices		
	d-observed	*d*-calculated		h	k	l
1	3.8470	3.8760	12	1	0	2
2	2.7265	2.7315	100	1	1	0
3	2.2281	2.2328	15	2	0	2
4	1.9313	1.9380	30	2	0	4
5	1.7290	1.7287	2	2	1	2
6	1.5779	1.5770	19	3	0	0
7	1.3674	1.3657	7	2	2	0
8	1.2238	1.2232	4	3	1	4

Table 3.16 Comparison of lattice parameters (*a* and *c* in Å) and unit cell volume (*V* in $(Å)^3$) of $(Na_{0.5}Bi_{0.5})_{(1-x)}Y_xTi_{(1-x/4)}O_3$.

x	*a*	*c*	Volume(V)
0.0	5.4880(43)	13.5384(43)	353.116
0.02	5.4873(81)	13.4791(81)	351.485
0.04	5.4873(91)	13.4501(91)	350.738
0.06	5.4845(74)	13.4427(74)	350.176
0.08	5.4832(70)	13.4412(70)	349.974

Under the reported conditions of calcinations of La/Y/Zr modified NBT, the formation of impurity phases cannot be avoided. But our observations suggest that the impurity phases are of minor in nature so far as their fraction in the sample is concerned. So the presence of impurity phases could be neglected for all practical purposes in the present analysis.

3.3 Scanning electron microscope

The microstructural and surface morphological studies of the sintered ceramic pellets were carried out using SEM (JEOL JSM-6480 LV). The sample pellets were platinum coated prior to being scanned under high-resolution field emission gun scanning electron microscope.

3.3.1 $Na_{0.5}Bi_{0.5}TiO_3$

The SEM micrograph of sintered pellet of $Na_{0.5}Bi_{0.5}TiO_3$ is shown in Fig. 3.5. SEM micrograph shows the polycrystalline microstructure with nearly rectangular grains of different grain sizes and they are in-homogeneously distributed throughout the sample surface. The grains and grain boundaries are well defined and clearly visible. The microstructure is overall dense, but a few scattered pores are observed which indicates that there is a certain degree of porosity in the sample. The average grain size lies between 1 to 3 μm.

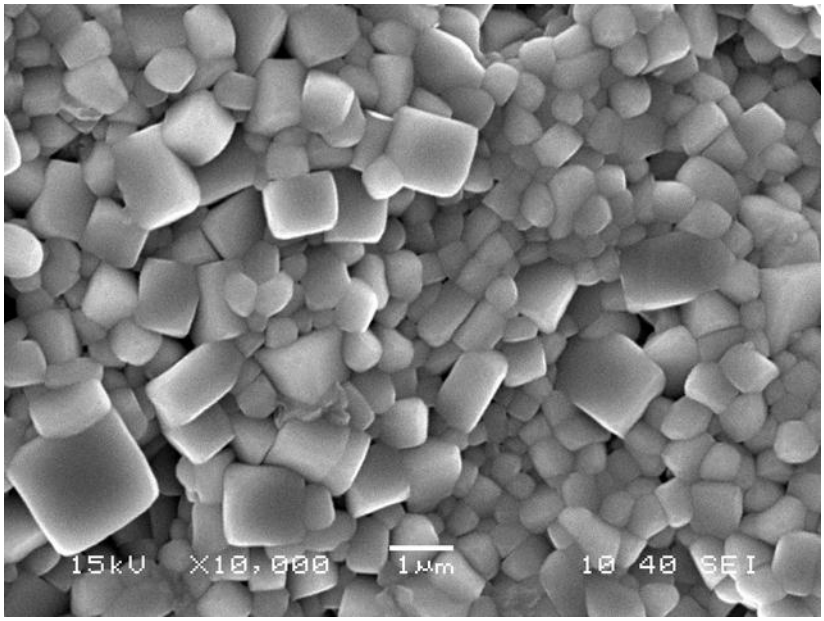

Fig. 3.5 SEM micrograph of $Na_{0.5}Bi_{0.5}TiO_3$ at room temperature.

3.3.2 La modified NBT

The SEM micrographs of $(Na_{0.5}Bi_{0.5})_{(1-x)}La_xTi_{(1-x/4)}O_3$, x=0.0, 0.02, 0.04, 0.06, 0.08 sintered pellets are shown Fig. 3.6 (a-e). The micrographs reveal a non-uniform

distribution of grains of varying size and shape. The grain sizes are significantly reduced from 2 to 0.5 μm with increase in La concentration from 0–8 %.

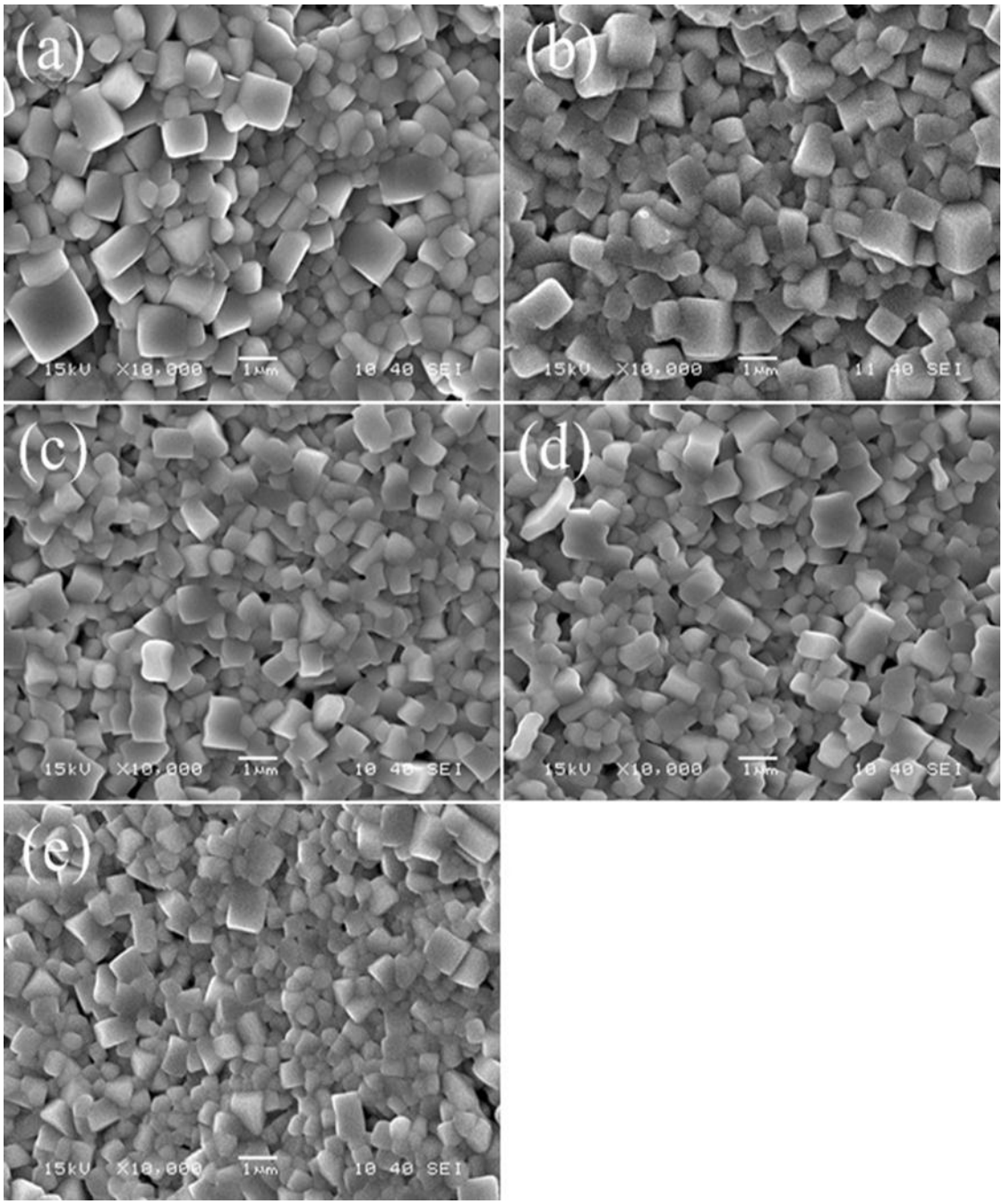

Fig. 3.6 SEM micrographs of $(Na_{0.5}Bi_{0.5})_{(1-x)}La_xTi_{(1-x/4)}O_3$, (a) x=0.0, (b) x=0.02, (c) x=0.04, (d) x=0.06, (e) x=0.08 at room temperature.

3.3.3 Zr modified NBT

The SEM micrographs of as sintered surface of $(Na_{0.5}Bi_{0.5})Ti_{(1-x)}Zr_xO_3$, x=0.0, 0.05, 0.1, 0.2, 0.3 are shown in Fig. 3.7 (a-e). The shapes of the particles are rectangular with different size and are randomly distributed on the surface. The average grain size is observed to be more in comparison to the pure NBT. The grain and grain boundary are well observed from the figure.

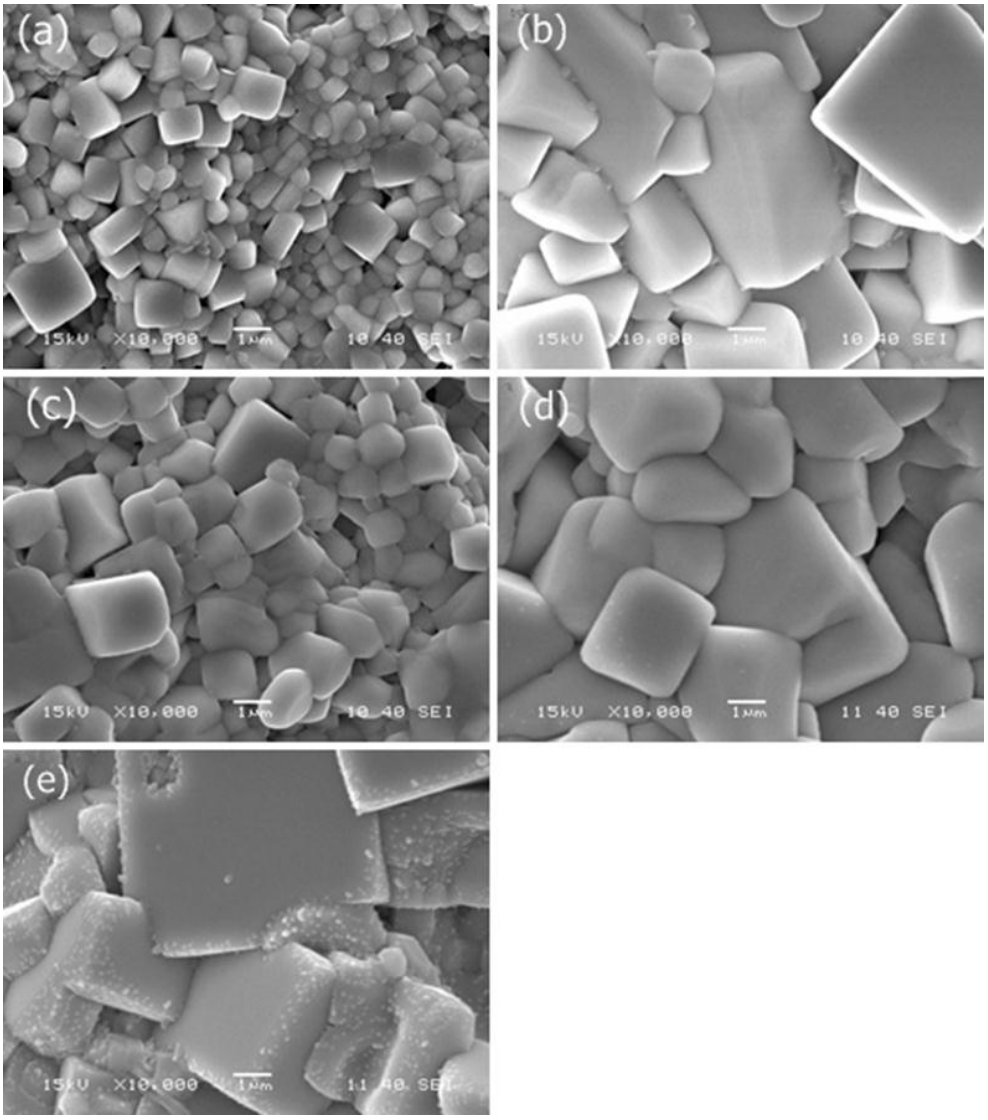

Fig. 3.7 SEM micrographs of $(Na_{0.5}Bi_{0.5})Ti_{(1-x)}Zr_xO_3$, (a) x=0.0,(b) x=0.05, (c)x=0.1, (d) x=0.2, (e) x=0.3 at room temperature.

3.3.4 Y Modified NBT

The SEM micrographs of $(Na_{0.5}Bi_{0.5})_{(1-x)}Y_xTi_{(1-x/4)}O_3$, x=0.0, 0.02, 0.04, 0.06, 0.08 are shown in Fig. 3.8 (a-e). Nearly rectangular shaped particles with different sizes are randomly distributed on the surface. The grain and grain boundary are well observed from the SEM micrographs. The average grain size decreases with an increase in the doping concentration of yttrium in NBT.

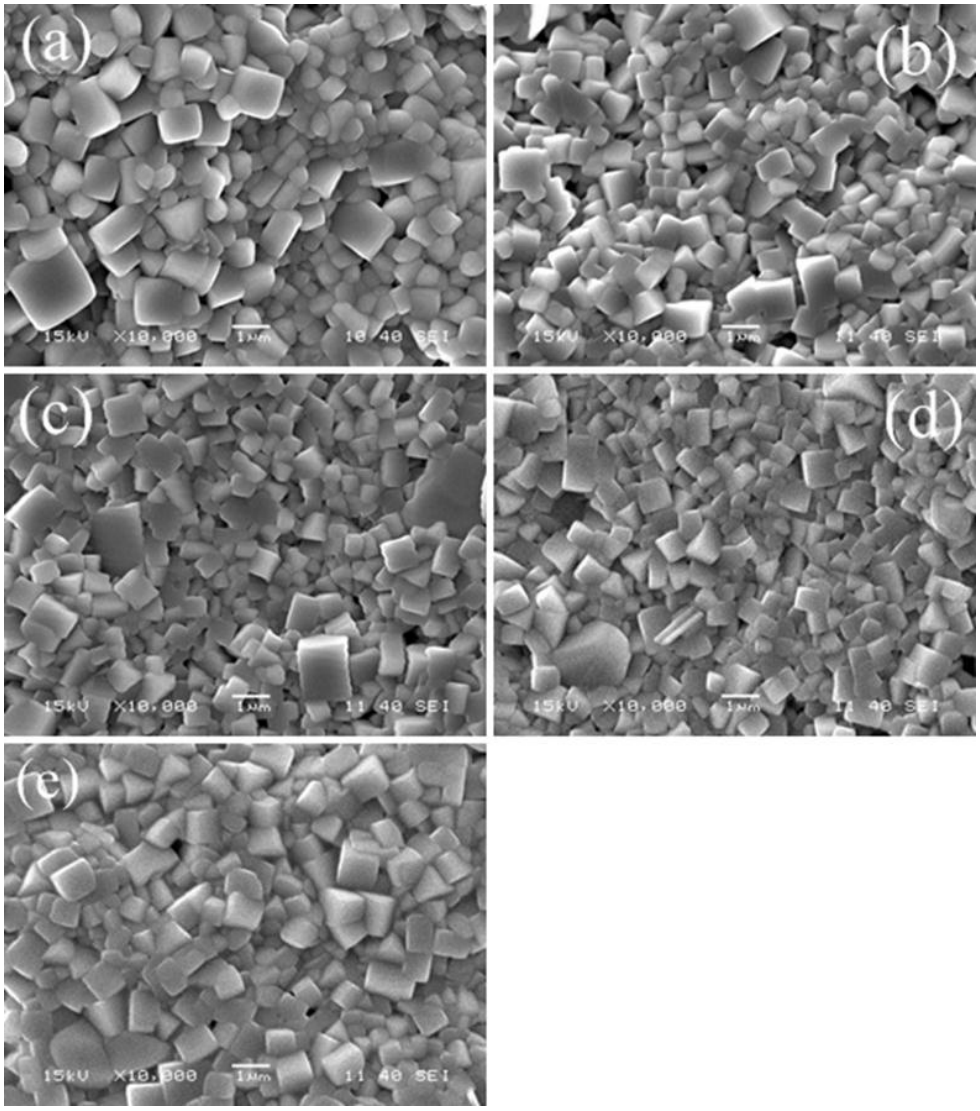

Fig. 3.8 SEM micrographs of $(Na_{0.5}Bi_{0.5})_{(1-x)}Y_xTi_{(1-x/4)}O_3$, (a) x=0.0, (b) x=0.02, (c) x=0.04, (d) x=0.06, (e) x=0.08 at room temperature.

3.4 Vibrational Study

The vibration characterization of material was carried out in FTIR spectrometer (Perklin Elmer FTIR spectrometer spectrum RX-1). The absorption spectra were scanned on a thin pellet made up of pinch of powder sample and spectroscopic graded KBr as an infrared transparent material. The FTIR spectrum of the sample has been recorded in the wave number range of 400 to 4000 cm^{-1}. In order to remove moisture from powder samples were dried before pelletizing.

3.4.1 La modified NBT

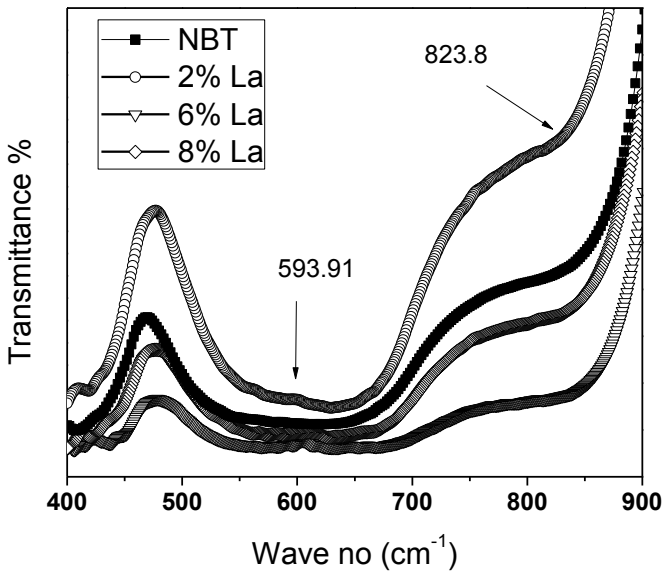

Fig. 3.9 FTIR spectra of $(Na_{0.5}Bi_{0.5})_{(1-x)}La_xTi_{(1-x/4)}O_3$, x=0.0, 0.02, 0.06, 0.08 at room temperature.

The FTIR spectra are characterized by appearance of several deeps in the curve corresponds to the vibrational bands in the compounds in transmittance mode of measurement. Figure 3.9 shows the FTIR spectra of $(Na_{0.5}Bi_{0.5})_{(1-x)}La_xTi_{(1-x/4)}O_3$,

x=0.0, 0.02, 0.06, 0.08 in the region 400-900 cm^{-1}. All the compounds show identical vibration of asymmetric bands around 593 cm^{-1} and a shoulder around 823 cm^{-1} is assigned to the Ti-O streching vibration of octahedral groups in the perovskite structure [3-5]. At lower frequency region (400-430 cm^{-1}) a small deep has been observed, that may corresponds to the Ti-O bending vibration of the compounds [6]. Hence the spectra represent the characteristic peaks of perovskite phase and confirm that TiO_6 octahedra have been formed. No appreciable change in bands corresponds to the characteristic TiO_6 octahedra have been observed as the substitution is at the A-site of the compound.

3.4.2 Zr Modified NBT

Figure 3.10shows the FTIR spectra of$(Na_{0.5}Bi_{0.5})Ti_{(1-x)}Zr_xO_3$, x= 0.0, 0.05, 0.1, 0.2, 0.3 in the range of 400 to 900 cm^{-1}. Similarly the Ti-O absorption mode has been observed at low frequency region (400-430 cm^{-1}) [6]. The characteristic modes of vibration of TO6 octahedral are observed around 586 cm^{-1} and the shoulder around 828 cm^{-1} [5]. It has been observed with increase in Zr concentration, the characteristics band of TO_6 octahedral around 586 cm^{-1} gets broadened and the intensity decreases, which may be due to the substitution of Zr^{4+} on Ti^{4+} site.

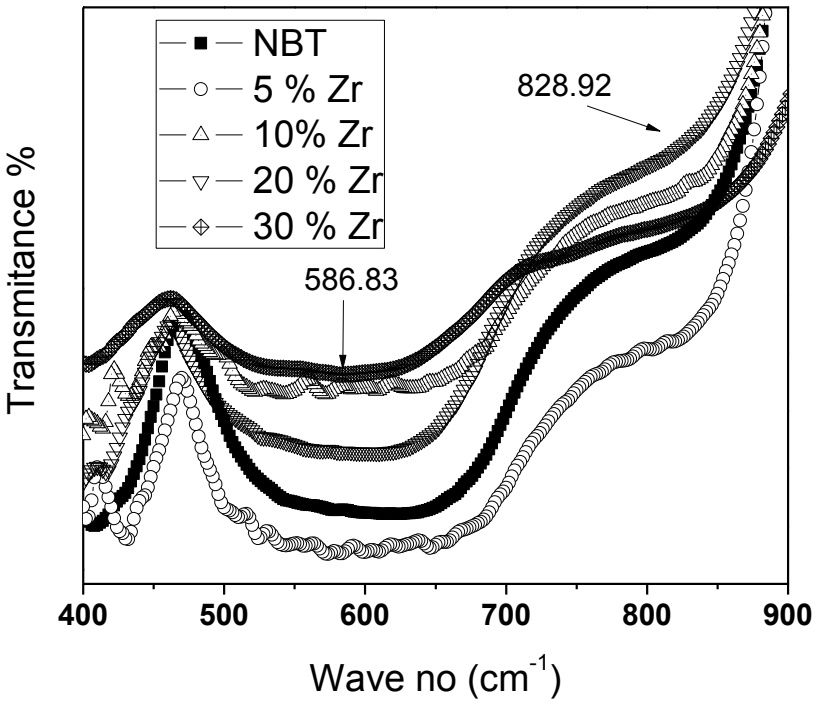

Fig. 3.10 FTIR spectra of$(Na_{0.5}Bi_{0.5})Ti_{(1-x)}Zr_xO_3$, x=0.0, 0.05, 0.1, 0.2, 0.3 at room temperature.

3.4.3 Y Modified NBT

The FTIR spectra of $(Na_{0.5}Bi_{0.5})_{(1-x)}Y_xTi_{(1-x/4)}O_3$, x=0.0, 0.02, 0.04, 0.06, 0.08 in the range of 400 to 900 cm^{-1} is shown in Fig. 3.11. All the samples display Ti–O bending absorptions band around 420 cm^{-1} [6] and characteristic vibrations of $[TiO_6]^{-2}$ octahedron in NBT crystal around 593 cm^{-1}along with a shoulder of TiO_6 octahedral around 830 cm^{-1}[5]. This again confirms the formation of perovskite phase. As the substitution is at the A-site of the compounds, no appreciable change in bands corresponds to the characteristic TiO_6 octahedra of the perovskite structure.

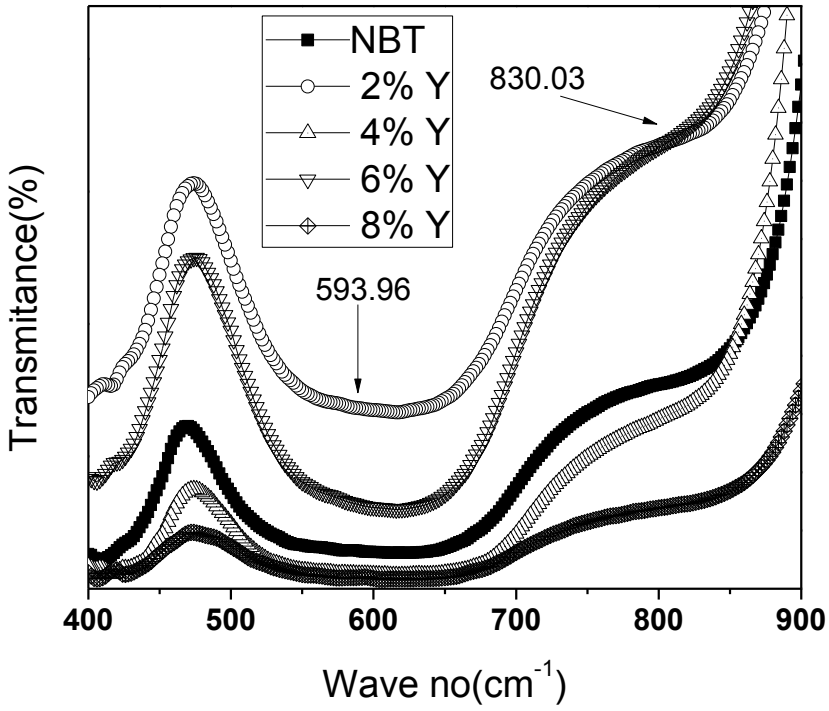

Fig. 3.11 FTIR spectra of $(Na_{0.5}Bi_{0.5})_{(1-x)}Y_xTi_{(1-x/4)}O_3$, x=0.0, 0.02, 0.04, 0.06, 0.08 at room temperature.

All the characteristic features of modified NBT samples shown in the IR spectra suggest that the lattice of the modified perovskite has distorted BO_6 octahedra which produces the dipole moment and hence creates ferroelcticity. It needs further experiments/studies to address the change in electrical properties on substitutions at A/B site of the NBT ceramics oxides.

References

[1] Peak Fit version 4.02, Jandel Scientific Software, 1991

[2] POWD-an Interactive Powder Diffraction Data Interpretation and indexing Program Version 2.2 by E.Wu, School of Physical sciences, Flinder University of South Australia Bedford Park, S. A. 5042, Australia.

[3] S. E. Perk, S. J. Chung, I. T. Kim and K. S. Hong, Nonstoichiometry and the Long-Range Cation Ordering in Crystals of $(Na_{1/2}Bi_{1/2})TiO_3$. Journal of American Ceramic Society 77 (1994) 2641.

[4] J. T. Last, Infrared-absorption studies on barium titanate and related materials. Physical Review B, 105 (1957) 1740.

[5] C. A. Guarany, L. H. Z. Pelaio, E. B. Araujo, K. Yukimitu, J. C. S. Moraes and J. A. Eiras, Infrared studies of the monoclinic–tetragonal phase transition in $Pb(Zr,Ti)O_3$ ceramics. Journal of Physics: Condensed Matter, 15 (2003) 4851.

[6] S. Dutta, R. N. P. Choudhary, P. K. Sinha, and A. K. Thakur, Microstructural studies of $(PbLa)(ZrTi)O_3$ ceramics using complex impedance spectroscopy. Journal of Applied Physics, 96(2004) 1607.

Chapter 4

DIELECTRIC STUDY

4.1 Introduction

The dielectric properties of ferroelectrics depend on the field strength at which it is measured. It is a consequence of non-linear relation between polarization and electric field. For ferroelectric materials, the dielectric constant increases up to the transition temperature and after that it obeys the Curie-Weiss law. There are various methods for dielectric measurements, among them the most convenient impedance method has been used to study the dielectric properties of materials. In the impedance method, input voltage is applied and corresponding impedance and phase angle are measured at different frequencies. From the impedance and phase angle, other electrical parameters are calculated. The aim of this chapter is to study the dielectric properties of the synthesized materials as a function of frequency and temperature, which may provide information regarding the existence of ferroelectricity, the nature of the phase transition in them and the effect of substitution on dielectric properties of the proposed compounds.

A sample holder has been specially designed for electrical measurement with an attachment of thermocouple for temperature measurement. The silver electrode samples were kept in a sample holder such as it works as a capacitor. For temperature variable electrical measurement the sample holder containing sample was then kept inside a handmade furnace and a variac voltage regulator was used to control the current to the heating coil for uniform and the slow heating environment. The temperature inside the sample holder was measured by measuring the current of the thermocouple using a milli-voltmeter and converting that current to temperature by a conversion table. Electrical parameters i.e., the impedance (Z), parallel capacitance (C_p), phase (θ), and dielectric loss (D) were measured as a function of frequency (100 Hz to 1MHz) at steps of 5 ^{0}C intervals from room temperature to 500 ^{0}C with the application of an a.c. input signal voltage of 1Vrms. The dielectric constant is calculated using an empirical formula: $\epsilon = C_p/C_0$, where C_0 is the air capacitance.

4.2. Measurement of ϵ_r and tanδ with frequency

4.2.1.$(Na_{0.5}Bi_{0.5})TiO_3$

The variation of relative dielectric constant (ϵ_r) with frequency of NBT at different temperatures (i.e. from 30 to 500 ^{0}C) is shown in Fig. 4.1 (a). It is observed that ε_r decreases monotonically with increasing frequency for all the temperature, which is a normal behavior of polar dielectric materials [1]. The ε_r value observed to be increases with rise in temperature for all frequency, but the increase in the ε_r value is more in the low frequency region as compared to the high frequency region.

The variation of dielectric loss (tanδ) of $(Na_{0.5}Bi_{0.5})TiO_3$ with frequency at different temperatures is shown in Fig. 4.1 (b). The variation of tanδ with frequency also follows the similar nature as dielectric constant, except the appearance of a peak in the spectrum above 225 ^{0}C. The observed peak shifted towards the higher frequency side on increasing temperature. At higher temperature (≥ 300 ^{0}C) the peak is beyond the measured of frequency range used.

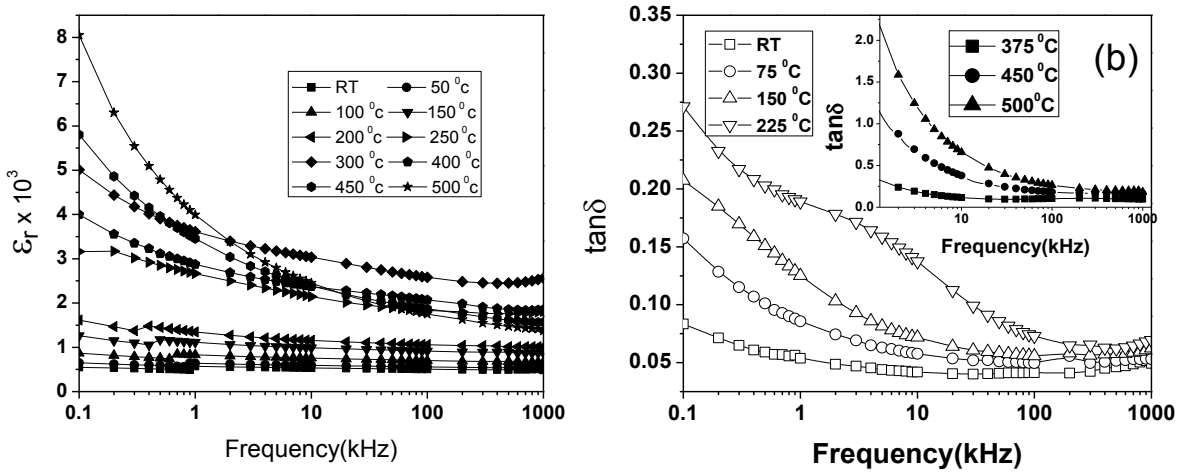

Fig 4.1 Variation of (a) dielectric constant and (b) tanδ of $(Na_{0.5}Bi_{0.5})TiO_3$ with frequency at various temperature, respectively.

4.2.2 La modified NBT

The variation of dielectric constant of $(Na_{0.5}Bi_{0.5})_{(1-x)}La_xTi_{(1-x/4)}O_3$, x=0.0, 0.02, 0.04, 0.06, 0.08 are compared in Fig. 4.2(a). The normal dielectric behavior of La modified NBT has been observed from the variation of dielectric constant with frequency. It also can be seen that the dielectric constant at room temperature

increases with increase in lanthanum concentration up to 6%, then decreases for 8% of La modified NBT.

The variation of dielectric loss with frequency of $(Na_{0.5}Bi_{0.5})_{(1-x)}La_xTi_{(1-x/4)}O_3$, x= 0.0, 0.02, 0.04, 0.06, 0.08 at room temperature is compared in Fig. 4.2 (b). The dielectric loss is observed to be higher at low frequency and decreases with increase in frequency which is similar in behavior to that the variation of dielectric constant. Also the dielectric loss is more in lanthanum substituted NBT than pure NBT at low frequency.

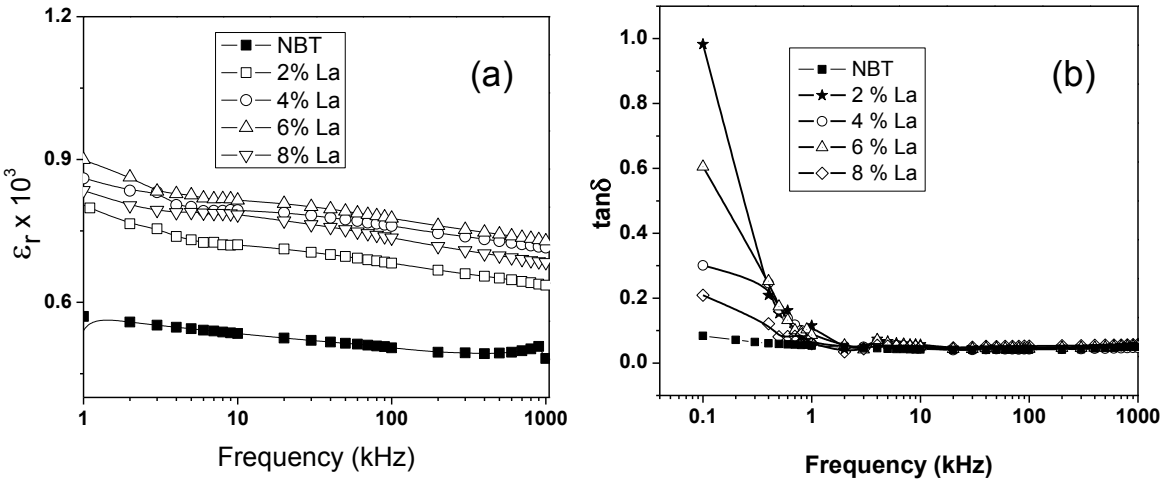

Fig. 4.2 Variation of (a) dielectric constant & (b) tanδ with frequency of La modified NBT at room temperature.

4.2.3 Zr modified NBT

Figure 4.3 (a) compares the variation of dielectric constant of $(Na_{0.5}Bi_{0.5})Ti_{(1-x)}Zr_xO_3$, x=0.0, 0.05, 0.1, 0.2, 0.3 at room temperature. The dielectric constant decreases with a rise in frequency for all composition. The dielectric constant is found to be more for 20 and 30 % Zr substituted NBT than pure NBT.

The nature of variation of tanδ of 5, 10, 20, 30 % zirconium modified NBT at room temperature is shown in Fig 4.3 (b). The variation of tanδ shows the same behavior as that of the dielectric constant with frequency as shown in fig. 4.3 (a).

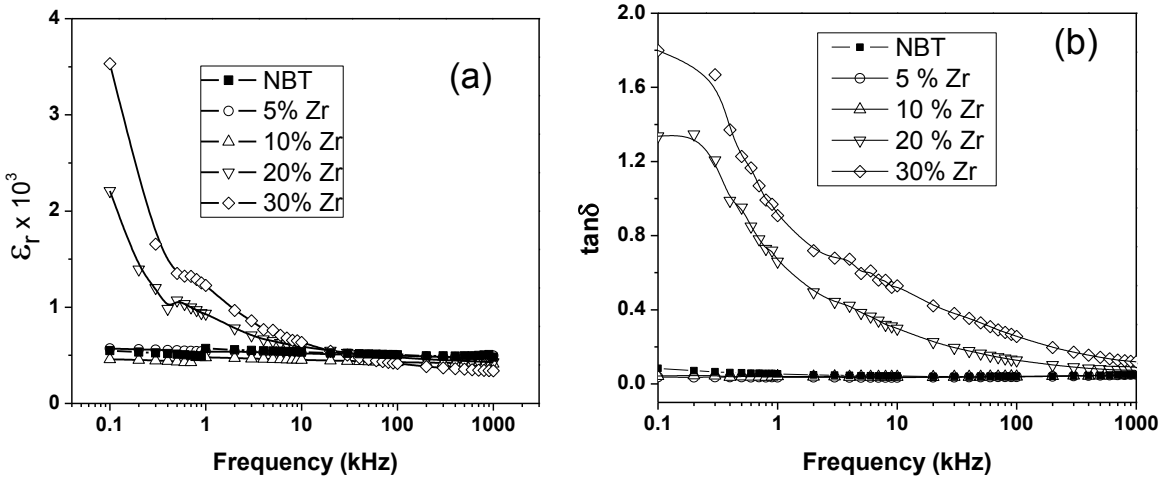

Fig. 4.3 Variation of (a) ϵ_r & (b) tanδ with frequency at room temperature of Zr substituted NBT.

4.2.4 Y modified NBT

The variation of dielectric constant of $(Na_{0.5}Bi_{0.5})_{(1-x)}Y_xTi_{(1-x/4)}O_3$, x= 0.0, 0.02, 0.04, 0.06, 0.08 at room temperature is compared in Fig. 4.4 (a). The dielectric constant decreases with increase in frequency for all compositions. Also the higher value of dielectric constant is observed for higher Y content as compared to NBT at room temperature.

The comparison of variation of dielectric loss with frequency of $(Na_{0.5}Bi_{0.5})_{(1-x)}Y_xTi_{(1-x/4)}O_3$, x= 0.0, 0.02, 0.04, 0.06, 0.08 at room temperature is shown in Fig. 4.4 (b). It has been observed that the dielectric loss decreases with increase in frequency. Also the loss decreases with increases in yttrium concentration at lower frequencies.

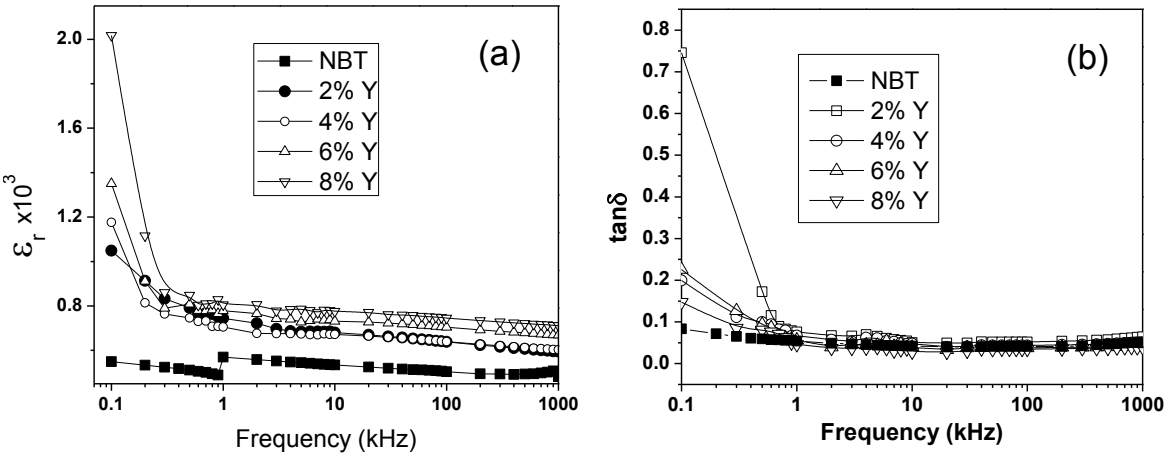

Fig. 4.4 Variation of (a) dielectric constant and (b) tanδ with frequency of Y modified NBT at room temperature.

4.3 Measurement of ϵ_r and tanδ with temperature

4.3.1 $(Na_{0.5}Bi_{0.5})TiO_3$

The variation of dielectric constant with temperature at the few selected frequencies of NBT is shown in Fig. 4.5 (a). It can be seen that dielectric constant increases with increase in temperature to its maximum value (ε_{max}) and then decreases. The dielectric anomaly is observed around 300 ^{0}C representing the antiferroelectric-paraelectric phase transition, which is of diffuse in nature. The peak in the pattern appears at the same temperature irrespective of the frequency. It is also observed that around the temperature 200 ^{0}C, there is a bifurcation in dielectric constants for different frequencies, which may be due to the ferroelectric to antiferroelectric phase transition of NBT. Further, the relative dielectric constant at low frequency observed to be increased with the increase in temperature above phase transition temperature, which may be due to space charge polarization and its conductivity.

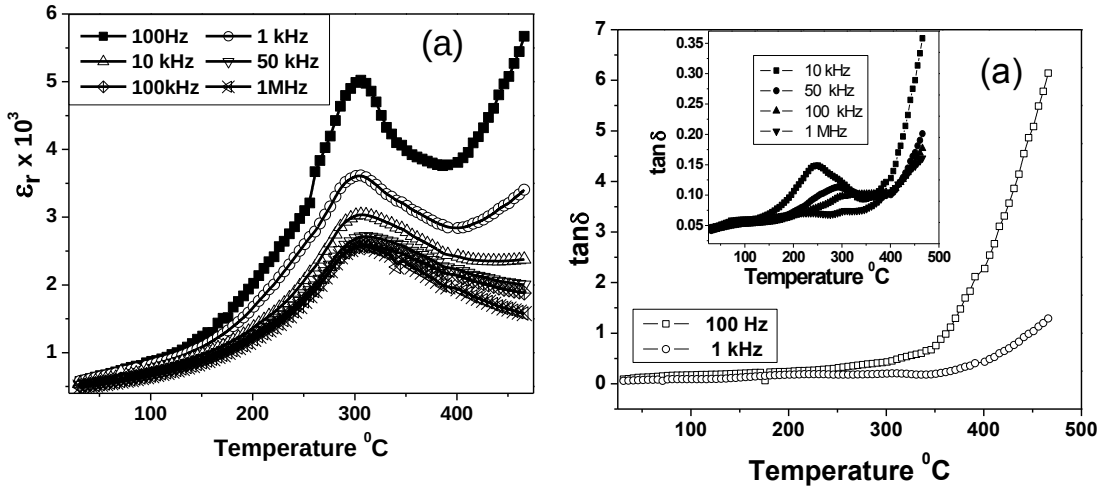

Fig. 4.5 Variation of (a) dielectric constant and (b) tanδ with temperature of $(Na_{0.5}Bi_{0.5})TiO_3$ at various frequencies.

The variation of tanδ with the temperature at different frequencies of NBT is shown in Fig. 4.5 (b). It is observed that the tangent loss increases with increase in temperature at all frequencies. The increase in tanδ value of NBT is very small up to 350 ^{0}C and above this temperature there is a sudden increase in the tanδ value with rise in temperature. Inset of Fig. 4.5 (b) shows the variation of tanδ with temperature for the frequencies of 10 kHz, 50 kHz, 100 kHz, and 1MHz. A peak has been observed at 250 ^{0}C for 10 kHz and this peak is more broadened and shifted to higher temperature side with an increase in frequency. The peak positions are observed to be in the temperature between 200 ^{0}C to 300 ^{0}C. The increasing trend in tanδ values at higher temperature region for all frequencies may be due to space charge polarization [2].

4.3.2 La modified NBT

The variation of dielectric constant with temperature at various frequencies of $(Na_{0.5}Bi_{0.5})_{(1-x)}La_xTi_{(1-x/4)}O_3$, x= 0.02, 0.04, 0.06, 0.08 are shown in Fig. 4.6 (a, b, c, d), respectively. Three dielectric anomalies are observed from room temperature to 500 ^{0}C. Around the temperature 100 ^{0}C, there is a hump in the temperature dependent dielectric constants for all frequencies, which may be due to the ferroelectric to antiferroelectric phase transition (T_d). The dielectric anomaly is observed around 300 ^{0}C representing the antiferroelectric-paraelectric phase transition (T_c), which is of diffuse in nature. There is another anomaly observed in between T_d and T_c, which may be due to the transition from rhombohedral to tetragonal structure [3]. The transition temperatures and maximum permittivity at the transition temperature of La modified

NBT are given in the Table 4.1. The transition temperatures are calculated from phase angle (θ) verses temperature graph.

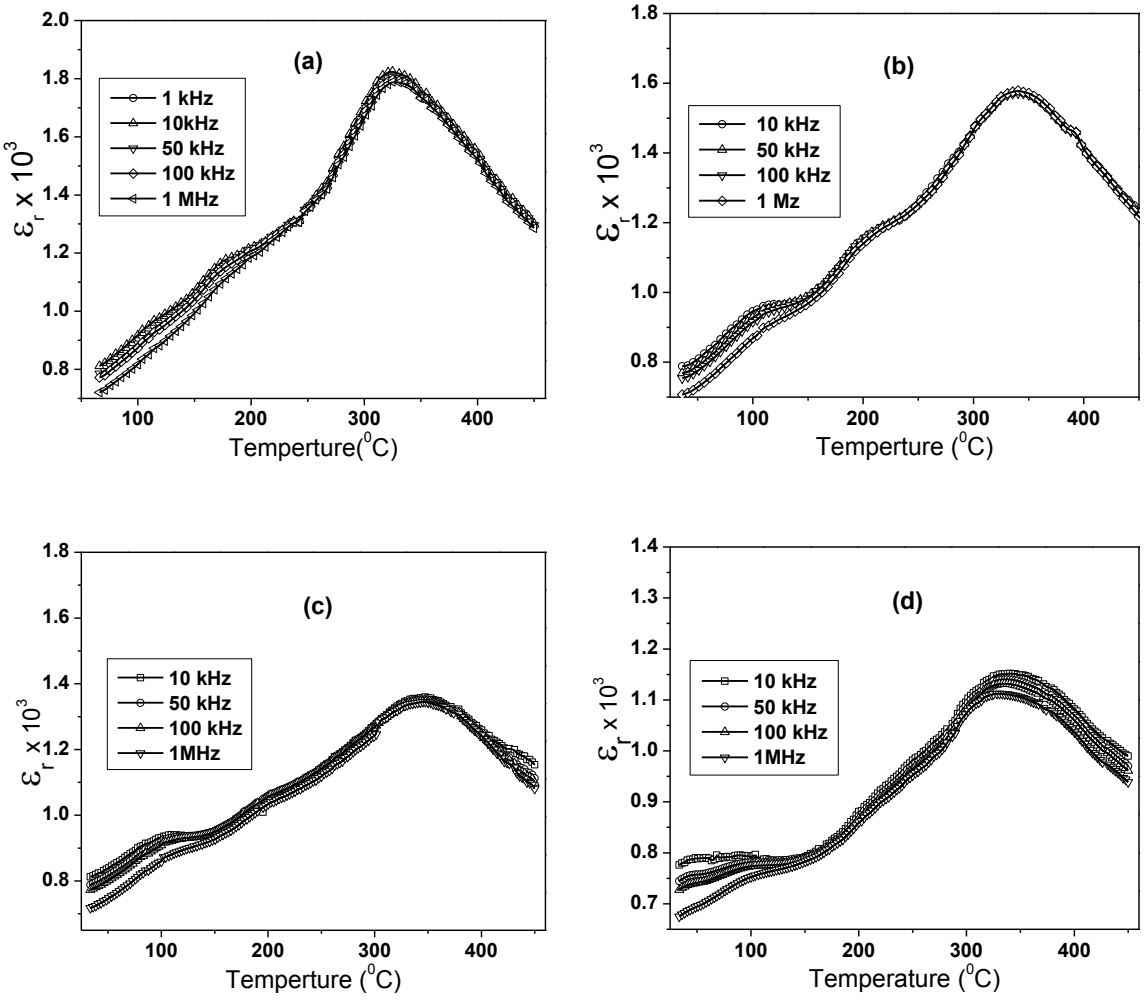

Fig. 4.6 Variation of ε_r with temperature at different frequencies of $(Na_{0.5}Bi_{0.5})_{(1-x)}La_xTi_{(1-x/4)}O_3$, (a) x=0.02, (b) x=0.04, (c) x=0.06, (d) x=0.08.

The variation of tanδ with temperature of $(Na_{0.5}Bi_{0.5})_{(1-x)}La_xTi_{(1-x/4)}O_3$, x= 0.02, 0.04, 0.06, 0.08 is shown in Fig. 4.7 (a, b, c, d), respectively. The dielectric loss decreases with the rise in temperature. There are frequency dependent humps observed from the

graph in the temperature range of 200 to 320 ^{0}C except 6% La- modified NBT. The dielectric loss of La modified NBT is less in comparison to pure NBT and also the dielectric loss of NBT at high temperature has been significantly reduced. The La modification results in the formation of cation vacancies which efficiently reduces the concentration of oxygen vacancies which in turn significantly reduces the dielectric loss.

Table 4.1 Comparison of T_d, T_{R-T}, T_c, and ε_{max} of $(Na_{0.5}Bi_{0.5})_{(1-x)}La_xTi_{(1-x/4)}O_3$ ceramic.

x	**T_d(^{0}C)**	**T_{R-T}(^{0}C)**	**T_c(^{0}C)**	$\boldsymbol{\varepsilon_{max}}$
0.02	158	238	326.	1795
0.04	159	227	340.	1571
0.06	154	248	345	1346
0.08	158	302	336	1131

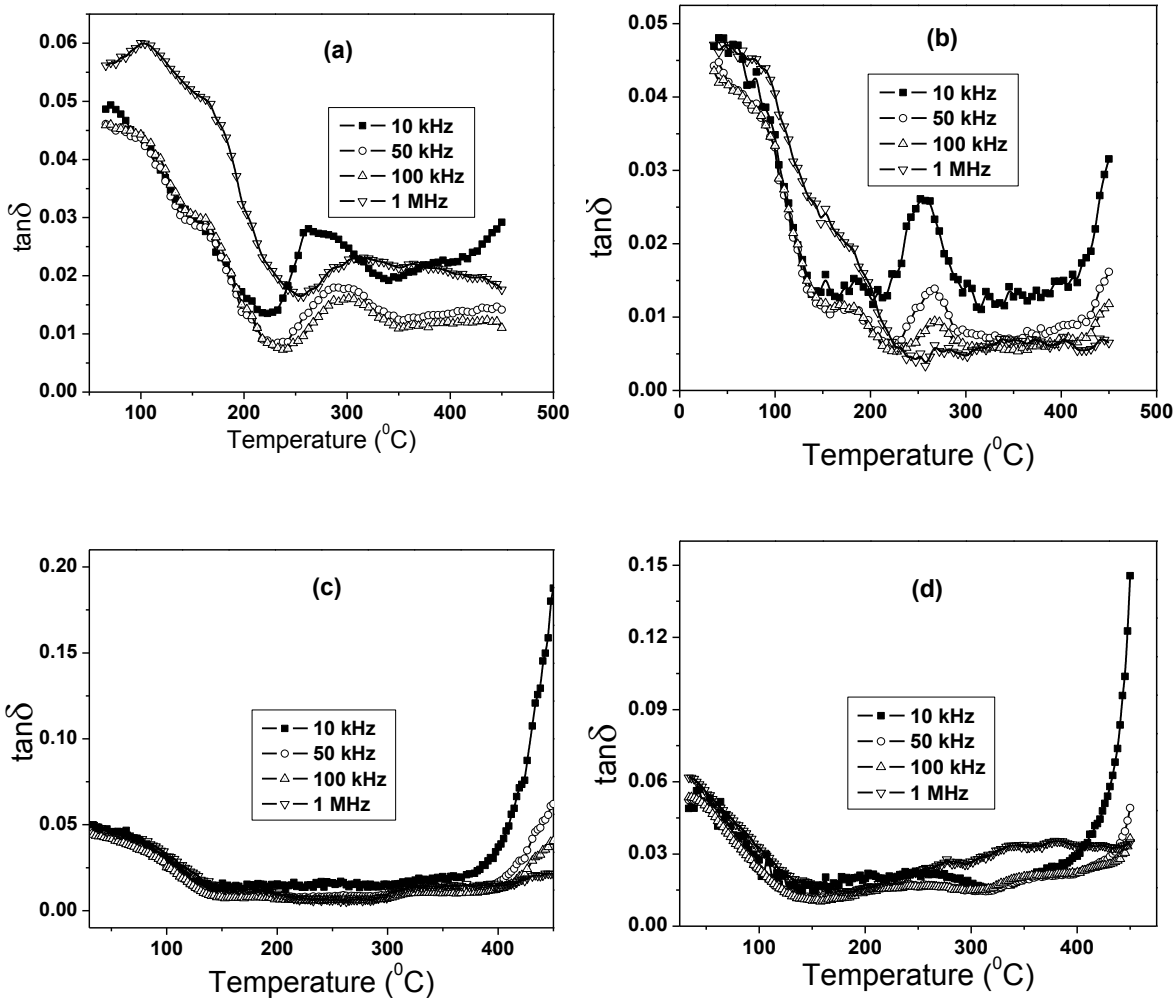

Fig. 4.7 Variation of tanδ with temperature at different frequencies of $(Na_{0.5}Bi_{0.5})_{(1-x)}La_xTi_{(1-x/4)}O_3$, (a) x=0.02, (b) x=0.04, (c) x=0.06, (d) x=0.08.

4.3.3 Zr modified NBT

The temperature dependence of dielectric constant of $(Na_{0.5}Bi_{0.5})Ti_{(1-x)}Zr_xO_3$, x=0.05, 0.1, 0.2, 0.3 at different frequencies is shown in Fig. 4.8 (a, b, c, d), respectively. The dielectric constant increases with rise in temperature for 1, 10, 50 kHz frequency but at higher frequency 100 kHz and 1 MHz it decreases after attaining a maximum

value (ϵ_{max}). The observed broad peak at around 320 ^{0}C corresponds to the antiferroelectric to paraelectric phase transition. In case of low frequencies, the sudden increase of dielectric constant on and above the phase transition temperature may be due to the space charge polarization [4]. The bifurcation has been observed in between temperature 175-200 ^{0}C, may be due to the transition of ferroelectric to antiferroelectric phase. The ε_{max} value at transition temperature decreases with increase in the concentration of Zr in NBT. The transition temperature and maximum permittivity at transition temperature of Zr modified NBT are given in Table 4.2.

Table 4.2 Comparison of ε_{max}, and T_c of $(Na_{0.5}Bi_{0.5})Ti_{(1-x)}Zr_xO_3$ ceramics.

x	**T_c(^{0}C)**	**ε_{max}**
0.05	313	1618
0.1	311	1160
0.2	345	955
0.3	338	627

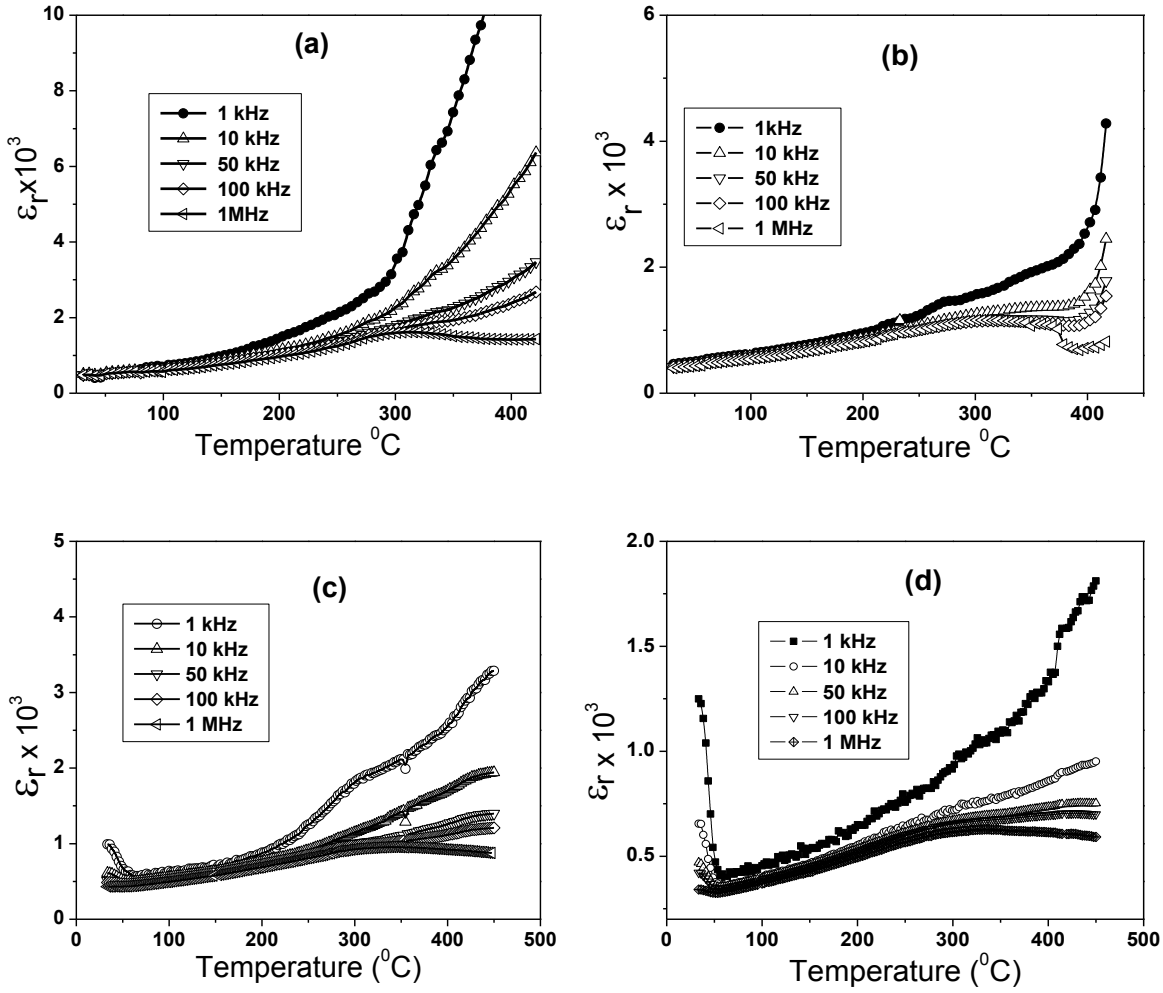

Fig. 4.8 Variation of dielectric constant with temperature at different frequencies of $(Na_{0.5}Bi_{0.5})Ti_{(1-x)}Zr_xO_3$, (a) x=0.05, (b) x= 0.1, (c) x=0.2, (d) x=0.3.

The temperature dependence of dielectric loss of $(Na_{0.5}Bi_{0.5})Ti_{(1-x)}Zr_xO_3$, x=0.05, 0.1, 0.2, 0.3 at various frequencies are shown in Fig. 4.9 (a, b, c, d), respectively. The dielectric loss is very less up to 250 ^{0}C and then increases with rise in temperature. The high value of dielectric loss at low frequency and high temperature may be due to the release of space charge. A small peak is observed in 10 and 20 % Zr modified NBT around 300 ^{0}C.

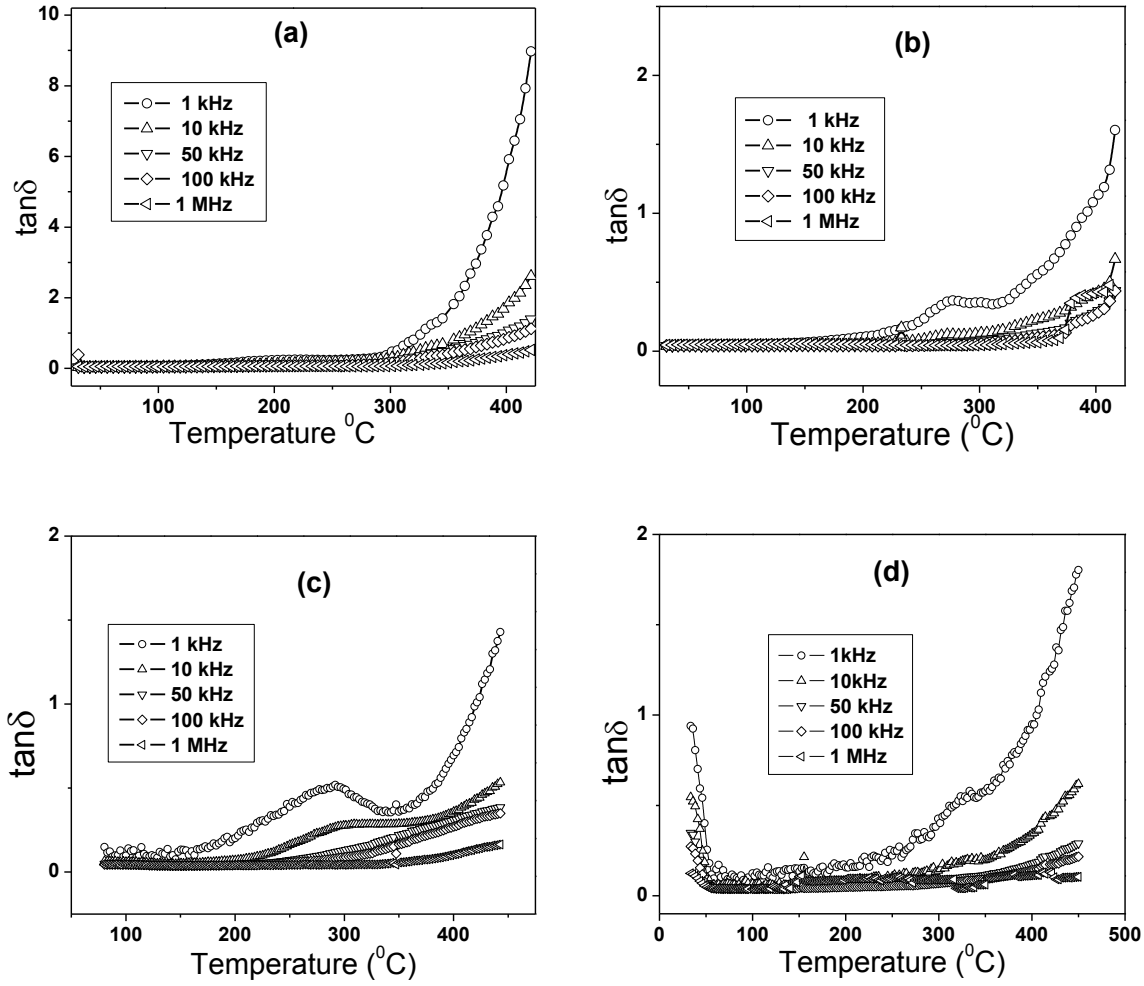

Fig. 4.9 Variation of tanδ with temperature at different frequencies $(Na_{0.5}Bi_{0.5})Ti_{(1-x)}Zr_xO_3$, (a) x=0.05,(b) x= 0.1, (c) x=0.2, (d) x=0.3.

4.3.4 Y modified NBT

The variation of dielectric constant with temperature at various frequencies of $(Na_{0.5}Bi_{0.5})_{(1-x)}Y_xTi_{(1-x/4)}O_3$, x=0.02, 0.04, 0.06, 0.08 are shown in Fig. 4.10 (a, b, c, d), respectively. There are appearance of three different peaks in the temperature range of

RT to 500 ^{0}C. The peak at temperature ~125 ^{0}C is the depolarization temperature (T_d) which may correspond to ferroelectric to antiferroelectric phase transition.

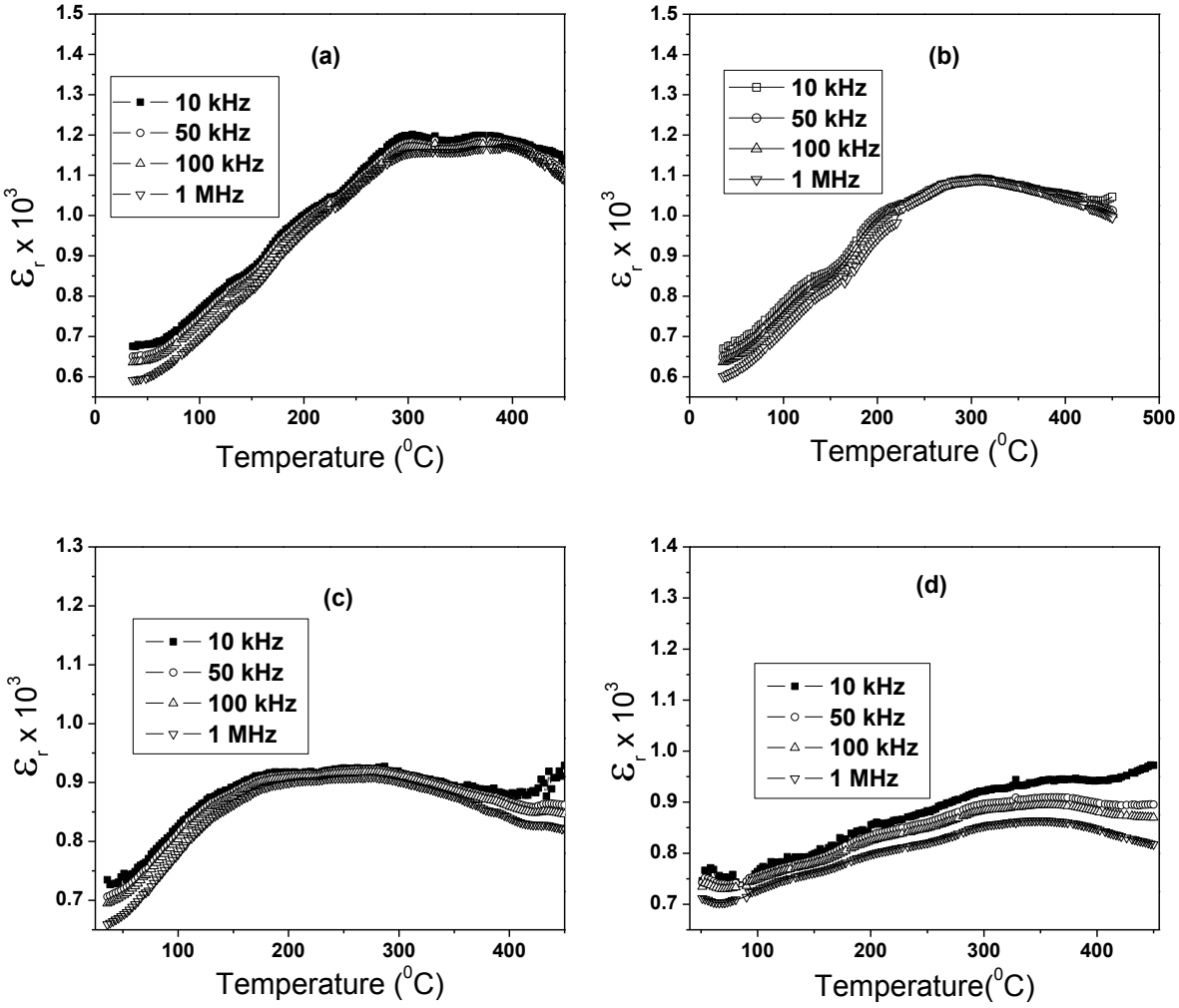

Fig. 4.10 Variation of dialectic constant with temperature at different frequencies of $(Na_{0.5}Bi_{0.5})_{(1-x)}Y_xTi_{(1-x/4)}O_3$, (a) x=0.02, (b) x=0.04, (c) x=0.06, (d) x=0.08.

A small dielectric hump is observed at temperature ~200 ^{0}C may be due to the transition from rhombohedral to the tetragonal phase. The maximum dielectric constant peak at around 300 ^{0}C is the transition from antiferroelectric to paraeleatric

phase. The maximum value of dielectric constant at transition temperature (T_m) decreases with an increase in yttrium concentration in NBT.

The transition temperatures and maximum permittivity at transition temperature (obtained from phase angle (θ) vs. temperature graph) of Y modified NBT are given in table 4.1

Table 4.3 Comparison of T_d, T_{R-T}, Tc and ε_{max} of $(Na_{0.5}Bi_{0.5})_{(1-x)}Y_xTi_{(1-x/4)}O_3$.

x	T_d(^{0}C)	T_{R-T}(^{0}C)	T_c(^{0}C)	ε_{max}
0.02	153	232	337	1170
0.04	161	232	347	1090
0.06	141	222	337	918
0.08	133	232	320	885

The variation of dielectric loss with temperature at different frequencies of $(Na_{0.5}Bi_{0.5})_{(1-x)}Y_xTi_{(1-x/4)}O_3$, x=0.0, 0.02, 0.04, 0.06, 0.08 is shown in Fig. 4.11 (a, b, c, d). The dielectric losses almost remain constant up to 375^{0}C and above 400 ^{0}C it increases rapidly due to release of space charge in the sample.

For La and Y modified NBT, we have observed mainly three phase transitions i.e., ferroelectric to antiferroelectric phase transition (T_d), antiferroelectric-paraelectric phase transition (T_c) and transition from rhombohedral to tetragonal structure. Temperature dependent ferroelectric loop measurement and temperature dependent

Raman spectroscopy measurement can be employed to support the above phase transitions, which are observed in temperature dependent dielectric constant plot.

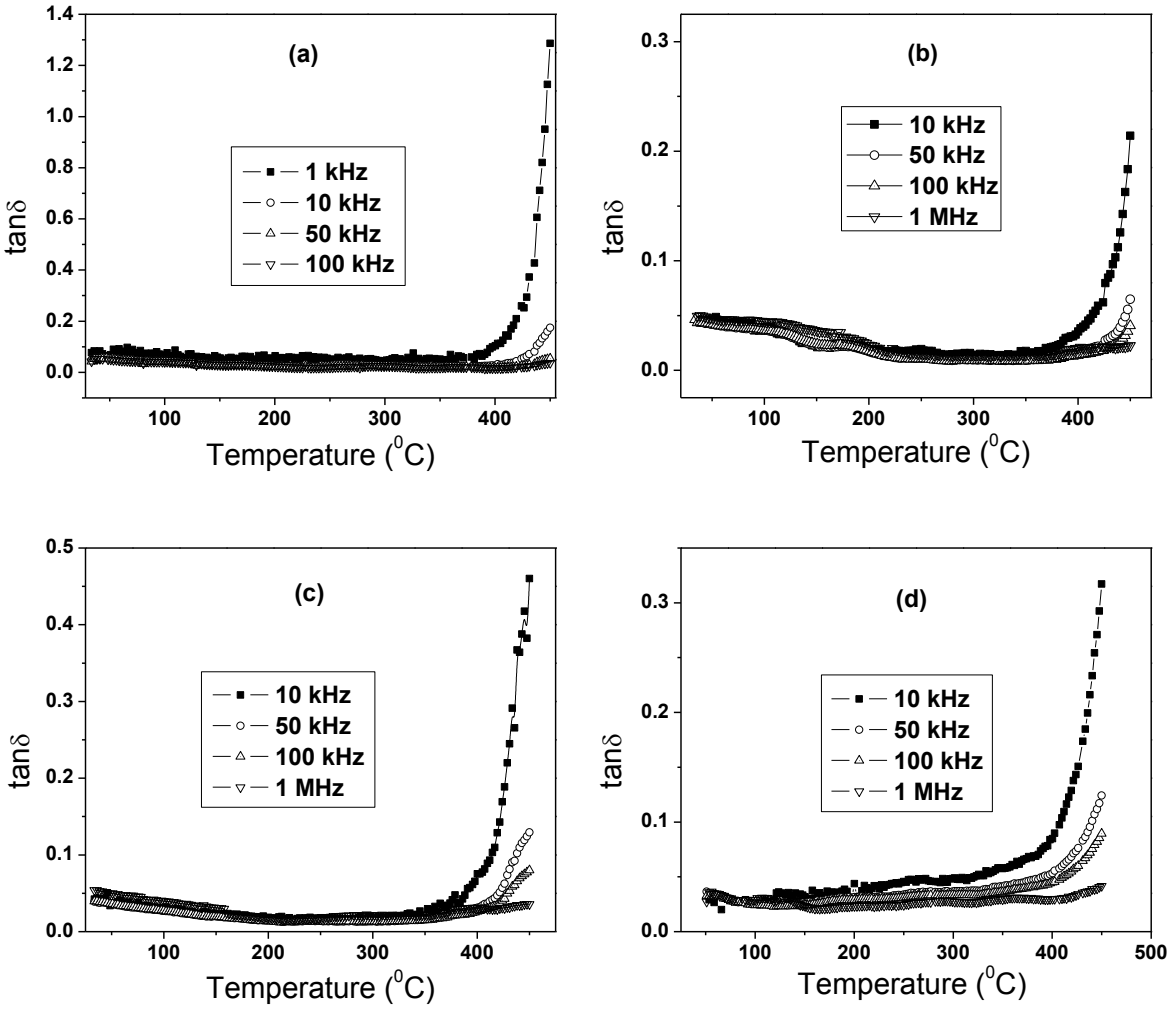

Fig. 4.11 Variation of tanδ with temperature at different frequencies of $(Na_{0.5}Bi_{0.5})_{(1-x)}Y_xTi_{(1-x/4)}O_3$, (a) x=0.02, (b) x=0.04, (c) x=0.06, (d) x=0.08.

4.3.5 Diffuse phase transition

The broad peak at phase transition (T_c) temperature in dielectric constant verses temperature curves indicates the transition is of diffuse type. The broad peak

implies that the phase transition does not occur at discrete temperature but smears out over a temperature range [5]. The broadening or diffuseness of the peak may be due to the substitution disordering in the arrangement of cations at one or more crystallographic sites in the lattice structure leading to heterogeneous domains or may be due to the defect induced relaxation at high temperature [6]. The variation of dielectric constant with temperature after the phase transition (T_c) was analyzed by modified Curie-Wiess law: $1/\varepsilon - 1/\varepsilon_m = (T - T_m)^{\gamma}/C$, where γ is the diffusivity, C is the Curie Weiss constant, ε is dielectric constant at a temperature T and ε_{max} is dielectric constant at T_c. The diffusion factor (γ) can be employed to describe the degree of diffusivity of the phase transition [7].

Figure 4.11 (a, b, c, d) shows the diffusivity curve of NBT, La, Zr, and Y modified NBT, respectively. The calculated value of γ for NBT is found to be1.53 at10 kHz, which clearly shows that the phase transition in NBT is a diffuse phase transition. The values of γ for La, Zr, and Y modified NBT are given in the Table 4.4. The calculated *γ* values indicate that the phase transition is a diffuse type and diffusivity increases with the increase in substitution. The diffuse nature of the phase transition may be due to disorder in A/B site of the material and defects. The cation disorder and defect induces the formation of micro-polar regions and each of such regions has its own transition temperatures, hence the transition occurred in a temperature range rather than at a particular temperature.

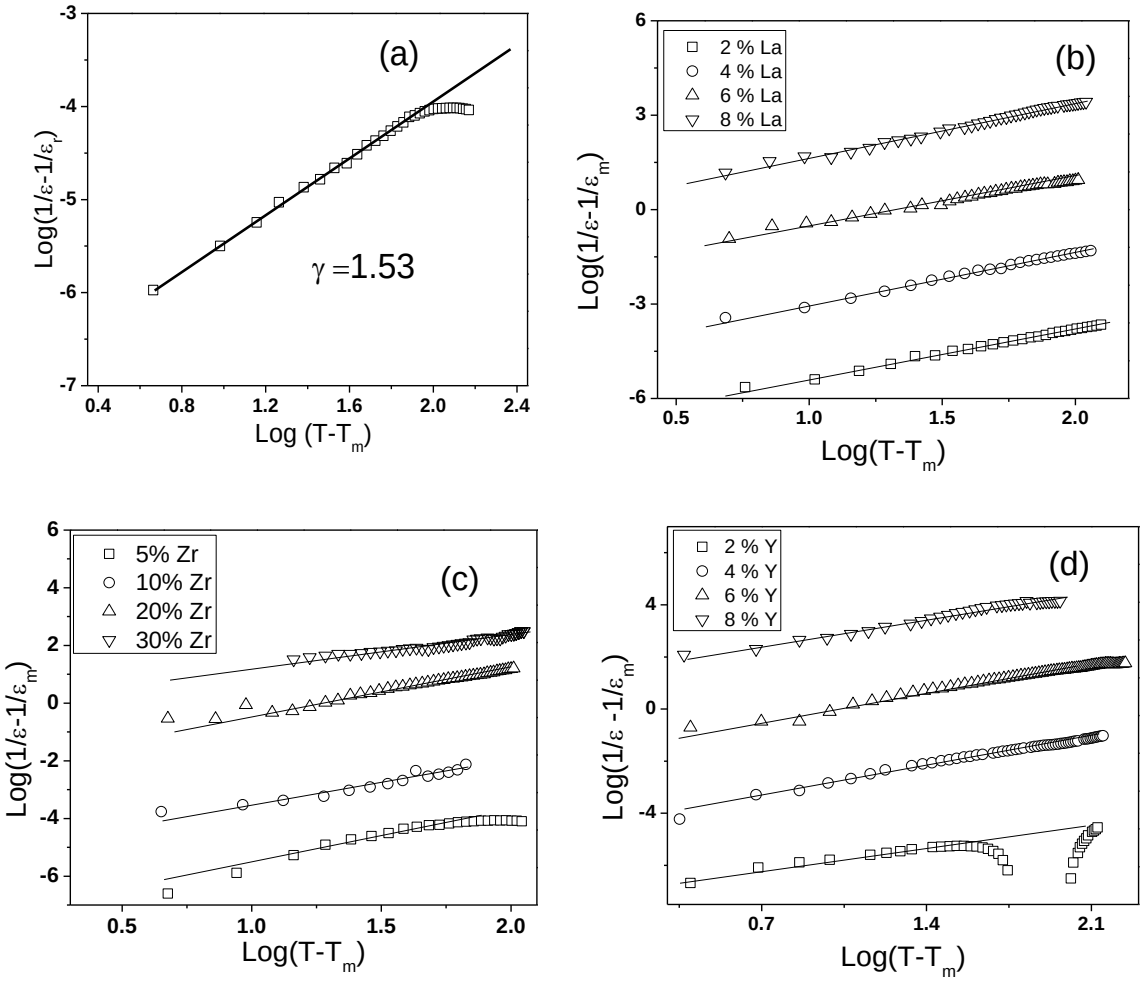

Fig. 4.12 Diffusivity curve for (a) NBT, (b) La modified NBT, (c) Zr modified NBT, (d) Y modified NBT.

Table 4.4 Comparison of γ (diffusivity) of NBT and modified NBT.

La modified NBT		**Zr modified NBT**		**Y modified NBT**	
2%	1.61	5%	1.81	2%	1.27
4%	1.69	10%	1.59	4%	1.64
6%	1.60	20%	1.73	6%	1.63
8%	1.73	30%	1.22	8%	1.71

References

[1] R.N.P. Choudhary, D. K. Pradhan, G.E. Bonilla, R.S. Katiyar, Effect of La-substitution on structural and dielectric properties of $Bi(Sc_{1/2}Fe_{1/2})O_3$ ceramics. Journal of Alloys and Compound, 437 (2007) 220.

[2] D. Maurya, S. Tiwari, J. Kumar and P. Chand Dielectric-spectroscopic and a.c. conductivity investigations on copper doped layered $Na_{1.8}K_{0.2}Ti_3O_7$ ceramics. Solid State Communication, 139 (2006) 295.

[3] I. G. Siny, C. S. Tu, and V. H. Schmidt, Critical acoustic behavior of the relaxor ferroelectric $Na_{1/2}Bi_{1/2}TiO_3$ in the intertransition region. Physics Review B, 51 (1995) 5659.

[4] P. K. C. Pillai and S. Chandrasekhar, Dielectric changes in ZnTe. Applied Physics A: Material Science Processes, 20 (1979) 175.

[5] Y. Zhu, X. Zhang, P. Gu, P. C. Joshi and S. B. Desu, Electrical properties of ferroelectric $(SrBi_2Ta_2O_9)_{1-x}(BiTiNbO_9)$ solid solution. Journal of Physics: Condensed Matter, 9 (1997) 10225.

[6] R. Rai, S. Sharma and R. N. P. Choudhary, Dielectric and piezoelectric studies of Fe doped PLZT ceramics. Materials Letter, 59 (2005) 3921.

[7] X. D. Betriu, J. E. Garcia, C. Ostos, A. U. Boya, D. A. Ochoa, L. Mestres and R. Perez Phase transition characteristics and dielectric properties of rare-earth (La, Pr, Nd, Gd) doped $Ba(Zr_{0.09}Ti_{0.91})O_3$ ceramics. Materials Chemistry and Physics, 125 (2011) 493.

Chapter 5

CONDUCTIVITY, IMPEDANCE,

AND MODULUS SPECTROSCOPIC STUDIES

5.1 A.C. Conductivity Study

Ferroelectric materials are polar dielectrics which normally possess small but finite electrical conductivity. The conduction at lower temperature is due to the impurities and defects while at higher temperature it is the intrinsic property of the material [1]. All the mechanisms of conduction in ferroelectric material are temperature dependent phenomena and follows Arrhenius behavior in a particular temperature range. The a.c. conductivity of the material contains frequency independent a.c. conductivity in the low frequency region and frequency dependent a.c. conductivity in the high frequency region. The variation of a.c. conductivity with temperature shows maxima around the ferroelectric-paraelectric phase transition temperature for all frequencies. This behavior can be attributed to the relaxation

process associated with the domain reorientation, domain wall motion, and the dipolar behavior [2].

5.1.1 $(Na_{0.5}Bi_{0.5})TiO_3$

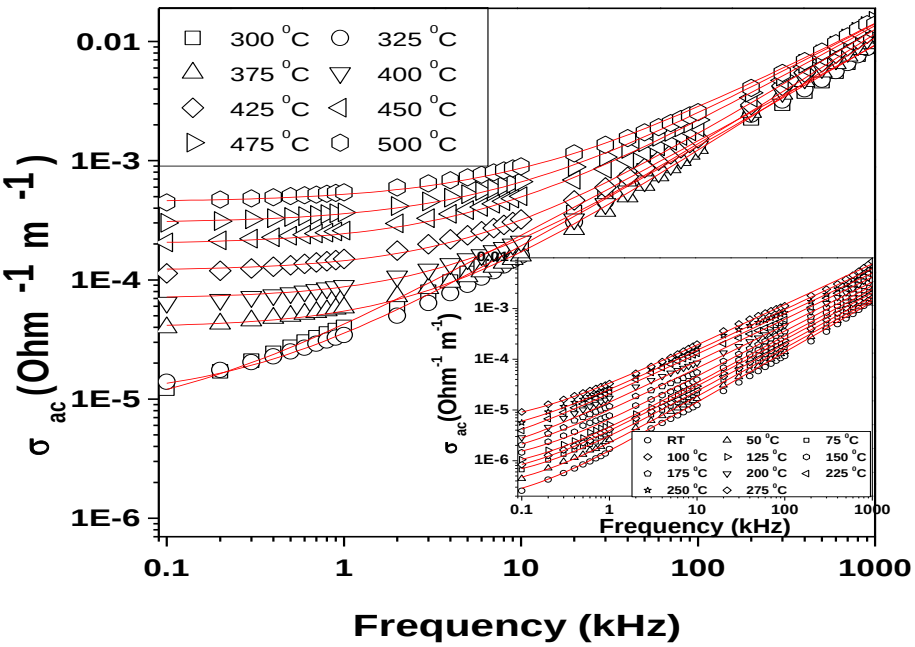

Fig. 5.1 Variation of a.c. conductivity with frequency at different temperature of $(Na_{0.5}Bi_{0.5})TiO_3$.

The a.c. conductivity is calculated from dielectric data using the relation: $\sigma_{ac}=\varepsilon_o\varepsilon_r\omega\tan\delta$. The variation of a.c. electrical conductivity (σ_{ac}) of $(Na_{0.5}Bi_{0.5})TiO_3$ as a function of frequency at different temperatures is shown in Fig. 5.1. The conductivity spectrum displays characteristic conductivity dispersion throughout the frequency range below 325 ^{0}C. At higher temperatures (≥ 325 ^{0}C), a low frequency independent plateau is observed, whereas in the higher frequency region dispersion of

conductivity is still retained. The crossover from the frequency independent region to the frequency dependent regions shows the onset of the conductivity relaxation, indicating the transition from long range hopping to the short range ionic motion. The frequency of onset of conductivity relaxation shifts with temperature to higher frequency side. The frequency dependence of a.c. conductivity obeys Jonscher's power law. $\sigma_{ac}=\sigma_0+A\omega^n$, where σ_0 is frequency independent conductivity (which is related to d.c. conductivity), A is the temperature dependent pre-exponential factor and n is frequency exponent, ($0 \leq n \leq 1$). In the conductivity spectra, the symbols denote the experimental data and the solid line represents the fitting of the experimental data to Jonscher's power law. The A, n and σ_{dc} are the fitted parameters. A close agreement between the experimental data and the fitted solid line has been observed from Fig. 1.

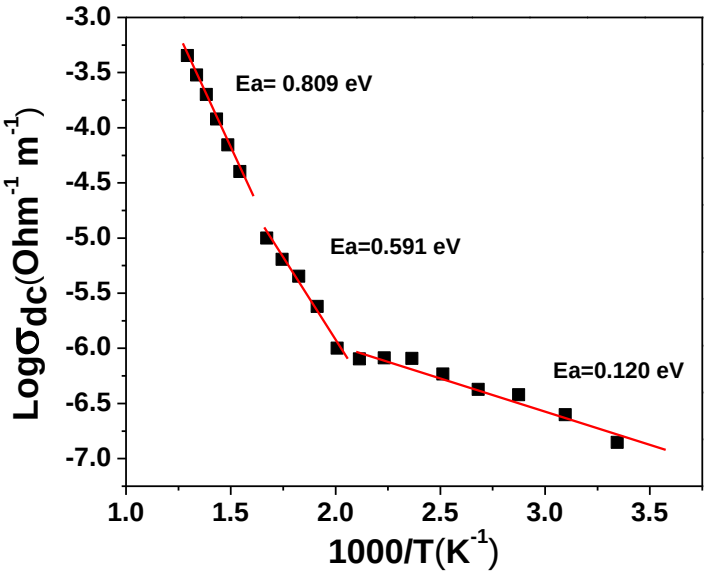

Fig 5.2 Variation of d.c. conductivity with inverse of absolute temperature of $(Na_{0.5}Bi_{0.5})TiO_3$.

The variation of d.c. conductivity with inverse of absolute temperature (i.e. log σ_{dc} vs. $10^3/T$) of $(Na_{0.5}Bi_{0.5})TiO_3$ is shown in Fig. 5.2. The temperature dependence of d.c. conductivity can be explained by the empirical relation: $\sigma=\sigma_p exp(-E_a/kT)$, (k = Boltzmann constant, E_a= activation energy and σ_p = pre-exponential factor). The value of E_a can be calculated from the slope of log σ_{dc} vs. $10^3/T$ (K^{-1}) plot. From the figure, it has been observed that there are three different slopes in the temperature range from room temperature to 500 ^{0}C and each slope corresponds to the activation energy in some particular temperature ranges. Hence, there are distinct value of activation energies in the different temperature ranges; (i) from room temperature to 200 ^{0}C, activation energy found to be 0.12 eV, ii) from 225 ^{0}C to 300 ^{0}C, activation energy is found to be 0.59 eV, and (iii) from 325 ^{0}C to 500 ^{0}C, activation energy found 0.81 eV.

The motion of domain wall (both migration and gliding along with spatial domain configuration) becomes complex when there is a structural phase change of rhombohedral to tetragonal and in coexistence region. The different activation energy in different temperature region is due to the different in conductivity mechanism and domain configuration [3]. The obtained low value of E_a (0.12eV) in the rhombohedra structural phase may be due to the carrier transport mechanism associated with the hopping between localized states $Ti^{4+}+e^{-1}\rightarrow Ti^{3+}$ by oxidation or reduction process in a disordered manner by n/p type hopping charge carrier. The intermediate value of the activation energy (0.59eV) may be attributed to the small polarons created by the electron and/or hole-phonon interaction which is enhanced by the structural deformation by the transition between rhombohedral and tetragonal phases. The higher value of activation energy (0.81 eV) may be due to the oxygen vacancy [3].

Also the motion of domain wall occurs with the increase of temperature but pinning of the motion of domain walls arises due to the deposition of excess oxygen vacancy at higher temperature. It is also responsible for higher activation energy at high temperatures. The high value of conductivity in NBT may be considered due to (i) Bi vacancies (ii) oxygen vacancies, ($V^{\cdot}$ or $V^{\cdot\cdot}$) creation during the sintering process. The conductivity of NBT increases with rise in temperature. It confirms the negative temperature coefficient of resistance (NTCR) behavior similar to that of semiconductors.

5.1.2 La modified NBT

The variation of a.c. conductivity with frequency at different temperature of$(Na_{0.5}Bi_{0.5})_{(1-x)}La_xTi_{(1-x/4)}O_3$, x=0.02, 0.04, 0.06, 0.08 are shown in Fig. 5.3 (a, b, c, d), respectively. The double power law has been used to fit the a.c. conductivity of the material is given by: $\sigma_{ac}=\sigma_{dc}+A\omega^n+B\omega^m$ where σ_{dc} is frequency independent conductivity related to d.c. conductivity, *A* and *B* are the temperature dependent pre-exponential factor, and *n* and *m* are frequency exponent. The value of *n* less than unity corresponds to the translational hopping motion, whereas the value of *m* less than two corresponds to a localized or representational hopping motion [4]. Three regions are observed in the conductivity spectrum. The long-range translational hoping in the low frequency region gives rise to σ_{dc}. The short-range translational hoping at intermediate frequency and localized or representational hopping motion at high frequency are assigned by $A\omega^n$ and $B\omega^m$ terms, respectively. The σ_{ac} decreases noticeably by the addition of La into NBT throughout the frequency range. As σ_{ac}

increases with rise in temperature, all the compounds have a negative temperature coefficient of resistance (NTCR) behavior. The observed conduction spectra can be explained by jump relaxation model (JRM) and grain boundaries conduction [5]. As per the JRM model, at the low frequency, the conductivity is mainly due to the substantial successful hopping of ions between A–site and B–site but more and more hops are significantly restricted at higher frequency. The frequency dispersion is due to the change in ratio of successful to unsuccessful hops on increase in the frequency. The JRM suggests that different activation energies are associated with successful and unsuccessful hopping processes [6].

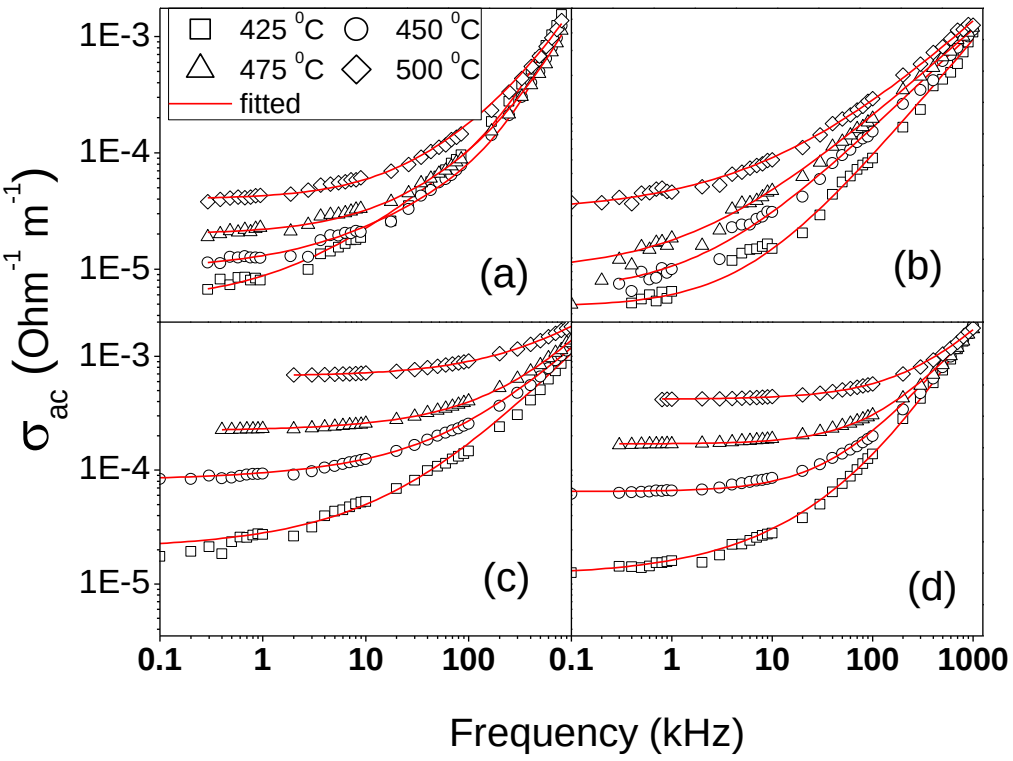

Fig. 5.3 Variation of a.c. conductivity with frequency at different temperatures of $(Na_{0.5}Bi_{0.5})_{(1-x)}La_xTi_{(1-x/4)}O_3$, (a) x=0.02, (b) x=0.04, (c) x=0.06, (d) x=0.08.

The variation of d.c. conductivity with absolute temperature of $(Na_{0.5}Bi_{0.5})_{(1-x)}La_xTi_{(1-x/4)}O_3$, x= 0.02, 0.04, 0.06, 0.08 are shown in Fig. 5.4. It can be seen from the figures that the d.c. conductivity of La modified NBT shows Arrhenius behavior. The calculated activation energy is found to be 1.22, 0.89, 2.06, 2.10 eV for 2, 4, 6, 8 % La modified NBT, respectively. The high values of activation energy may be due to oxygen vacancies and/or A-site cation vacancies at high temperature (above 325 ^{0}C) [7].

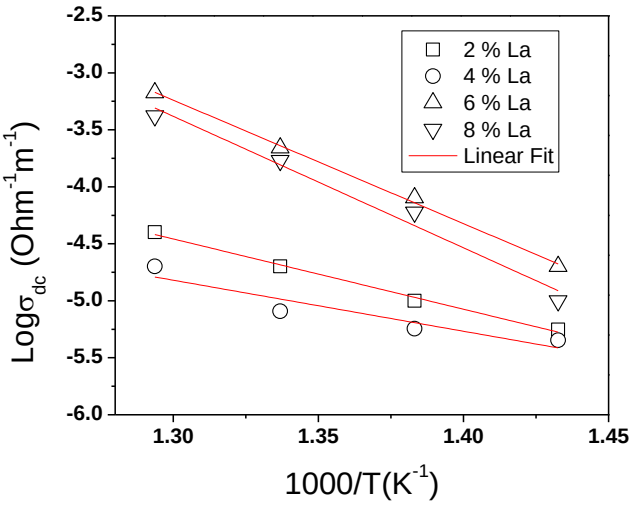

Fig. 5.4 Variation of d.c. conductivity with inverse of absolute temperature of $(Na_{0.5}Bi_{0.5})_{(1-x)}La_xTi_{(1-x/4)}O_3$, x=0.02, 0.04, 0.06, 0.08.

5.1.3 Zr modified NBT

The variation of a.c. conductivity with frequency at different temperature of $(Na_{0.5}Bi_{0.5})Ti_{(1-x)}Zr_xO_3$, x=0.05, 0.1, 0.2, 0.3 are shown in Fig. 5.5 (a, b, c, d), respectively. The Jonscher power law has been used to fit the a.c. conductivity data of

the material. There is a close agreement between the experimental and fitted data have been observed. The conductivity decreases with increase in the concentration of zirconium in NBT as well as with the increase in temperature.

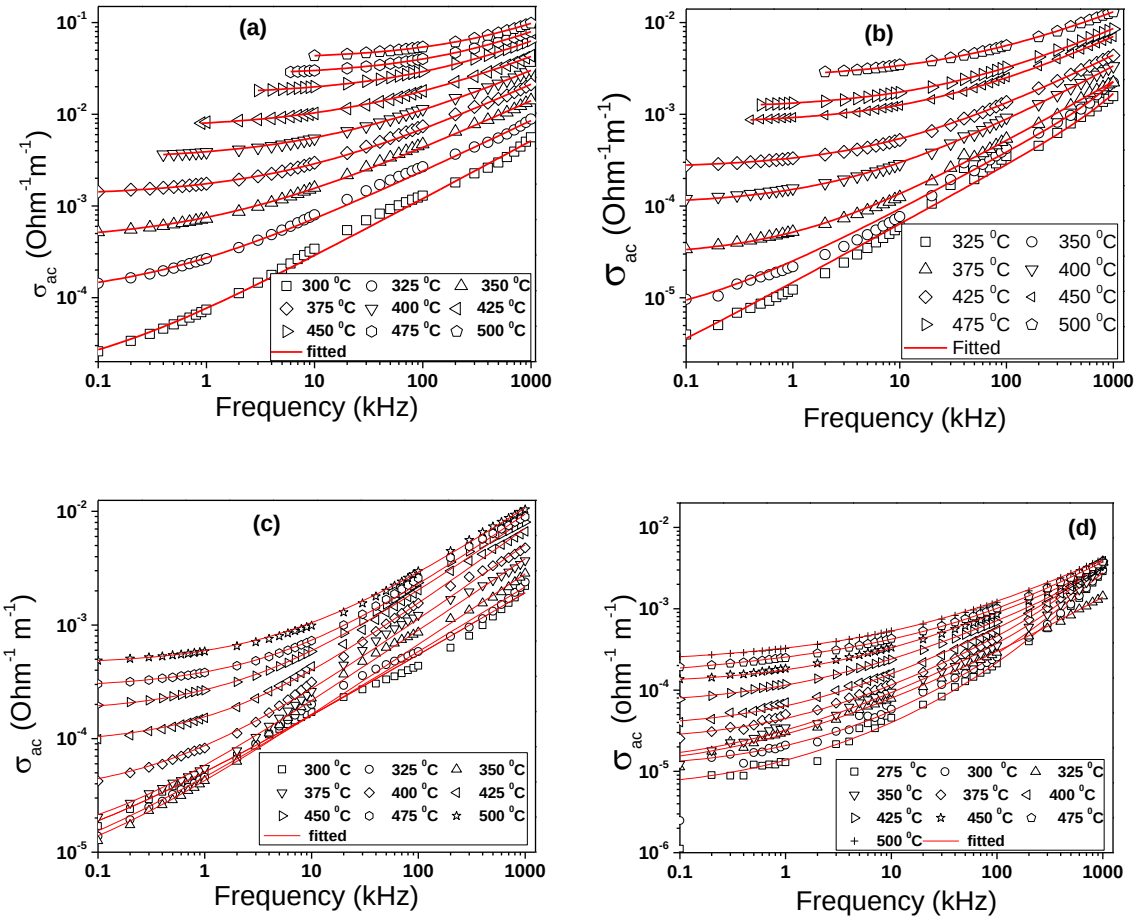

Fig. 5.5 Variation of a.c. conductivity with frequency at different temperatures of $(Na_{0.5}Bi_{0.5})Ti_{(1-x)}Zr_xO_3$, (a) x=0.05, (b) x= 0.1, (c) x=0.2, (d) x=0.3.

The variation of d.c. conductivity with inverse of absolute temperature of $(Na_{0.5}Bi_{0.5})Ti_{(1-x)}Zr_xO_3$, x=0.05, 0.1, 0.2, 0.3 are shown in Fig. 5.6. The temperature dependent d.c. conductivity of Zr modified NBT follows Arrhenius behavior. The

calculated activation energies are found to be1.37, 1.56, 1.19, and 0.65, for5, 10, 20, 30 % Zr modified NBT ceramics, respectively. The activation energy is observed to be increased with increase in Zr concentration up to 10 % then decreases may be due to the compositional variation. The high values of activation energy may be due to oxygen double ion vacancies at high temperature (above 300 ^{0}C) [7].

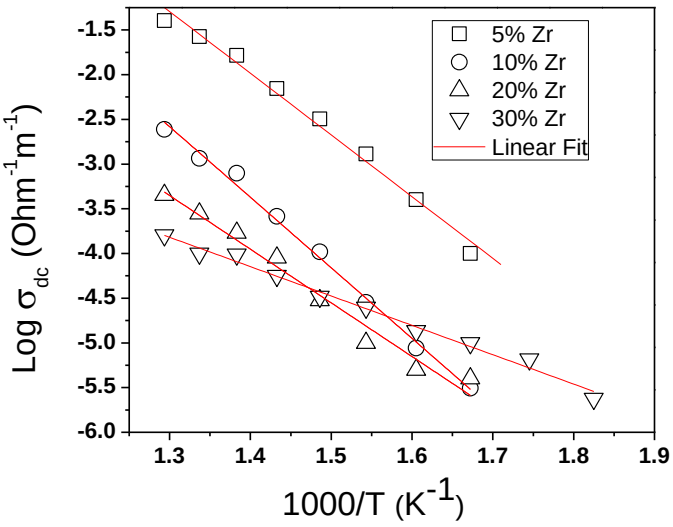

Fig. 5.6 Variation of d.c. conductivity with inverse of absolute temperature of $(Na_{0.5}Bi_{0.5})Ti_{(1-x)}Zr_xO_3$, x=0.05, 0.1, 0.2, 0.3.

5.1.4 Y modified NBT

The log-log plot of a.c. conductivity verses frequency at different measuring temperatures of $(Na_{0.5}Bi_{0.5})_{(1-x)}Y_xTi_{(1-x/4)}O_3$, x= 0.02, 0.04, 0.06, 0.08 are shown in Fig. 5.7 (a, b, c, d), respectively. It has been observed that the d.c. conductivity (i.e., frequency independent plateau in the figure) increases with increase in temperature

irrespective of Y modification. The a.c. conductivity spectrum of Y modified NBT obeys double power law feature.

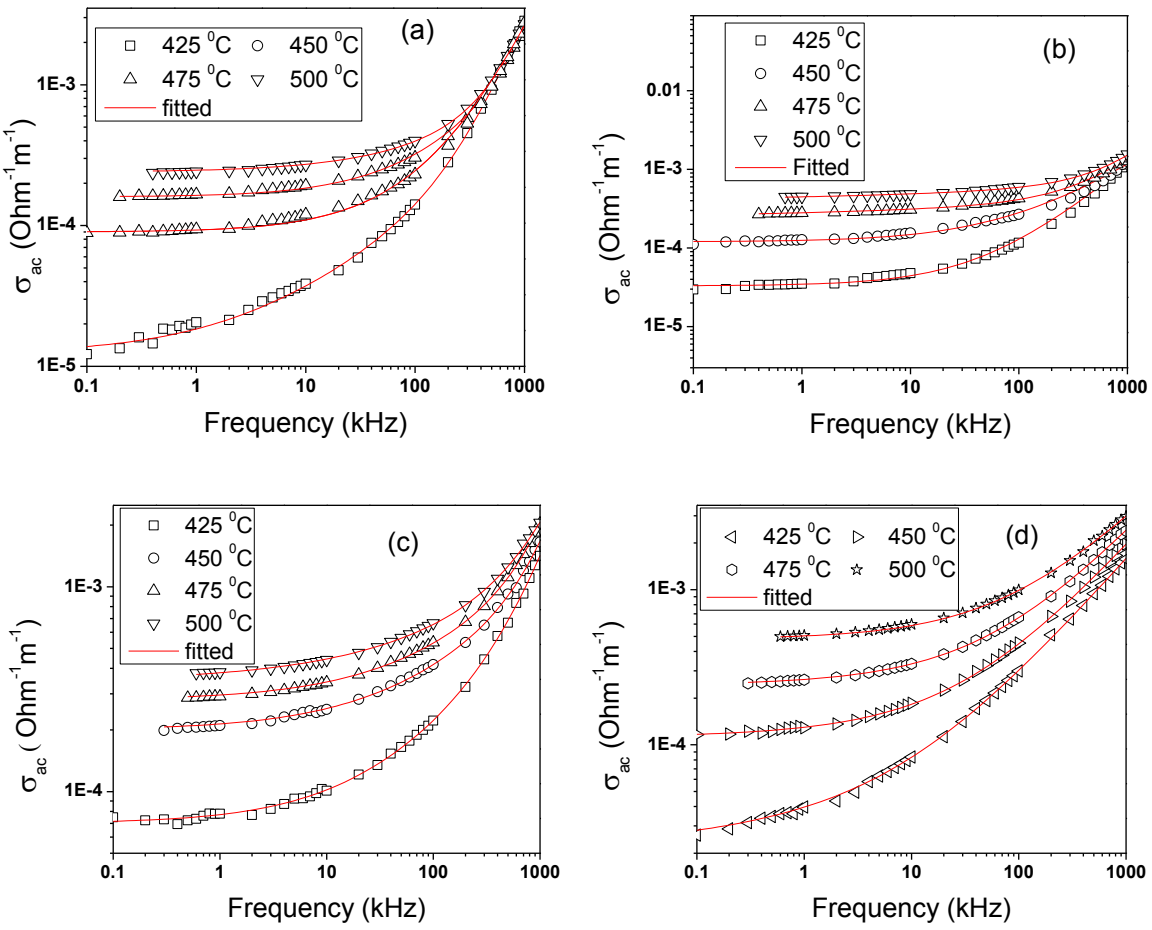

Fig. 5.7 Variation of a.c. conductivity with frequency of $(Na_{0.5}Bi_{0.5})_{(1-x)}Y_xTi_{(1-x/4)}O_3$, (a) x=0.02, (b) x=0.04, (c) x=0.06, (d)x=0.08 at different temperatures.

The variation of d.c. conductivity with inverse of absolute temperature of $(Na_{0.5}Bi_{0.5})_{(1-x)}Y_xTi_{(1-x/4)}O_3$, x=0.02, 0.04, 0.06, 0.08 are shown in Fig. 5.8. The d.c.

conductivity of Y modified NBT follows Arrhenius behavior. The calculated activation energy is 1.30, 1.26, 1.10, 1.80, for 2, 4, 6, 8 % of Y modified NBT ceramics.

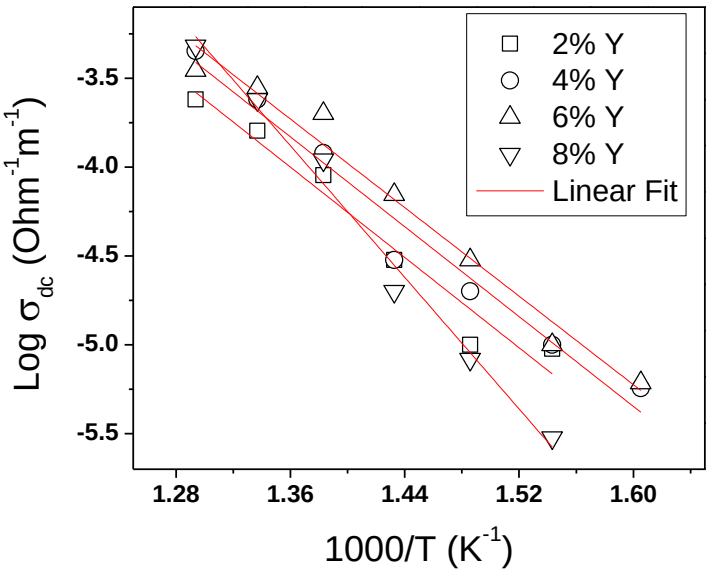

Fig. 5.8 Variation of d.c. conductivity with inverse of absolute temperature $(Na_{0.5}Bi_{0.5})_{(1-x)}Y_xTi_{(1-x/4)}O_3$, x=0.02, 0.04, 0.06, 0.08.

5.2 Impedance and modulus Spectroscopic Studies

The complex impedance spectroscopy (CIS) is a non-destructive method, used to analyze the electrical response of polycrystalline sample in a wide range of frequencies and temperatures [8]. In CIS a constant current signal (I) of variable frequency is applied to the object under test (OUT) and the potentials (V) developed across the OUT are measured at each frequency. Dividing the voltage measured by the applied current, the complex impedance is estimated. The complex impedance (Z) is a function of material properties which create a phase difference (θ) between I and V

[9]. Complex impedance formalism offers wide scope for a graphical analysis of the various parameters under different conditions of temperature and frequency.

The CIS technique easily separates bulk (grain), grain boundary, and material electrode contributions in the electrical properties of the materials. Sometimes it is difficult to interpret the data whether the response is due to long-range conductivity (delocalized) or dipole relaxation (localized) of materials. Both localized and delocalized conduction are bulk processes, and therefore this gives rise to the same geometrical capacitance. The use of the imaginary part of the impedance (Z'') and conductance (Y'') is particularly appropriate for resistive and/or conductive analysis (when the long range conductivity is dominant) whereas the imaginary part of the permittivity (ε'') and electrical modulus (M'') are suitable when localized relaxation dominates. In the case of multiferroic materials, a combination of all the impedance formalisms is the best strategy to distinguish between the ferroelectric and non-ferroelectric properties of the materials.

5.2.1 $(Na_{0.5}Bi_{0.5})TiO_3$

The variations of imaginary part of impedance with frequency at different temperatures of $(Na_{0.5}Bi_{0.5})TiO_3$ are shown in Fig. 5.9(a). The value of Z'' decreased with increase in frequency at low temperatures. On and above 375 ^{0}C, a peak is appearing. The peak position shifts towards higher frequency side with rise in temperature. As well as the width of the peak also broadened with increasing temperature. The asymmetric broadening of peaks in Z'' with frequency suggests that there is a spread of relaxation time. Also the shifting of relaxation peak indicates

the existence of a temperature dependent electrical relaxation phenomenon in the material.

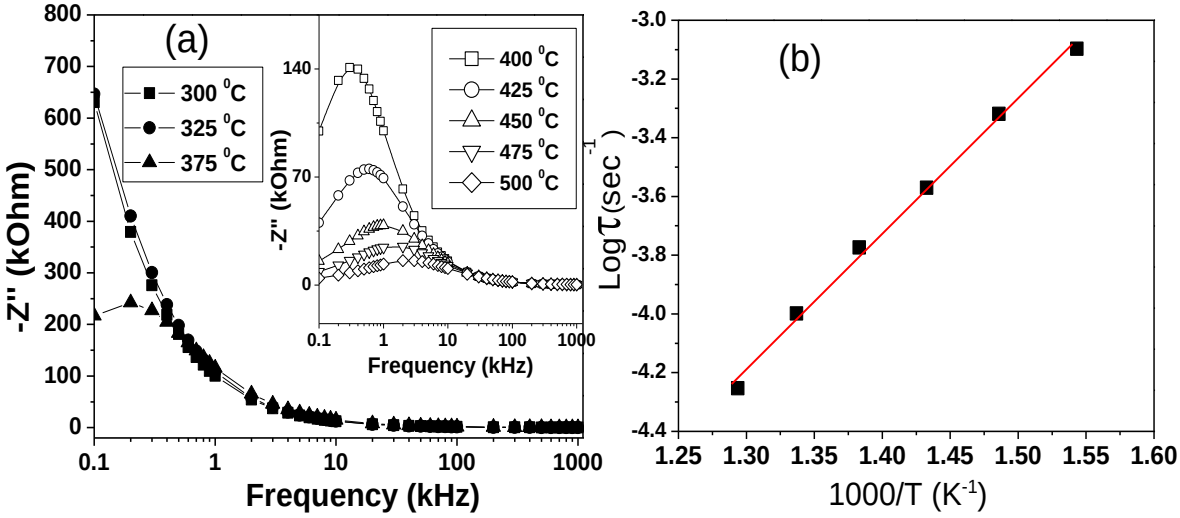

Fig. 5.9 (a, b) Variation of Z'' with frequency at various temperatures and Log τ_Z Vs. 1000/T of $(Na_{0.5}Bi_{0.5})TiO_3$, respectively.

The variation of relaxation time with the inverse of absolute temperature of $(Na_{0.5}Bi_{0.5})TiO_3$ is shown in Fig. 5.9 (b). The relaxation time $\tau_{Z''}$ is calculated from Z'' vs. frequency plot using the formula $\omega_{max}\tau=1$. The temperature dependence of relaxation time follows the Arrhenius behavior govern by the relation, $\tau = \tau_0 \exp(E_a/kT)$ where τ_0 is a pre-exponential factor, E_a is the activation energy, k is the Boltzmann constant, and T is the absolute temperature. The activation energy evaluated from the slope of log $\tau_{Z''}$ against $10^3/T$ curve is found to be 0.91 eV. The activation energy obtained from the Z'' spectra represent the localized conduction (i.e., dielectric relaxation) of the material.

The complex impedance spectrum (Nyquist plot) of $(Na_{0.5}Bi_{0.5})TiO_3$ at different temperatures is shown in Fig.5.10 (a). The temperature dependence of Nyquist plots show a clear change in the pattern of evolution of impedance spectrum. At low temperatures (≤ 325 ^{0}C) straight line is observed indicating the insulating properties of the material. Above 375 ^{0}C, a semicircular arc start forming and finally semicircular arcs become more resolved with rise in temperature. The presence of single semicircular arc is due the bulk property of material. At higher temperature (> 450 ^{0}C) the plot can be characterized by the presence of two overlapping of semicircular arcs with their centers lying below the real axis. The high frequency semicircle could be attributed to the bulk (grain) property of the material. The low frequency arc of the impedance spectrum (at elevated temperatures) has been attributed to the presence of grain boundary. The assignment of the two semi-circular arcs to the electrical response due to grain interior and grain boundary is consistent with the *brick-layer* model for a polycrystalline material. The comparison of imaginary component of complex impedance and that of electrical modulus versus frequency is shown in Fig. 5.10 (b) as representatively. It has been found that both the Z'' and M'' peaks as a function of frequency differ in symmetry and the peak position. It suggests the departure from the ideal Debye behavior and justifies the presence of a constant phase element (CPE) [13] in fitting of the circuit. The CPE admittance is generally represented as: $Y(\mathrm{CPE}) = A_0(j\omega)^n = A\omega^n + jB\omega^n$, [10] where, $A = A_0\mathrm{Cos}(n\pi/2)$ and $B = A_0\mathrm{Sin}(n\pi/2)$. A_0 and n are frequency independent but temperature dependent parameters, A_0 determines the magnitude of the dispersion and it varies between zero to one ($0 \le n \le 1$). The CPE describes an ideal capacitor for n=1 and an ideal

resistor for *n*=0. The equivalent circuit for the observed two overlapping semicircular arcs of the impedance spectrum can be modeled by a series array of parallel combination of (i) a resistance (bulk resistance), capacitance (bulk capacitance) and a CPE, with another parallel combination of (ii) a resistance (grain boundary resistance), capacitance (grain boundary capacitance) as shown in Fig. 5.10(a).

The impedance data (symbols) have been fitted (solid line) with the proposed model by commercially available software ZSIMP WIN Version 2 as shown in Fig.5.10 (a). It has been found that there is a close agreement between the observed and fitted values. The grain and grain boundary resistances decreases as the intercept of semicircular arc on real axis reduced with the rise in temperature. It suggests that with increase in temperature the bulk conductivity increases, which is a typical behavior of semiconductors.

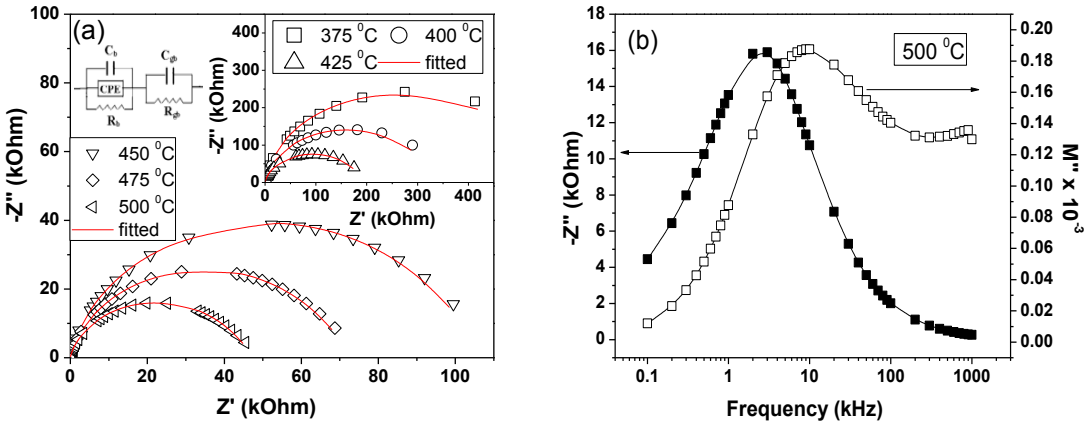

Fig. 5.10 Nyquist plot of $(Na_{0.5}Bi_{0.5})TiO_3$ at various temperatures (a) and variation of imaginary electrical modulus (M'') and imaginary impedance (Z'') with frequency of $(Na_{0.5}Bi_{0.5})TiO_3$ at 500 ^{0}C (b).

Electrical response of the ferroelectric material can also be analyzed using complex electric modulus formalism. The complex electric modulus formalism is based on polarization analysis. Complex impedance plot is more effective for the elements with the high resistance but complex electric modulus plots useful for smallest capacitance elements [11]. Using the complex electric modulus formalism the inhomogeneous nature of polycrystalline ceramics can be separated into bulk and grain boundary effects, which is some time not clearly distinguished from complex impedance plots. One of the interesting advantages of the electric modulus formalism is that it suppresses the electrode effect [12].

The variation of imaginary part of electrical modulus (M'') of $(Na_{0.5}Bi_{0.5})TiO_3$ with frequency at different temperatures is shown in Fig. 5.11(a, b) as representatively. It is observed that M'' decreases with increase in frequency at lower temperatures but above 200 ^{0}C, variation of M'' with frequency attains a maximum value (peak) at a particular frequency, and that peak is shifted to higher frequency with rise in temperature. These peaks indicate the transition from long range to short range mobility with increase in frequency. At the low frequency (of the peak), the ions are capable of moving long distances, (i.e., performing successful hopping from one site to the neighboring site). But for the high frequency side of peak, the ions are spatially confined to their potential wells and can execute only localized motion within the well [13]. Again above 375 ^{0}C another peak appears. The appearance of two peaks in M'' verses frequency plots again confirms the presence of both grain and grin boundary effect in the material. These capacitances of different contributor (grain and grain boundary) are comparable even with large difference between the

two resistances contributions. So two resolve peaks are observed in M'' verses frequency plots, which is not clearly observed in Z''vs. frequency plot. The peak indicates the conductivity relaxation occurring in the material.

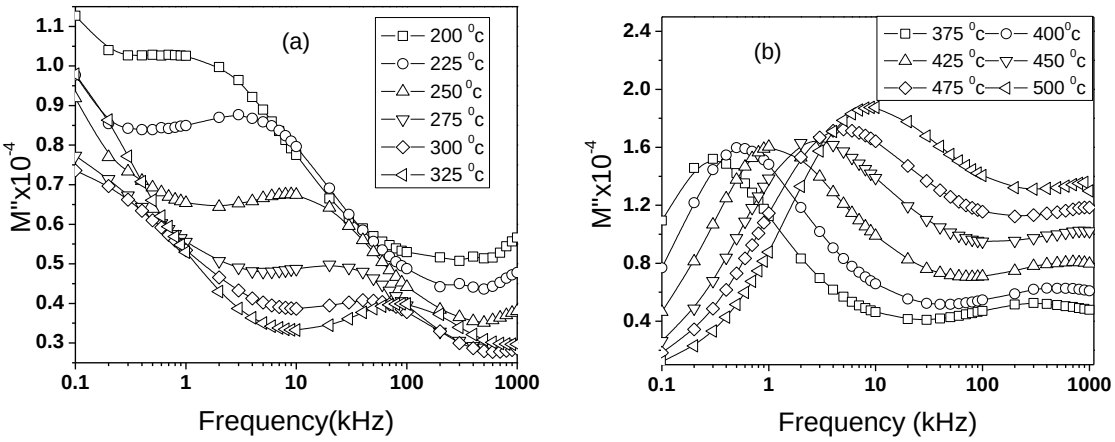

Fig. 5.11 (a, b) Variation of M'' with frequency at different temperature of $(Na_{0.5}Bi_{0.5})TiO_3$.

The peak in the M″ vs. frequency plot is asymmetric in nature indicating the spread of relaxation time. The asymmetric nature of the modulus peak indicates the stretched exponential character of relaxation time. It can be explained by Kularch-William-Watt (KWW) stretched non-exponential function. $\phi(t) = \exp(-t/\tau)^{\beta}$ where $\phi(t)$ is the relaxation of electric field,τ is the characteristic time and β is the relaxation parameter denoting the distribution of relaxation time[10]. This behavior may be due to the non-exponential process, such as correlated diffusive motion of the ions or non-uniform microstructure in the material [14]. The FWHM of the peak is observed to be more than Debye peak (1.14 decades). It also suggests that the relaxation process is non-Debye type. The peaks are got more broadened after phase

transition with increase of temperature showing the increase of non-Debye behavior. This temperature dependent of relaxation time follows the Arrhenius behavior.

5.2.2 La modified NBT

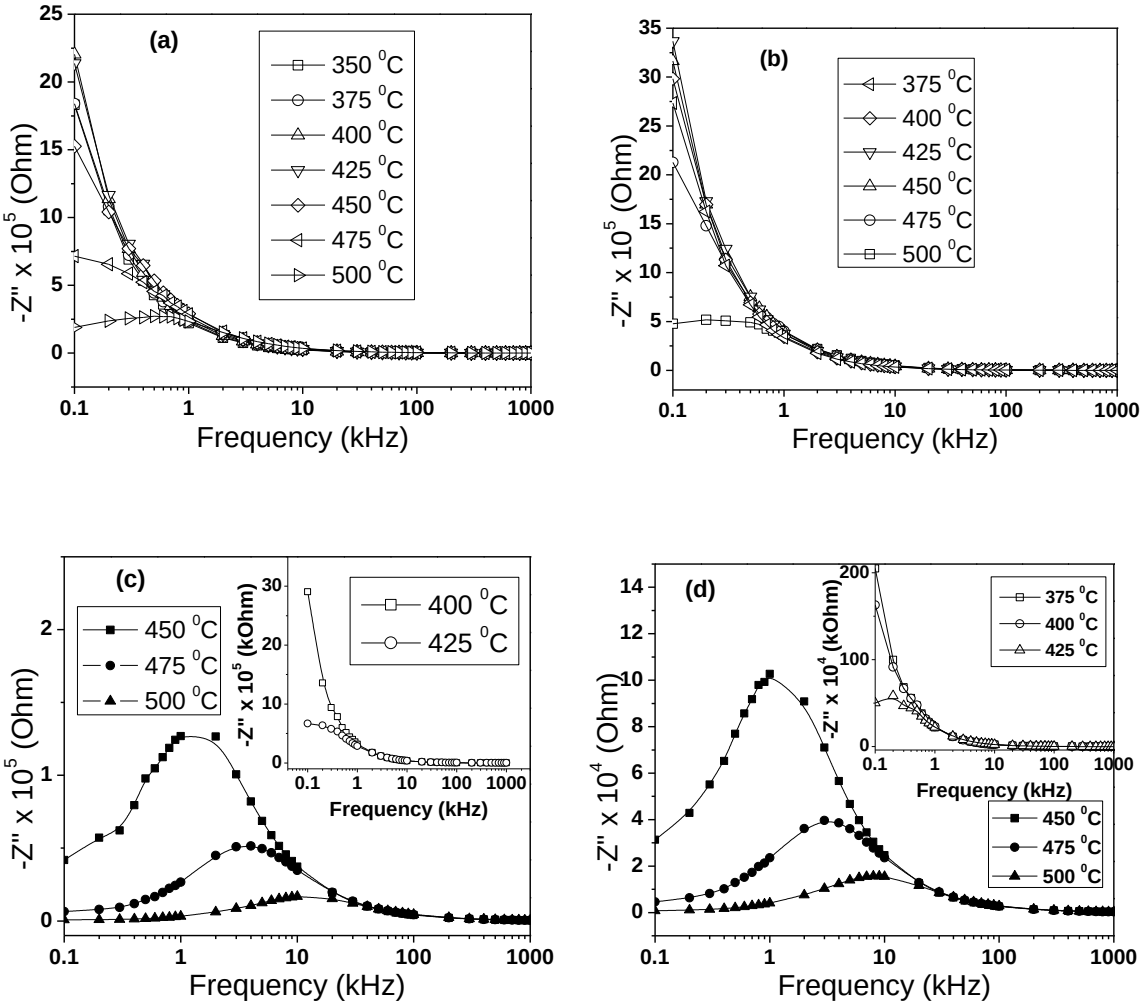

Fig. 5.12 Variation of imaginary part of impedance with frequency of $(Na_{0.5}Bi_{0.5})_{(1-x)}La_xTi_{(1-x/4)}O_3$, (a) x=0.02, (b) x=0.04, (c) x=0.06, (d) x=0.08 at various temperatures.

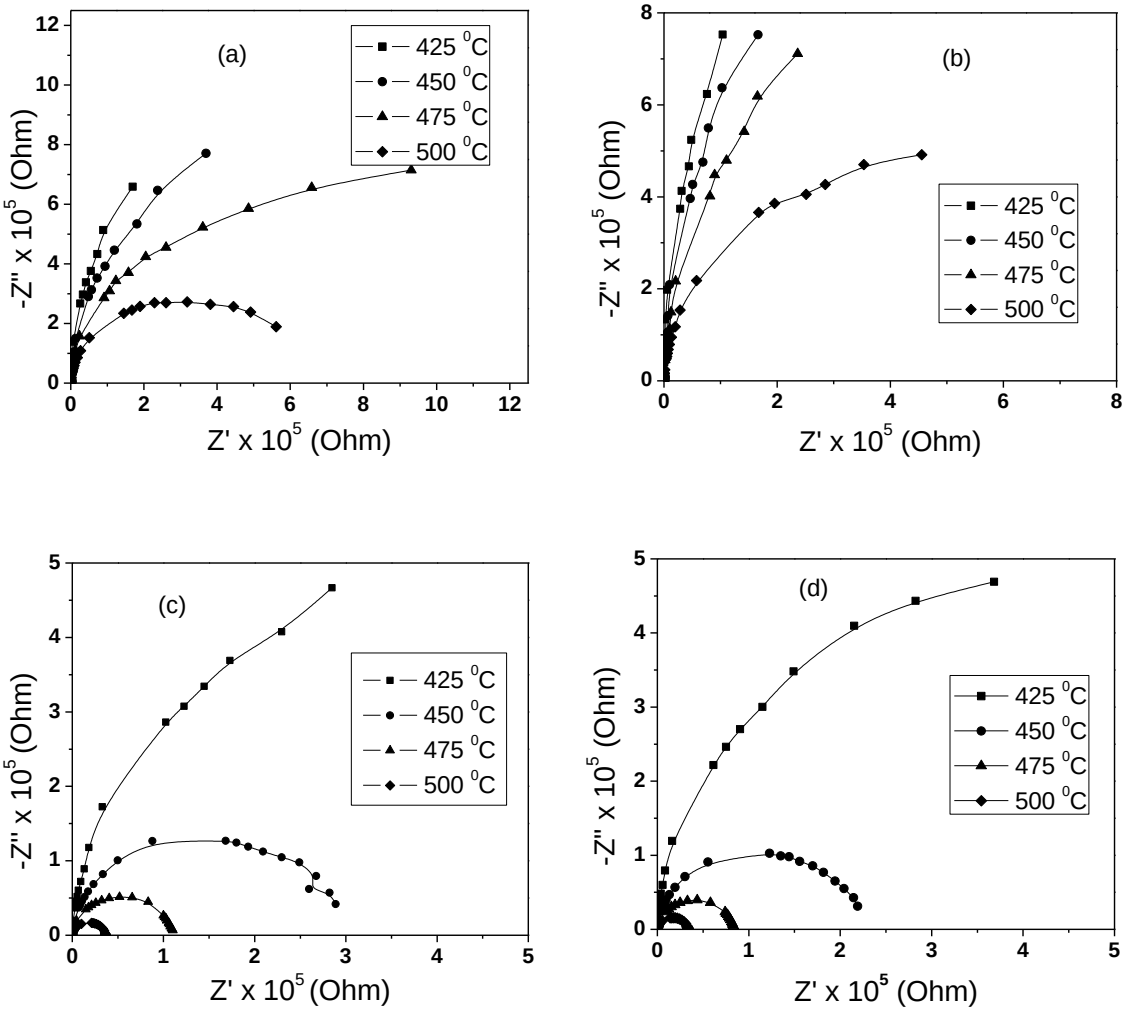

Fig. 5.13 Nyquist plot of $(Na_{0.5}Bi_{0.5})_{(1-x)}La_xTi_{(1-x/4)}O_3$, (a) x=0.02, (b) x=0.04, (c) x=0.06, (d) x=0.08 at various temperatures.

The variation of imaginary part of impedance as a function of frequency of $(Na_{0.5}Bi_{0.5})_{(1-x)}La_xTi_{(1-x/4)}O_3$, x= 0.02, 0.04, 0.06, 0.08 are shown in Fig. 5.12 (a, b, c, d), respectively. The magnitude of Z″ at the peak (Z''_{max}) decreases with increase in temperature and the corresponding f_{max} shifts towards higher frequency side. This indicates the decrease of relaxation time with increase in temperature. The

asymmetric broadening of the peaks of Z″ with frequency plot suggests the presence of distributed relaxation process. The observed peak position and the value of (Z''_{max}) are different for different La content in NBT at a constant temperature.

The temperature dependence of complex impedance spectra (Nyquist plot) of $(Na_{0.5}Bi_{0.5})_{(1-x)}La_xTi_{(1-x/4)}O_3$, x= 0.02, 0.04, 0.06, 0.08 are shown in Fig. 5.13 (a, b, c, d), respectively. The linear variation of Z″ with Z′ between room temperature and 400 ºC (not shown) is observed. Above 400 ^{0}C, a trend of formation of circular arc is started due to the increase in conductivity. The impedance plots (Fig. 5.13) seem to have over lapping of two semicircles. The observed depressed semicircular arcs have center lies below real impedance (Z′) axis. The relaxation process associated with this observation is non-ideal in nature. This non-ideal behavior may be originated from the several factors such as grain orientation, grain size distribution, grain boundaries, atomic defect distribution, and stress–strain phenomena [15]. It is seen from the Fig. 5.13, that the d.c. resistance sharply decreases with increase in the temperature as well as the La content in NBT.

5.2.3 Zr modified NBT

The variation of imaginary part of impedance with frequency at different temperature of $(Na_{0.5}Bi_{0.5})Ti_{(1-x)}Zr_xO_3$, x= 0.05, 0.1, 0.2, 0.3 are shown in Fig.5.14 (a, b, c, d), respectively. The values of Z'' decreases with rise in frequency at lower temperatures. At higher temperature a peak is observed in all compounds but the appearance of peak at a particular temperature are different for different compounds (325 ^{0}C for 5 %, 350 ^{0}C for 10 %, 400 ^{0}C for 20 and 30 % of Zr content in NBT).

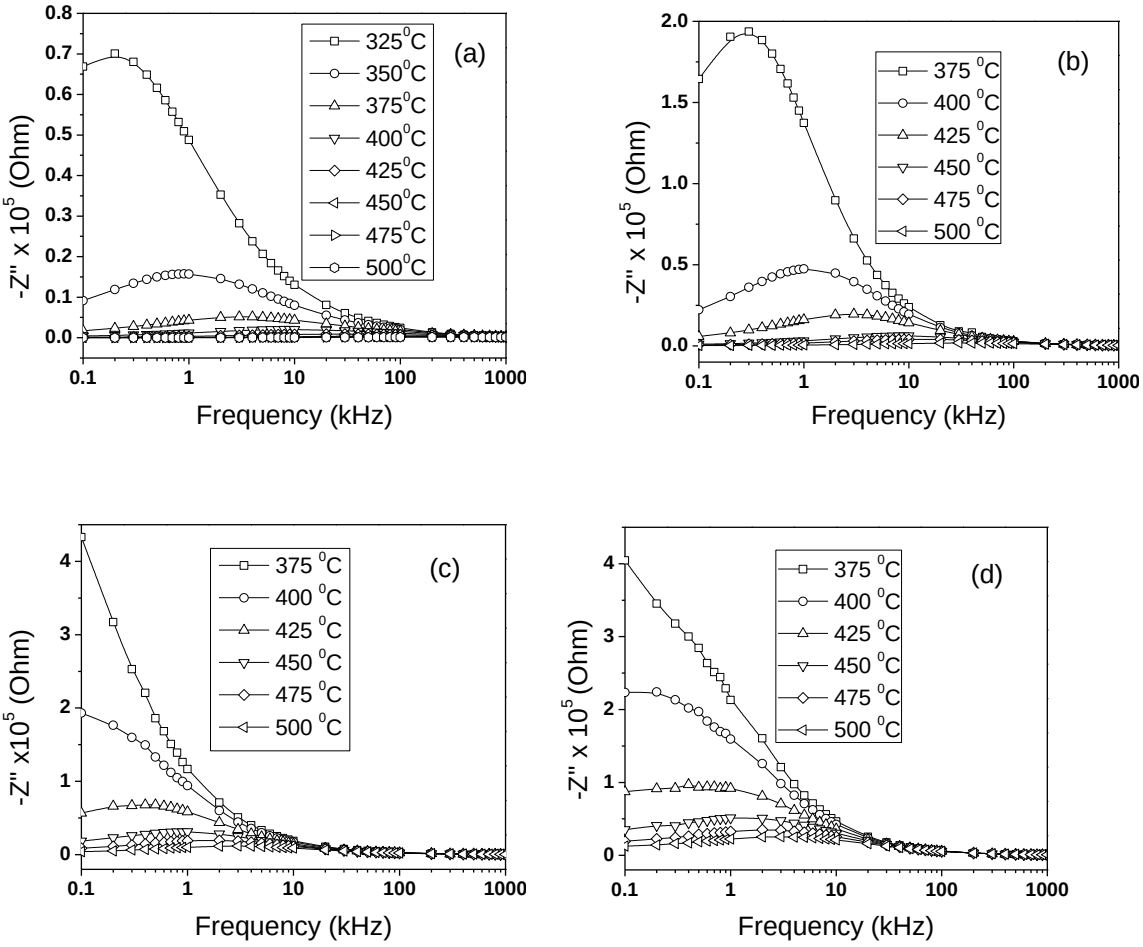

Fig. 5.14 Variation of Z'' with frequency of $(Na_{0.5}Bi_{0.5})Ti_{(1-x)}Zr_xO_3$, (a) x=0.05,(b) x= 0.1, (c) x=0.2, (d) x=0.3.

The variation of relaxation time with inverse of temperature of $(Na_{0.5}Bi_{0.5})Ti_{(1-x)}Zr_xO_3$, x= 0.05, 0.1, 0.2,0.3 are shown in Fig. 5.15. The temperature dependence of relaxation frequency follows the Arrhenius behavior. The activation energy evaluated from the slope of log Z'' against $10^3/T$ curve is found to be 1.609, 1.047, 1.319, 0.728 eV for 5 %, 10 %, 20 % and 30 % Zr modified NBT, respectively.

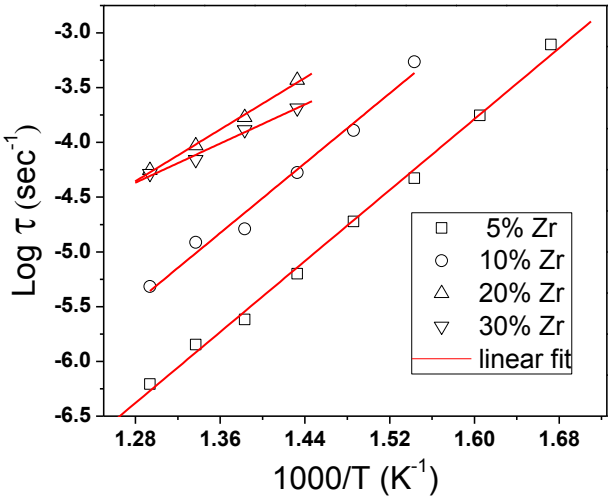

Fig. 5.15 Variation of τ_z with inverse of absolute temperature of $(Na_{0.5}Bi_{0.5})Ti_{(1-x)}Zr_xO_3$,(a) x=0.05,(b) x=0.1, (c) x=0.2, (d) x=0.3.

The complex impedance spectrum of $(Na_{0.5}Bi_{0.5})Ti_{(1-x)}Zr_xO_3$, x= 0.05, 0.1, 0.2, 0.3 at different temperatures are shown in Fig.5.16 (a, b, c, d), respectively. The presence of a single semicircular arc up to a temperature of 375 ^{0}C indicates that the electrical processes in the material may be due to bulk properties. The impedance patterns appear to be overlapping of two semicircular arcs with rise in temperature (> 450 ^{0}C) indicates the appearance of grain boundary contribution. An equivalent electrical circuit can be modeled for the observed electrical phenomena in the material, according to brick layer model. It has been observed that both the grin and grain boundary resistances decreases with rise in temperature.

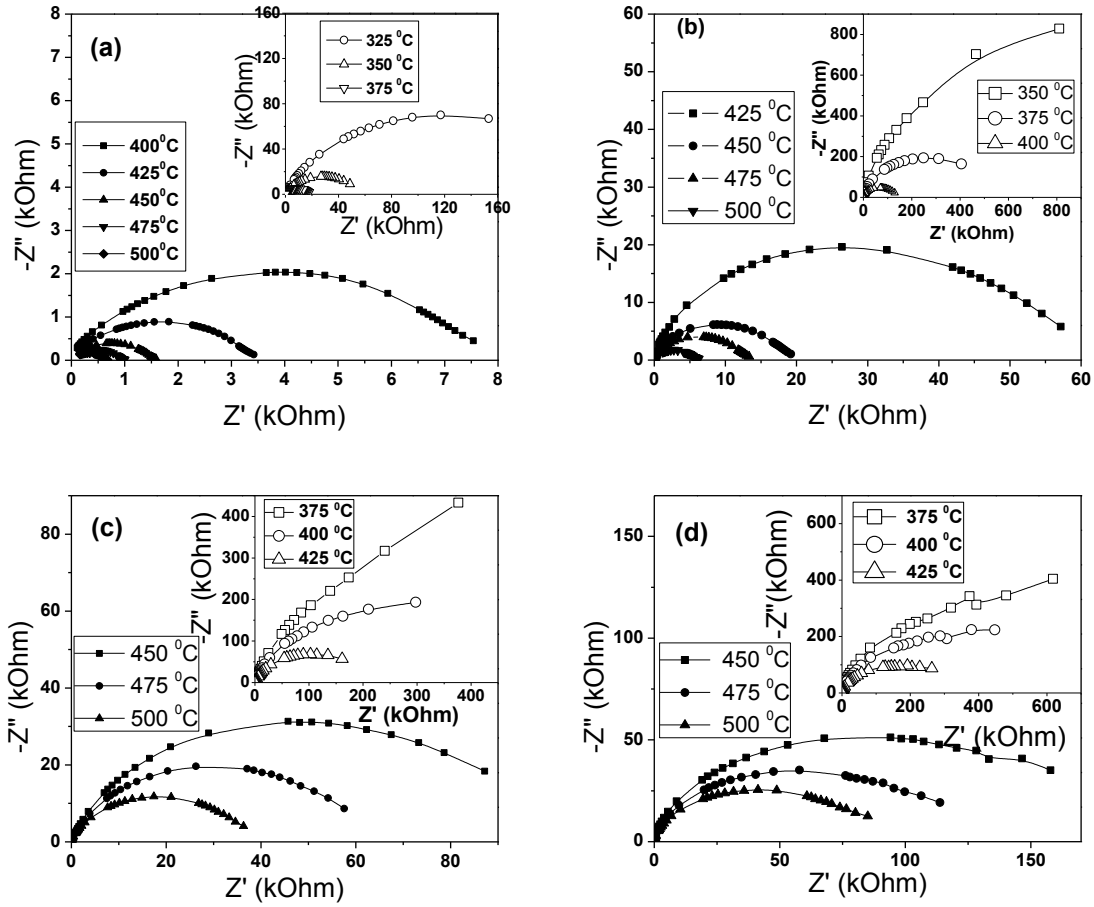

Fig. 5.16 Nyquist plots of $(Na_{0.5}Bi_{0.5})Ti_{(1-x)}Zr_xO_3$, (a) x=0.05,(b)x=0.1, (c)x=0.2, (d) x=0.3.

5.2.4 Y modified NBT

The variation of imaginary part of impedance with frequency at different temperature of $(Na_{0.5}Bi_{0.5})_{(1-x)}Y_xTi_{(1-x/4)}O_3$, x=0.02, 0.04, 0.06, 0.08 are shown in Fig. 5.17 (a, b, c, d), respectively. On and above 375 ^{0}C a peak is appearing. The peak position shifts to higher frequency side with rise in temperature. As well as the width of the peak also get broadened with increasing temperature. The asymmetric

broadening of peaks in Z'' with frequency suggests that there is a spread of relaxation time.

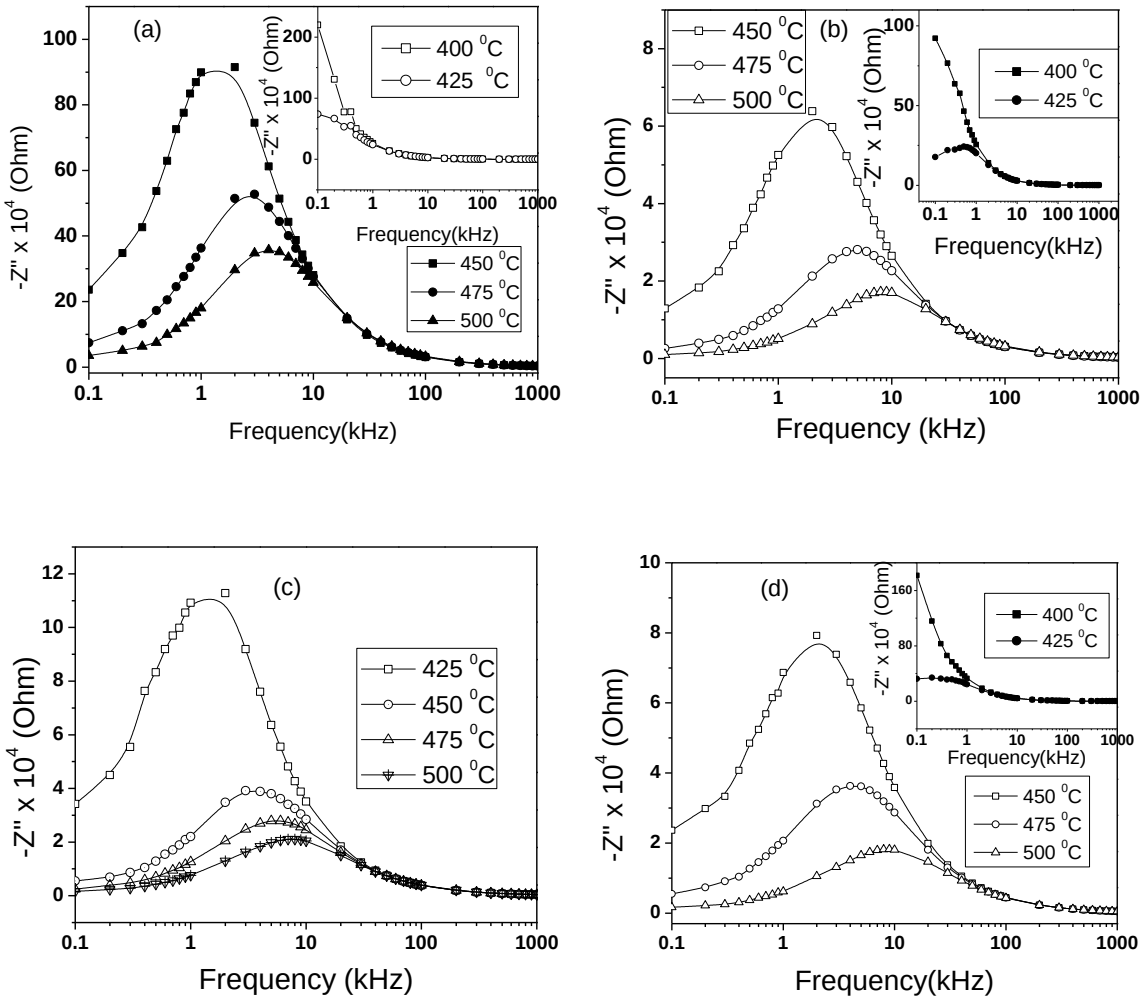

Fig. 5.17 Variation of Z'' with frequency of $(Na_{0.5}Bi_{0.5})_{(1-x)}Y_xTi_{(1-x/4)}O_3$, (a) x=0.02, (b) x=0.04, (c) x=0.06,(d) x=0.08.

The variation of relaxation time with inverse of temperature of $(Na_{0.5}Bi_{0.5})_{(1-x)}Y_xTi_{(1-x/4)}O_3$, x=0.02, 0.04, 0.06,0.08 are shown in Fig 5.18. The temperature dependence of relaxation time follows the Arrhenius behavior. The activation energy

is evaluated from the slope of log Z'' against 10^3/T curve. It is found to be 1.047, 1.319, 0.7283, 1.379 eV for 2, 4, 6, 8 % Y modified NBT, respectively.

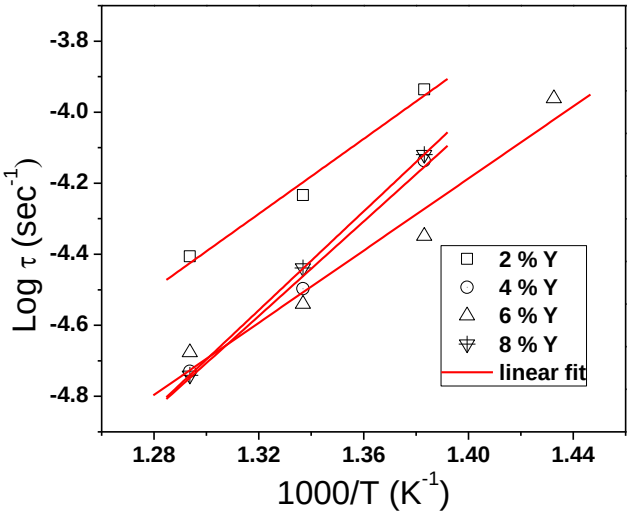

Fig. 5.18 Variation of τ_z with inverse of absolute temperature of $(Na_{0.5}Bi_{0.5})_{(1-x)}Y_xTi_{(1-x/4)}O_3$, (a) x=0.02, (b) x=0.04, (c) x=0.06, (d) x=0.08.

The complex impedance spectrum (Nyquist plot) of $(Na_{0.5}Bi_{0.5})_{(1-x)}Y_xTi_{(1-x/4)}O_3$, x=0.02, 0.04, 0.06,0.08 at different temperatures are shown in Fig. 5.19 (a, b, c, d), respectively. At low temperature (>425 ^{0}C), the complex impedance spectra is a single semicircular arc, with rise in temperature (> 450 ^{0}C) the spectra are composed of two overlapping semicircular arcs having their centers lying below the real axis. The diameter of the semicircle decreases with rise in temperature that signifies a reduction in resistive behavior of the material.

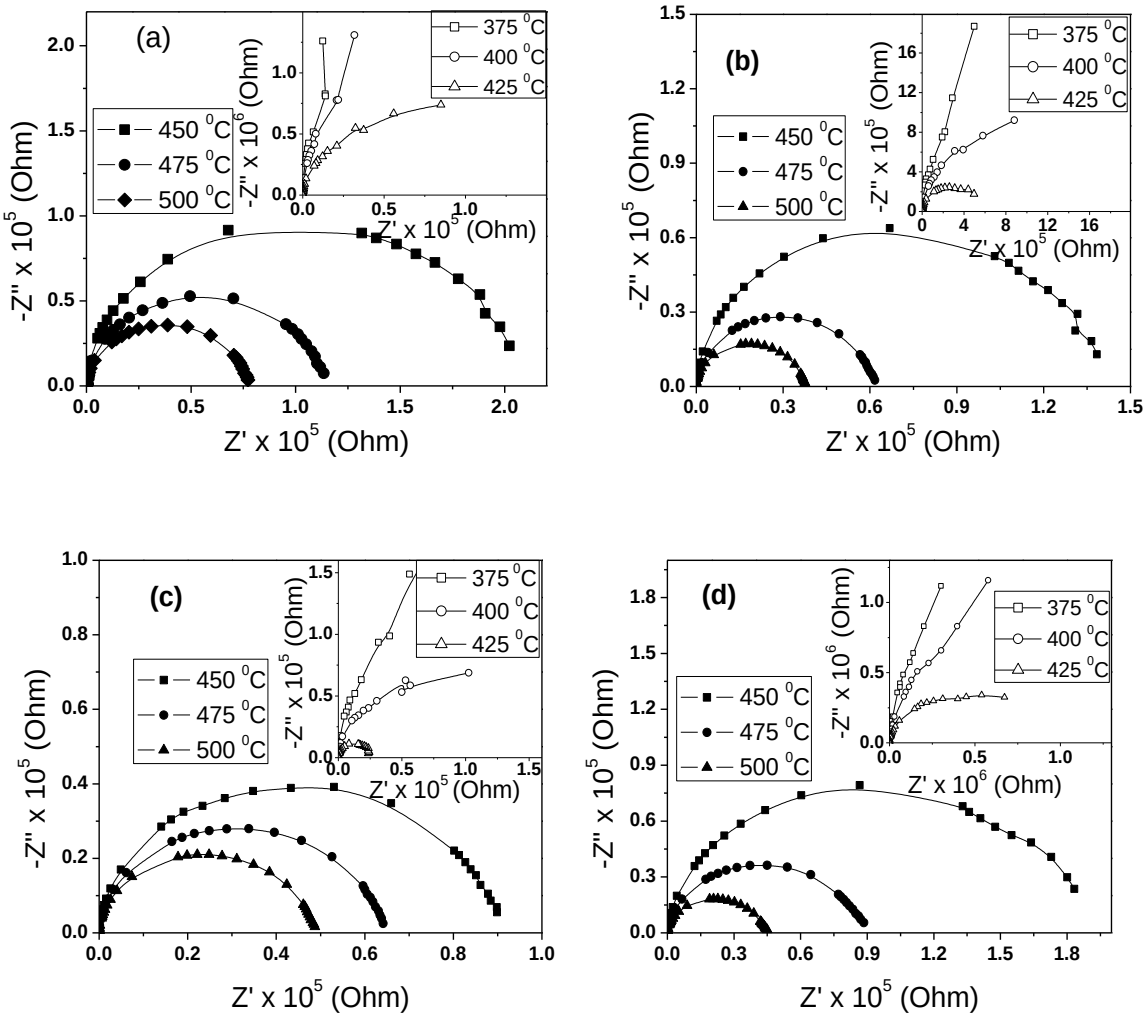

Fig. 5.19 Nyquist plots of $(Na_{0.5}Bi_{0.5})_{(1-x)}Y_xTi_{(1-x/4)}O_3$, (a) x=0.02, (b) x=0.04, (c) x=0.06, (d) x=0.08 at various temperatures.

References

[1] F. Kochary, M. D. Aggarwal, A. K. Batra, R. Hawrami, D. Lianos and A. Burger, Growth and electrical characterization of lead magnesium niobate–lead titanate (PMN-PT) single crystal for piezoelectric devices. Journal of Materials Science: Materials in Electronics, 19 (2008) 1058.

[2] L. E. Cross, Relaxor ferroelectrics. Ferroelectrics, 76 (1987) 241.

[3] O. Raymond, R. Font, N. S. Almodovar, J. Portelles and J. M. Siqueiros, Frequency-temperature response of ferroelectromagnetic $Pb(Fe_{1/2}Nb_{1/2})O_3$ ceramics obtained by different precursors. Part I. Structural and thermo-electrical characterization. Journal of Applied Physics, 97 (2005) 084107.

[4] K. Funke, Jump relaxation in solid electrolytes. Progress in Solid State Chemistry, 22 (1993) 111.

[5] N. Ortega, A. Kumar, P. Bhattacharya, S. B. Majumder and R. S. Katiyar, Impedance spectroscopy of multiferroic $PbZr_xTi_{1-x}O_3/CoFe_2O_4$ layered thin films. Physical Review B: Condens. Matter, 77 (2008) 014111.

[6] A. A. A. Youssef, The Permittivity and AC Conductivity of the Layered Perovskite $[(CH_3)(C_6H_5)_3P]_2\ HgI_4$. Z. Naturforsch, 57a (2002) 263.

[7] Gurvinderjit Singh and V. S. Tiwari, Effect of Zr concentration on conductivity behavior of (1−x)PMN-xPZ ceramic: An impedance spectroscopy analysis. Journal of Applied Physics, 106 (2009) 124104.

[8] J. R. MacDonald, Impedance Spectroscopy, Wiley, New York, NY, USA, 1987.

[9] I. M. Hodge, M. D. Ingram and A. R. West, Impedance and modulus spectroscopy of polycrystalline solid electrolytes. Journal of Electroanalytical Chemistry, 74 (1976) 125.

[10] D. K. Pradhan, R. N. P Choudhary. C. Rinaldi and R. S. Katiyar, Effect of Mn substitution on electrical and magnetic properties of $Bi_{0.9}La_{0.1}FeO_3$. Journal of Applied Physics, 106 (2009) 024102.

[11] R. N. P. Choudhary, D. K. Pradhan, C. M. Tirado, G. E. Bonilla and R. S. Katiyar,Impedance characteristics of $Pb(Fe_{2/3}W_{1/3})O_3$–$BiFeO_3$ composites. Physica Status Solidi (b), 244 (2007) 2254.

[12]W. Chen, W. Zhu, O. K. Tan and X. F. Chen, Frequency and temperature dependent impedance spectroscopy of cobalt ferrite composite thick films. Journal of applied physics, 108 (2010) 034101.

[13] J. Liu C. G Duan, W. G. Yin, W. N. Mei, R. W. Smith and J. R. Hardy, Dielectric permittivity and electric modulus in $Bi_2Ti_4O_{11}$. Journal of Chemical Physics, 119 (2003) 2812.

[14] J. Liu, C. G. Duan, W. G. Yin, W. N. Mei, R. W. Smith and J. R. Hardy, Large dielectric constant and Maxwell-Wagner relaxation in $Bi_{2/3}Cu_3Ti_4O_{12}$. Physical Review B, 70 (2004) 144106.

[15] S. Sen, R. N. P. Choudhary, A. Tarafdar and P. Pramanik, Impedance spectroscopy study of strontium modified lead zirconate titanate ceramics. Journal of Applied Physics, 99 (2006) 24114.

Chapter 6

MAJOR CONCLUSIONS AND FUTURE WORK

8.1 Conclusions

In search of suitable lead free ferroelectric ceramics for the environmental concern, the structural, microstructural and electrical properties of sodium bismuth titanate (NBT) and modified NBT have been investigated. The work contributes to the research and development of lead free perovskite ferroelectric material in the following aspects:

- The samples were prepared using a two-step high-temperature solid-state reaction route at an optimized calcination (950, 1000 ^{0}C) and sintering temperature (1080 ^{0}C).
- The formations of the compounds were confirmed by XRD analysis. Preliminary structural analysis showed all compounds possess rhombohedral crystal system with hexagonal axis.

- SEM micrograph shows the polycrystalline microstructure with a certain degree of porosity in the samples. The average grain size is found to be 1 to 5 μm. The grain size of La and Y modified NBT decreases whereas the reverse is observed in case of Zr modified NBT.
- FTIR spectrum confirms the formation of perovskite phase by showing the characteristic peak of BO_6 octahedral at around 600 cm^{-1}.
- Dielectric measurement of NBT and modified NBT showed the decrease in the value of dielectric constant at the Curie temperature (T_c) with the modification, which may be due to the reduction of distortion in the unit cell.
- The Curie temperature (T_c) has been found to be increased with the La, Y and Zr modification.
- The nature phase transition of NBT and modified NBT is diffuse type and it increases with increase in the concentration of substitutions. This diffuse behavior may be due to the disorder of the cations in the material.
- Temperature dependent dielectric constant of La and Y modified NBT showed three dielectric anomalies, i.e., ferroelectric to antiferroelectric phase transition ~150 ^{0}C (T_d), transition of rhombohedral to tetragonal structure ~220 ^{0}C (T_{R-T}) and antiferroelectric to paraelectric phase transition (T_c) ~330 ^{0}C.
- The conductivity of NBT and Zr modified NBT obeys Jonscher Power law. The conductivity spectrum shows frequency independent plateau at low frequency but dispersion at higher frequency.

- In the case of La and Y modified NBT, conductivity spectrum obeys the double power law for the observed three distinct regions in conductivity spectra. A frequency independent plateau at low frequency, short range hopping conductivity at intermediate frequency region and localized conductivity at high frequency region were observed. The Jump Relaxation Model (JRM) has been used to describe the conductivity spectrum.
- The onset frequency of dispersion shifts to the higher frequency with rise in temperature. The temperature dependent d.c. conductivity follows Arrhenius behavior. The calculated activation energy shows the conduction mechanism may be due to oxygen vacancy and A-site ionic vacancies.
- NBT has three different types of activation energy for different temperature range. This may be due to different conduction mechanisms and domain configuration of various structural phases of materials.
- Impedance spectroscopy has been used to establish microstructure-electrical properties relationship in the material. The existence of grain and grain boundary phenomena in the material are more distinctly separated in complex modulus formalism than complex impedance formalism.
- Impedance spectroscopy showed the existence of non-Debye type relaxation phenomena in the materials.
- An equivalent electrical circuit has been proposed on the basis of brick layer model which is a combination of two parallel RC elements connected in series for the electrical response of the material.

- The reduction of grain and grain boundary resistances (R_g and R_{gb}) of materials with increase in temperature showed the negative temperature coefficient of resistance (NTCR) type behavior.
- The relaxation peak of both imaginary part of impedance and modulus shift with temperature and follows Arrhenius behavior.
- The complex modulus formalism confirms the contribution of grain and grain boundary phenomena in the material at higher temperatures.

8.2 Future Work

This thesis investigates the synthesis, phase formation, structural, dielectric and electrical properties of bulk ceramics. A lot of further studies on different aspects are possible for academic/fundamental interest, and also for potential applications of the material.

The study of crystal structure at various temperature by temperature dependent X-ray diffraction from synchrotron radiation, neutron diffraction analysis and Raman spectroscopy can be performed.

In-situ TEM and HRTM study is necessary for the domain wall motion and degree of ordering.

Novel techniques (microwave, mechanochemical alloying and chemical synthesis) can be adopted for synthesis of modified NBT ceramics.

Study of dielectric, piezoelectric and ferroelectric properties of thin films and single crystal of NBT based materials can be developed for application point of view.

Dependence of grain size and other properties (piezoelectric, ferroelectric etc.) on sintering temperature can also be studied.

List of Publications based on the research work

A. Paper presented at National/International Conferences:

1. **B K Barick**, R N P Choudhary and Dillip K Pradhan, Studies of relaxatation phenomena in $Na_{0.5}Bi_{0.5}TiO_3$ ferroelectric ceramics. National Seminar on *Physics& Technology of Novel Materials* (PTNM 2010),25-27 February, 2010, Department of Physics, Sambalpur University, Sambalpur (ORISSA)
2. **B K Barick**, R N P Choudhary and Dillip K Pradhan, Dielectric and impedance spectroscopic study of La modified sodium bismuth titanate. *National Seminar on Ferroelectrics & Dielectrics* (NSFD-XVI), 2-4 December, 2010, Department of Pure & Applied Physics, Guru Ghasidas Vishwavidyalaya, Bilaspur (C. G.)

B. National/International Journal Papers:

1. **B K Barick**, K K Mishra, A K Arora, R N P Choudhary and Dillip K Pradhan, Impedance and Raman spectroscopic studies of $(Na_{0.5}Bi_{0.5})TiO_3$ (*Journal of Physics D: Applied Physics* 44 (2011) 355402)
2. **B K Barick**, R N P Choudhary, Dillip K Pradhan, Effect of Lanthanum modification on the phase transition and electrical properties of sodium bismuth titanate (Revised manuscript to be submitted on *Materials Chemistry and Physics*)